LIBRARY DECLARATION AND DEPOSIT AGREEMENT

STUDENT DETAILS

Full name: .....
University ID number: .....

THESIS DEPOSIT

I understand that under my registration at the University, I am required to deposit my thesis with the University in both hard copy and digital format.

The hard copy will be housed in the University Library. The digital version will be deposited in the University's Institutional Repository (WRAP). Unless otherwise indicated, this will be made openly accessible on the Internet and will be supplied to the British Library to be made available online via its Electronic Theses Online Service (EThOS) service.

In exceptional circumstances, the Chair of the Board of Graduate Studies may grant permission for an embargo to be placed on public access to the hard copy thesis for a limited period. It is also possible to apply separately for an embargo on the digital version.

Hard Copy

I hereby deposit a hard copy of my thesis at the University Library to be made publicly available to readers immediately.

I agree that my thesis may be photocopied.

Digital Copy

I hereby deposit a digital copy of my thesis to be held in the WRAP and made available via the EThOS.

My thesis can be made publicly available online.

GRANTING OF NON-EXCLUSIVE RIGHTS

I agree to the following:

Rights granted to the University of Warwick, the British Library, and the users of my thesis through this agreement are non-exclusive. I retain all rights in

my thesis in its present version or future versions. I agree that the institutional repository administrators and the British Library or their agents may, without changing content, digitize and migrate my thesis to any medium or format for the purpose of future preservation and accessibility.

DECLARATIONS

I declare that:

I am the author and owner of the copyright in my thesis and I have the authority of the authors and owners of the copyright in my thesis to make this agreement. Reproduction of any part of this thesis for teaching or in academic or other forms of publication is subject to the normal limitations on the use of copyrighted materials and to the proper and full acknowledgement of its source.

The digital version of my thesis I am supplying is the same version as the final, hardbound copy submitted in completion of my degree, once any minor corrections have been completed.

I have exercized reasonable care to ensure that my thesis is original, and does not to the best of my knowledge break any UK law or other intellectual property right, or contain any confidential material.

I understand that, through the medium of the Internet, my files will be available to automated agents, and may be searched and copied by, for example, text mining and plagiarism detection software.

I grant the University of Warwick and the British Library a licence to make available on the Internet my thesis in digitized format through the Institutional Repository and through the British Library via the EThOS service.

If my thesis does include any substantial subsidiary material owned by third-party copyright holders, I have sought and obtained permission to include it in any version of my thesis available in digital format and that this permission encompasses the rights that I have granted to the University of Warwick and to the British Library.

LEGAL INFRINGEMENTS

I understand that neither the University of Warwick nor the British Library have any obligation to take legal action on behalf of myself, or other rights holders, in the event of infringement of intellectual property rights, breach of contract or of any other right, in my thesis.

Student's signature: ..... Date: .....

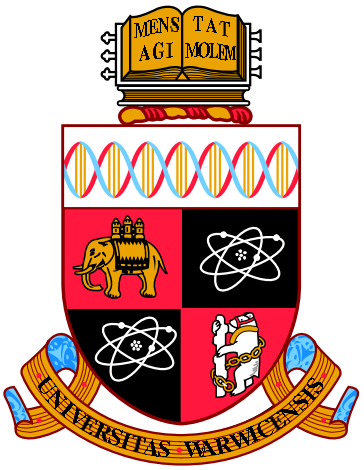

BIOLOGICALLY PLAUSIBLE ATTRACTOR NETWORKS

TRISTAN JAMES WEBB

THESIS

SUBMITTED TO THE UNIVERSITY OF WARWICK

FOR THE DEGREE OF

DOCTOR OF PHILOSOPHY

COMPLEXITY SCIENCE DOCTORAL TRAINING CENTRE

DEPARTMENT OF COMPUTER SCIENCE

MARCH 2013

THE UNIVERSITY OF WARWICK

CONTENTS

LIST OF FIGURES

LIST OF TABLES

ACKNOWLEGMENTS

During the course of my Ph.D., there have been many people that have supported and encouraged me. Without them, this thesis would not have been possible.

Foremost, I must thank my supervisors Jianfeng Feng and Edmund Rolls. I owe them both a great deal of inspiration. Professor Rolls in particular was very supportive of my work and a source of many ideas and feedback. It was a great learning experience to work alongside a scientist of his character. He has shown me the real importance and role that computational neuroscience will play in society. I feel very privileged to have had them both as my supervisors.

Dimitris Vavoulis has been a great friend, and the source of much conversation about computational neuroscience and programming ideas. His friendship has certainly shaped the work I have done.

I thank all of my colleagues in the Complexity Science DTC, and Computational Biology group. The community surrounding the DTC embodies an unique blend of theory and practice, and I am very pleased to have chosen it as the place to do my doctorate. I am also very grateful to the hardworking HPC staff at the University of Warwick for keeping our computing resources highly available.

Most importantly, I must thank my family. I also owe much to my parents, Karen and James Webb. My mother, a teacher, homeschooled me and instilled in me a strong desire for education. Without her long years of mentoring, I likely never would have have gotten this far. I wish that she could be here to celebrate this achievement. My father has been an unwaivering role model to me throughout my life. I must thank him for supporting me here in England both financially and emotionally. Thank you dad for being there on the weekend when I needed to phone home. It is impossible to express the great appreciation I feel for my fianceé Galina for being my everlasting support. She has kept me more than on track during my Ph.D. Thank you for all your love and being my best friend.

PUBLICATIONS

Rolls, E. T. and T. J. Webb (2011). "Cortical attractor network dynamics with diluted connectivity". *Brain Research* 1434, pp. 212–225.

Rolls, E. T. and T. J. Webb (2012). "Communication before Coherence". *European Journal of Neuroscience*, accepted.

Webb, T. J. et al. (2011). "Noise in attractor networks in the brain produced by graded firing rate representations". *PLoS One* 6, e23630.

ABSTRACT

Attractor networks have shown much promise as a neural network architecture that can describe many aspects of brain function. Much of the field of study around these networks has coalesced around pioneering work done by John Hopfield, and therefore many approaches have been strongly linked to the field of statistical physics. In this thesis I use existing theoretical and statistical notions of attractor networks, and introduce several biologically inspired extensions to an attractor network for which a mean-field solution has been previously derived. This attractor network is a computational neuroscience model that accounts for decision-making in the situation of two competing stimuli. By basing our simulation studies on such a network, we are able to study situations where mean-field solutions have been derived, and use these as the starting case, which we then extend with large scale integrate-and-fire attractor network simulations. The simulations are large enough to provide evidence that the results apply to networks of the size found in the brain. One factor that has been highlighted by previous research to be very important to brain function is that of noise. Spiking-related noise is seen to be a factor that influences processes such as decision-making, signal detection, short-term memory, and memory recall even with the quite large networks found in the cerebral cortex, and this thesis aims to measure the effects of noise on biologically plausible attractor networks. Our results are obtained using a spiking neural network made up of integrate-and-fire neurons, and we focus our results on the stochastic transition that this network undergoes. In this thesis we examine two such processes that are biologically relevant, but for which no mean-field solutions yet exist: graded firing rates, and diluted connectivity. Representations in the cortex are often graded, and we find that noise in these networks may be larger than with binary representations. In further investigations it was shown that diluted connectivity reduces the effects of noise in the situation where the number of synapses onto each neuron is held constant. In this thesis we also use the same attractor network framework to investigate the Communication through Coherence hypothesis. The Communication through Coherence hypothesis states that synchronous oscillations, especially in the gamma range, can facilitate communication between neural systems. It is shown that information transfer from one network to a second network occurs for a much lower strength of synaptic coupling between the networks than is required to produce coherence. Thus, information transmission can occur before any coherence is produced. This indicates that coherence is not needed for information transmission between coupled networks. This raises a major question about the Communication through Coherence hypothesis. Overall, the results provide substantial contributions towards understanding operation of attractor neuronal networks in the brain.

INTRODUCTION

The aim of this thesis is the study of stochastic neural networks for decision-making. The nervous systems consists of connected neural networks and is one of the most highly complex objects we have attempted to study in detail. There has been much progress in our theoretical understanding by using mathematics and dynamical systems theory as a basis to construct models of neural function. However, to pursue greater insight into the functioning of the actual brain, we must incorporate a biological understanding into these models. This thesis will describe how such mathematical models have been extended and simulated using techniques of computational neuroscience, so that they can be better applied to understanding brain function.

PROBLEM BACKGROUND

The function of the brain, and its relationship to intelligence, has been under consideration for hundreds of years, and now the structure of the brain is much more understood than in any other point in history. Nevertheless, we are a very long way from a full understanding of of this complex structure. We describe here basic neurophysiology at the neuron level, because this is the basic level at which information is transmitted in the nervous system. I also present the idea here that in order to understand the network level, that is the level of large scale complex systems, we must consider it from the perspective of computational neuroscience. Here I describe the promising area of attractor networks.

Basic neurophysiology

The Italian scientist Galvani first observed frog legs jumping to life when exposed to electricity over 200 years ago, which opened the door for the empirical neuroscience by enlightening us to the electrophysiological nature of the nervous system. The so-called age of the microscope that started in the 1800s allowed neuroscientists to be able to see the fine cellular makeup that dictates the brain's functioning. The "neuron doctrine" posed by Cajal, among others, (Bullock et al., 2005) has been verified through years of experimental neuroscience, and we now know that the brain is made up of individual neurons which communicate in a vast network through all or nothing electrical signals known as "action potentials". Still, until recently, neuroscience has been struggling with the problem of cataloging the incredible molecular complexity throughout the brain. Shepherd (1988) states in *Neurobiology* that

> *The major problem was the incredible diversity of cell types within the nervous system… Modern methods of molecular biology have changed all of this.*

Today these discoveries form the basis of many mathematical models of brain function.

The accepted understanding of a prototypical neuron is illustrated in Figure 1. Due to a careful balance of ions a neuron remains in an electrically polarized state from the surrounding inter-cellular fluid. Scientists such as Galvani were able to observe the affect an electrical stimulus had on a neuron, the generation of action potentials. When neurons fire naturally, the action potential impulse is very quick and can be thought of as a discrete event. Modelers can often think of these events as a "shot noise" and approximate the activity of a single action potential as a delta function. Once a neuron fires it reverts to a subthreshold state, and may remain in a refractory period in which it is less susceptible to input.

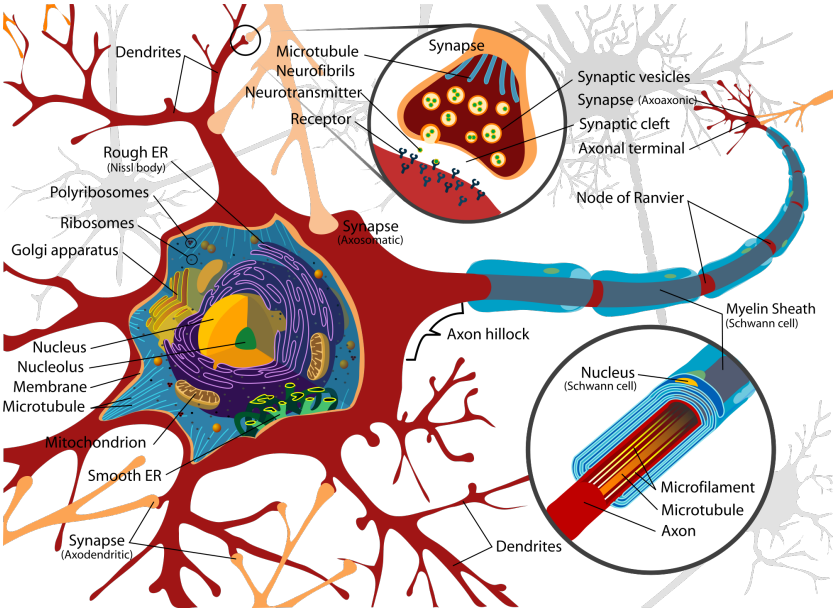

Figure 1: Artist's rendition of a typical neuron. Electrical activity is generated along the axon as a result of the input from other neurons. Detail shows Mylination of the Axon, which facilitates the speed of electrical impulses, and the connection points of neurons known as synapses. [1]

Of special interest to us is the *synapse*, or the small gap present at the connection between two neurons. Many of our recent investigations into molecular neurobiology have primarily been focused on categorizing the proteins responsible for neurotransmitter release at the synapse (Sudhof, 2004). The synaptic vesicle release cycle is the term used to describe the processes of communication that occurs at the synapse on the arrival of an electrical impulse, see Figure 2. We now know that this communication between neurons to be mediated by an electrochemical process. The chemicals released at synapse that signal an action potential are known as neurotransmitters. Their release is caused by Ca^2+ intake when an action potential arrives at the presynaptic terminal.

1 Figure taken from `http://en.wikipedia.org/wiki/File:Complete_neuron_cell_diagram_en.svg`, and used as released under the public domain

In this thesis, I will be examining three of the major neurotransmitters present in the brain, AMPA, NMDA, and GABA. AMPA and NMDA are excitatory neurotransmitter receptors, that implement the effect of glutamate (Purves, 2007). AMPA and NMDA differ in the speed at which the chemical signal is propagated to the post-synaptic neuron, with AMPA mediated potentials being much faster than NMDA. GABA is primary inhibitory neurotransmitter in the brain (Watanabe and Maemura, 2002).

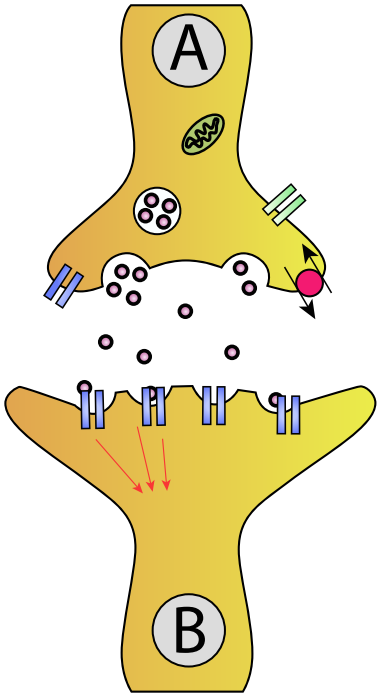

Figure 2: Illustration of the synaptic vesicle release cycle with neuron A transmitting to neuron B. [2]

Neurobiology of decision-making

What is the brain activity that is associated with making a decision, and what accounts for predictability of the choice? By decision-making, I refer to the process that we all go through when deciding an alternative between two or more choices. We have long known that this process is associated with an aspect of chance in the discrimination of stimuli (Thurstone, 1987). Tversky (1972) stated that "When faced with a choice among several alternatives, people often experience uncertainty and exhibit inconsistency" and went on to develop a probabilistic framework of decision-making. These questions have recently lead to experiments involving recording brain activity, and they have highlighted a few key areas of the brain that may be involved. Here, I will review them to provide a justification of the model of decision-making I use in this thesis.

2 Figure adapted from `http://en.wikipedia.org/wiki/File:Synapse_diag1.svg` under the Creative Commons Attribution-Share Alike 3.0 Unported license.

Key reviews of the neurobiology of decision-making have been produced by Gold and M. N. Shadlen (2007) and Schall (2001). The premise on which Gold and M. N. Shadlen (2007) argue is that somewhere in the brain are neurons specialized to the task of encoding a decision. We can think of this activity as being represented by a decision vector (DV). Gold and M. N. Shadlen (2007) identify this vector with all the internal "deliberations" that occur during a decision-making process, and assign it with a rule that signals the conclusion of decision. This approach leads to theories of decision making that can be verified by locating the decision vector in neurological data.

The brain processes sensory information in many specialized brain areas. For instance, the main sensory brain area for the sense of touch is the primary somatosensory cortex (S1) (Kandel, J. Schwartz, and Jessell, 2012). Neurons that are involved in the perception of vision during visual motion tasks have been found in the middle temporal (MT) area (K. Britten et al., 1993). These sensory areas are connected to areas of the brain that produces behavioral responses, such as the superior colliculus (SC), the lateral intraparietal area (LIP), and the frontal eye field (FEF), which all control eye movements (Schall, 2001).

Two perceptual tasks used in decision-making experiments are vibrotactile frequency discrimination (VTFD) and random dot motion (RDM). These experiments have been conducted alongside simultaneous recording of neurons using single- and multi-unit recording (Luna et al., 2005; Mountcastle, Steinmetz, and Romo, 1990; Romo and Salinas, 2003).

VTFD involves subjects discriminating between two flutter stimuli, f1 and f2, applied to their fingertips (Li Hegner et al., 2009). These stimuli are typically in the 5–50 Hz range, and there is a short time gap between their application. Work done by Romo and collaborators have found that neurons in S1 have firing rates that correspond to the frequency of each stimulus (Romo, Hernandez, and Zainos, 2004). It is not currently thought that neurons in S1 compare the two signals, because the neurons in S1 respond to both f1 and f2 and they do not seem to compute any stimulus comparison (Gold and M. N. Shadlen, 2007). Romo's lab found that activity in the secondary somatosensory cortex (S2) and dorsolateral prefrontal cortex (dlPFC), but to greatest extent activity in the ventral premotor cortex (VPC) and medial premotor cortex (MPC) reflected a comparison between the two stimuli (Hernandez, Zainos, and Romo, 2002; Romo, Brody, et al., 1999; Romo, Hernandez, and Zainos, 2004; Romo, Hernandez, Zainos, et al., 2002). The exact relationship between these different brain areas is still unknown, but these experiments have lead to proposed theoretical frameworks of decision making where activity in S1 encodes the stimulus and the VPC and MPC neurons encode a probabilistic response (Deco and E. T. Rolls, 2006; Deco, E. T. Rolls, et al., 2012).

RDM experiments involve tasks where an subject must decide the direction of dots having coherent motion in a random dot field. In primate experiments, monkeys were trained to indicate their choice by a saccade (rapid) eye movement. A major difference between VTFD and RDM tasks is that in the latter the subject does not need to hold a stimulus in working memory. Gold and M. N. Shadlen (2007) conclude that this fact gives it two advantages: one, is that RDM may be more linked to perception than cognition; and two, the DV is likely located in parts of the brain that control eye movements. Like the VTFD experiments, researchers have found an area of the brain that encodes the sen-

sory information, in this case the area is the MT area (K. Britten et al., 1993; W. T. Newsome, K. H. Britten, and J. A. Movshon, 1989). The position of the LIP area in between the MT area and the SC and FEF areas lead researchers to focus on the LIP area as possible area to encode a DV (Gold and M. N. Shadlen, 2007). Neural activity in this area has been found to correspond to decision performance on a RDM task (M. Shadlen and W. Newsome, 1996; M. Shadlen and W. Newsome, 2001). In addition, reaction time versions of the RDM tasks have produced results that have been reproduced in theoretical models of decision-making (Ditterich, Mazurek, and M. Shadlen, 2003; Vandekerckhove and Tuerlinckx, 2007; X.-J. Wang, 2002)

The experimental work done by Romo and Shadlen have shaped recent research in decision-making. Recent experiments using fRMI data gathered from humans subjects has pointed at the neural correlates of the speed-accuracy trade off (Criss, Wheeler, and McClelland, 2012; Ivanoff, Branning, and Marois, 2008; Van Veen, Krug, and C. Carter, 2008). Future experiments may help us soon locate more of the signaling pathways involved in decision making.

Computational neuroscience

Determining the structure of biological neural networks has been a very difficult task due to the high density of brain tissue. For years scientists relied primarily on the microscope and electrophysiological techniques such as voltage-clamp experiments. These limitation have recently been lifting in recent years with new optical imaging techniques that can complement electrophysiological techniques (Scanziani and Häusser, 2009).

While molecular biologists have explored the brain at smaller scales, larger neural systems have been investigated using functional magnetic resonance imaging (fMRI), electroencephalography (EEG), magnetoencephalography (MEG), and multielectrode array (MEA) data. Bullmore and Sporns (2009) review how these experimental techniques are used to map the functional systems of the brain and offer explanations for behavior and cognition. This last point emphasizes the need to synthesize the findings of experimental neuroscience with theory and computer simulations at the network level.

Computational neuroscience approaches the study of the brain by simulating its complex functioning using a synthesis of computers, theory, and experimental evidence. Since the term was first introduced by E. L. Schwartz (1990) to refer to already diverse field, computational neuroscience has grown to encompass many different levels of function. Deco, V. Jirsa, et al. (2008) surveyed the field and they describe the hierarchical nature of modeling the brain (models vary in space-time scope from the detailed single neuron level to the large scale neural system level). Detailed neuron models may not be needed explicitly in large scale population models. So in practice, along the way of building up scale, we abstract the perceived crucial functioning of detailed models into what becomes the components of larger scale models [3] Deco, V. Jirsa, et al. (2008) go on to describe how models (population models in particular) may be studied as

3 I note that one level of modeling is not necessarily more biologically correct than the other; rather, a detailed level and a more abstract level can both be "correct" at the level they describe, and that neither is truly biologically correct because, obviously, models never are. The major contributions of this thesis on the topic of noise are all reliant on the spiking neuron level of abstraction that we chose. I contrast the methods used in this thesis to more abstract models, such as race models,

purely theoretical models or be used as data generating models that can be verified with empirical results (EEG, MEG, MRI). All of this means, especially with the recent advances in gathering empirical results, computational neuroscience provides a theoretical means to model high-level traits, such as behavior and cognition, through models that have been devised from low level biological observations.

Neural network theory has long been connected to the study of physical systems and to associative memory systems in the brain (Little, 1974; Willshaw, Buneman, and Longuet-Higgins, 1969). Through work pioneered by John Hopfield, associative memory in neural networks was paralleled with statistical physics when he commented on an artificial neural network "This case is isomorphic with an Ising model" (Hopfield, 1982). Hopfield's work went further than work previously done by formulating a Lyapunov function that accounted for the dynamics of his network. This theory became a success because of the strong understanding of the statistical mechanics available at the time. For example, it became possible to compute the memory capacity of a neural network using just the information about its microscopic properties (A. Treves and E. T. Rolls, 1991). Work conducted by Daniel Amit, Nicolas Brunel, and Xiao-Jing Wang has lead to a time dependent spiking attractor network framework model of the areas of the brain associated with decision-making known to exist in the cerebral cortex (Amit and Brunel, 1997a; X.-J. Wang, 2002). Work like this has shown that simple models of the nervous system possess many complex properties. Feedback, an essential element of the actual nervous system, creates highly non-linear dynamics for these networks. In section 2.1, I describe a "balanced excitation-inhibition" network inspired by the work of Amit, Brunel, and Wang which is used for the computational modeling undertaken in this thesis.

In this thesis, I will be investigating the fundamental properties of the attractor network model and its biological significance. These networks can be used to model the functioning of the memory subsystems of the brain (B. McNaughton and Morris, 1987; E. T. Rolls, 1996). Or they can provide a model for learning, such as how Pavlov's classical conditioning may arise (Tesauro, 1986). Attractor networks have great explanatory power because stored memories can be recalled by a small fragment of that memory as a cue. The connections between neurons are also governed by the biologically accepted associative, or Hebbian, learning, named after the observations of Donald Hebb in his book *The Organization of Behavior* (Hebb, 1949). Hebbian learning has been almost universally accepted as describing the modifications of synaptic strength associated with long term potentiation (LTP), first experimentally observed by (Bliss and Gardner-Medwin, 1973), and its counterpart long term depression (LTD), discovered shortly afterwards by Lynch, Dunwiddie, and Gribkoff (1977).

---

of decision-making researched by other scientists, but such a contrast should not be perceived as negative one.

These other models that fall under the class of drift diffusion models are a valuable complement to our methods.

AIM OF THIS THESIS

Seminal work done by many theoretical neuroscientists has grounded the field in well established branches of mathematics. Modern attractor network theory has been rooted in statistical physics since the work of Hopfield (1982). Hopfield's contribution was deriving a model that used a Hebbian learning rule and also constructing a homeomorphism with the well known Ising model. Hopfield's model is regarded as a milestone is stimulating interest in the field of attractor networks, even though outside of Hebbian learning and the basic attractor network architecture it is not a biologically plausible model (Wilson, 2009). We shall see how models of spiking neurons, that have been studied as dynamical systems with a geometric interpretation by Rinzel (1986), among others, are used to make the basic notion of attractor networks more biologically plausible while still remaining true to the original theory. Furthermore, the biological abstractions in Hopfield networks allowed the proof of their ability to perform content addressable memory recall. The assumptions have made it easier to analyze these systems to determine quantities such as storage capacity using methods of statistical physics. We can therefore gauge the performance of an attractor network with a mean-field equivalent by knowing parameters such as connectivity, sparseness, and the memory pattern encoding. It is increasingly known the simplifications employed by Hopfield, such as assuming a binary firing distribution of neurons, may not apply in the brain. The distribution of neural firing rates in the brain is exponential (Baddeley et al., 1997; Franco et al., 2007; S. Treves A. P. et al., 1999), and the connectivity of neurons is diluted, with neurons in a given area connected to other local neurons with a value as low as 4% (Ishizuka, Cowan, and D. G. Amaral, 1995; Li et al., 1994; E. T. Rolls et al., 1997a).

Each of the chapters in turn will:

- Measure performance of realistic networks versus networks with mean-field equivalents.
- Quantify noise in biologically plausible neural networks.
- Test the Communication through Coherence Hypothesis using an attractor network model.

ORGANIZATION OF THIS THESIS

This thesis is split into two main parts, the first part being a description of attractor models and the spiking neural network I use, and the second part being three chapters that comprise the original research of this thesis. What follows is a brief description of each chapter.

Attractor Networks

In Chapter 1, I define attractor networks. Attractor networks are neural networks that are recurrently connected and settle into a stable pattern of firing.

Attractor networks posses rich information processing abilities. I show how they posses properties needed for memory, learning, and decision-making.

Spiking Neural Network Models

A computational neuroscience model of decision-making is presented in Chapter 2. I examine the stochastic methods used in neuroscience to model spiking neural networks, and present the major models used in the field to simulate decision-making. Finally, I define the model used in Chapter 3, Chapter 4, and Chapter 5.

Graded Firing Rates in the Brain

In Chapter 3, I discuss how representations in the cortex are often distributed with graded firing rates in the neuronal populations. The firing rate probability distribution of each neuron to a set of stimuli is often exponential or gamma (Baddeley et al., 1997; Franco et al., 2007; S. Treves A. P. et al., 1999). In processes in the brain, such as decision-making, that are influenced by the noise produced by the close to random spike timings of each neuron for a given mean rate, the noise with this graded type of representation may be larger than with the binary firing rate distribution that is usually investigated. In integrate-and-fire simulations of an attractor decision-making network, we show that the noise is indeed greater for a given sparseness of the representation for graded, exponential, than for binary firing rate distributions. The greater noise was measured by faster escape times from the spontaneous firing rate state when the decision cues are applied, and this corresponds to faster decision or reaction times. The greater noise was also evident as less stability of the spontaneous firing state before the decision cues are applied. The implication is that spiking-related noise will continue to be a factor that influences processes such as decision-making, signal detection, short-term memory, and memory recall even with the quite large networks found in the cerebral cortex. In these networks there are several thousand recurrent collateral synapses onto each neuron. The greater noise with graded firing rate distributions has the advantage that it can increase the speed of operation of cortical circuitry.

Diluted Connectivity

In Chapter 4, I discuss the role of dilution on spiking related noise in the cortex. The connectivity of the cerebral cortex is diluted, with the probability of excitatory connections between even neighboring pyramidal cells rarely more than 0.1, and in the hippocampus 0.04 (Ishizuka, Cowan, and D. G. Amaral, 1995; Li et al., 1994; E. T. Rolls et al., 1997a). To investigate the extent to which this diluted connectivity affects the dynamics of attractor networks in the cerebral cortex, I simulated an integrate-and-fire attractor network taking decisions between competing inputs with diluted connectivity of 0.25 or 0.1 but the same number of synaptic connections per neuron (80) for the recurrent collateral synapses within an attractor population as for full connectivity. The results indicated that there was less spiking-related noise with the diluted connectivity.

The decision times were a little slower with diluted than with complete connectivity (full connectivity 894 ms, 0.25 dilution 940 ms, and 0.1 dilution 1,013 ms). The accuracy of the correct decisions (with $\Delta\lambda = 6.4$) increased with dilution: full connectivity 64.3%, 0.25 dilution 75.7%, and 0.1 dilution 90.3%. The stability of the network when in the spontaneous state of firing was increased by dilution: full connectivity 11.4% of trial were unstable, 0.25 dilution 0.8% of trials, and 0.1 dilution 0% of trials. Given that the capacity of the network is set by the number of recurrent collateral synaptic connections per neuron, on which there is a biological limit, the findings indicate that the stability of cortical networks, and the accuracy of their correct decisions or memory recall operations, can be increased by utilizing diluted connectivity and correspondingly increasing the number of neurons in the network, with little impact on the speed of processing of the cortex. Thus, diluted connectivity can decrease cortical spiking-related noise.

Communication through Coherence

In Chapter 5, I test the Communication through Coherence Hypothesis. The communication through coherence hypothesis proposes that coherent or synchronous oscillations in connected neural systems can promote communication. I tested this in an integrate-and-fire network in which one network was connected to a second network by synaptic connection strengths that were systematically increased in strength in different simulations. Each of the networks was an attractor decision-making network, and the decision populations of neurons of the two networks were connected by associative connections such that a decision in the first network could, trigger a corresponding decision in the second network. Gamma oscillations could be induced by increasing the relative conductance of AMPA to NMDA excitatory synapses. It was found that very small connection strengths between the networks were sufficient to produce information transmission (measured by Shannon mutual information) such that the second network took the correct decision based on the state of the first network. Although gamma oscillations were present in both networks, the synaptic connections sufficient for perfect information transmission (100 percent correct, 1 bit of transmitted information) were insufficiently strong to produce coherence, phase locking or dependency, between the two networks, which only occurred when the synaptic strengths were increased more than 10 times. This indicates that information transmission can occur before synapses have been made sufficiently strong to produce coherence. Moreover, information transmission was as good when the AMPA to NMDA ratio was returned to its normal value, and oscillations were not present.

Part I

Background and Methods

1 ATTRACTOR NETWORKS

In this chapter I will consider how simple neural networks models can function as memory systems. The names *attractor network*, *autoassociator network*, and *associative memory network* all basically refer to the same thing; that is a neural network with enough feedback to provide itself with a tendency to settle in to a steady firing pattern, the attractor state (Eliasmith, 2007). Attractor networks came to be thought of as a type of memory system that would offer content addressing. This means that the network will reconstruct a stored memory, in the form of an attractor state, if it given an initial partial cue. This ability of attractor networks makes them likely to be involved in representing memory in the nervous system. It is theorized that these networks store patterns or memories for subsequent retrieval through the strength, or weight, of synapses (Amit, 1989).

1.1 PREVIOUS MODELING WORK

Attractor networks have been implicated as a basic building block of large scale neural networks, such as the thalamus and hippocampus (Rinzel et al., 1998), In the hippocampus, Buzsáki (1997) has suggested that it is an attractor network architecture that is responsible for the theta oscillations that have been observed through EEG recordings. The CA3 region of the hippocampus has been shown to posses the same feedback architecture that characterizes attractor networks (D. Amaral and Witter, 1989). The neurons in the CA3 region have both highly collateralized and spatially extensive axons that are connecting to other CA3 neurons in what are known as the associative projections (D. G. Amaral, 1993). In a rat study, Ishizuka, Cowan, and D. G. Amaral (1995) found that the CA3 dendritic trees contained a systematic variation in the dendritic length and proportion of the dendritic tree in other areas of the hippocampus as a function of the location of the cell in the CA3 region.

Recent studies help form a body of both theoretical studies and experimental evidence that suggest the presence of attractor-like connectivity in the brain. Some of the earlier experimental evidence for attractor networks has come from observations of hippocampus place cells forming a map-like description of the outside world (Tsodyks, 1999; Wills et al., 2005). More recently, there has been focus on the spontaneous activity in the cortex, and in particular this activity has been found to be highly structured with respect to space and time (Ringach, 2009). Studies have found that the resting state activity of the cat visual cortex was similar to the activity that was evoked by sensory stimulation (Braun and Mattia, 2010). These patterns of spontaneous activity in the primary visual cortex are theorized to result from an connectivity that is capable of producing attractor-like states (Goldberg, Rokni, and Sompolinsky, 2004). The connectivity pattern of neocortical microcircuits will produce a set of default states of

spontaneous activity. In experimental studies, both *in vivo* and *in vitro*, of these default states, neuron firing patterns show a temporal progression of activity that is similar to that observed when the area is exposed to stimulation (Luczak and MacLean, 2012).

It has been theorized that this architecture lets the CA3 system function as a single network with an approximate connectivity of 4% between CA3 cells (A. Treves and E. T. Rolls, 1994b). Many similar models that account for the storage of episodic memory in the hippocampus by the steady activation of cells in an attractor network have been suggested (B. L. McNaughton et al., 1996; O'Reilly and McClelland, 1994; E. T. Rolls, 2008). Another account of hippocampal function has stemmed from early work by O'Keefe and Nadel (1978) which discovered that the hippocampus contains place cells that seem to encode a cognitive map of an animal's environment. Lisman (2005) has suggested that hippocampal memory sequences are encoded in theta and gamma frequency oscillations that cue off the firing of place cells. Another model proposed by Alvarez and Squire (1994) differs from others in that cells in the hippocampus only facility the binding together of memories stored in neocortical areas.

Attractor network theory is also used to study the inferior temporal visual cortex (Deco and E. T. Rolls, 2004; Moreno-Bote, Rinzel, and Rubin, 2007), the olfactory bulb (Galán et al., 2004). A recent review by Braun and Mattia (2010) outlines the various supporting evidence and studies for attractor networks playing a role biological and physiological function. Here, Braun and Mattia (2010) propose that higher order mental activity could be generated through nested attractor networks. This is partially supported by the computational studies that reproduced characteristically the resting-state brain activity recorded from fMRI (Deco, V. K. Jirsa, and McIntosh, 2011; Lundervold, 2010). These networks are also theorized to account for the error related feedback observed in MRI experiments. Networks with Hopfield like recurrent layers providing feedback have been used to model a proposed functioning of the anterior cingulate cortex signaling conflict in information processing (Botvinick, J. D. Cohen, and C. S. Carter, 2004). This proposed theory has been supported by fMRI experiments showing that the dorsal anterior cingulate cortex shows a fast response to unexpected error signals (Holroyd et al., 2004).

1.1.1 Two alternative forced choice decision-making models

The simplest way to describe a decision-making task is to only allow two choices and demand that a decision is reached. A review of models that describe this task has been given by Bogacz, Brown, et al. (2006). One of the earliest models of this task was given by Ratcliff and McKoon (1978), which consisted of a random walk with a drift term and a barrier corresponding to a decision rule. This is one of the earliest descriptions of the drift diffusion model (DDM) of decision making; however, it was predicated by a simpler model (Feller, 1968). The DDM model was extended by embedding in the drift diffusion equation an Ornstien-Uhlenbeck process that possessed either a stable or unstable point corresponding to the mean of the decision distribution (Busemeyer, 1993). Another models that fits the DDM paradigm is the feedforward inhibition model (Ditterich, Mazurek, and M. Shadlen, 2003), and the line attractor model (Furman and X.-J. Wang, 2008). Finally, a new promising approach to model this

task is to use a Baysian formulation of neural variability (J. M. Beck et al., 2008; Ma, J. Beck, Pouget, et al., 2008). The advantages of this theory is that it may help deal with noisy experimental data.

In contrast to the models above based on one-dimensional stochastic processes, connectionist attractor neural networks (Deco and E. T. Rolls, 2006; X.-J. Wang, 2002; Webb et al., 2011) offer a more neurologically detailed account for the competition between neural populations and an arrival at an attractor state. The implementation of these models are done with spiking neurons arranged into decision populations. Analytically, it has been shown in some cases, their population firing rates reduce to lower dimensional stochastic processes (Bogacz, Brown, et al., 2006; Wong and X.-J. Wang, 2006; Wu, Hamaguchi, and Amari, 2008).

Another class of models, which can account for multiple decision outcomes, are known as accumulator or race models (Vickers, 1970, 1979). However, E. T. Rolls and Deco (2010) criticizes this model as biologically unrealistic, and Bogacz, Brown, et al. (2006) remarks that these models do not reduce to the drift diffusion model.

Before delving into the particulars of an attractor network I will first review the basic computational unit of the brain, the neuron, in its most basic terms. I will then describe the architecture of an attractor network. Finally, I will summarize the classic results of one of the most successful models of this architecture.

1.2 ARTIFICIAL NEURONS

A neuron is the fundamental computation unit of the brain. Biologically, it is an electrically excitable cell that receives inputs through cellular extensions called *dendrites* and sends an output signal through an *axon*. The soma or cell body is particularly relevant to us because it acts as a capacitive membrane that stores electrical charge. Communication between neurons takes place at *synapses*, which typically occur between axons and dendrites.

The concept I will first use to represent neurons is the McCulloch-Pitts formalism. In this formalism neurons are logical units that function as "all or none" units, that either emit a spikes or do not fire. McCulloch and Pits first used binary threshold neurons to construct more complicated logical structures, such as AND, XOR, and NOT logical gates (McCulloch and Pitts, 1943). The McCulloch-Pitts neuron model captures enough detail to provide a rate based interpretation of brain activity, and they form the basis of artificial neural networks such as the Hopfield model. Another important concept that this model cultivated early on in the computational neuroscience is the idea of neuronal inhibition playing a major role in steady state dynamics.

In the description given by McCulloch and Pitts (1943), see Figure 3, a neuron contains these components:

- A cell body, the soma, that consists of a post synaptic membrane potential(PSP), and an activation function that maps input into a measure of activation.
- A set of inputs, the synapses, from which the neuron receive spikes from other neurons.

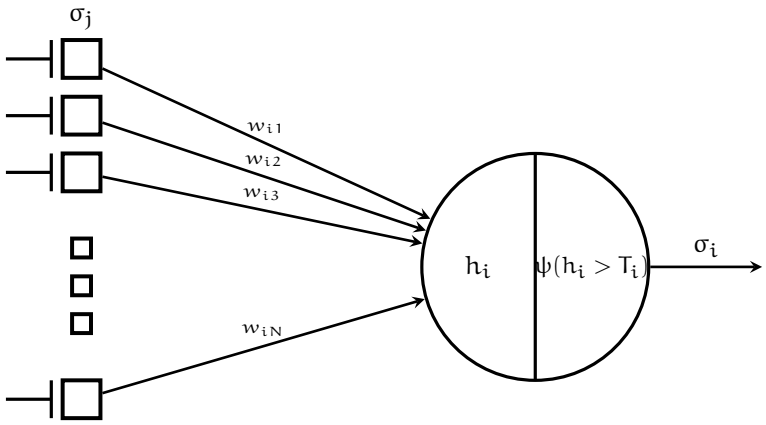

Figure 3: The major components of a McCulloch-Pitts artificial neuron. A neuron i receives spikes from presynaptic neuron j, with strength w_{ij}. Spikes are localized events in time, $\sigma_i(t)$ is a boolean variable that represents that presence of a spike at time t. h_i is the PSP at the soma, and $\psi(h_i)$ is a function which detects spikes, with θ_i representing a firing threshold. Figure adapted from Amit (1989).

- A single output, the axon, that transmits spikes to other neurons in the network.

In a logical framework it is useful to model the presence of a spike on the axon as a boolean variable σ_i, but here we give a neuron i a positive real valued firing rate r_i. Each synaptic connection is associated with a synaptic weight w_{ij} which signifies the amount to which the output firing rate of neuron i influences the activation of neuron j. A neuron accepts a set of inputs, and it maps these to its output, which represent the timing of output spikes. The process of computation takes place along the entire cell in the actual brain (Dayan and L. F. Abbott, 2001), with the spatial structure of the dendrites thought to play an increasing important role (London and Häusser, 2005), though we consider here only a single compartment of a cell's soma. Formally, this computation requires that each neuron's potential is associated with an activation function of its synaptic input, which we denote as h_i. As an example, consider a neuron that simply integrates synaptic, and input:

$$h_i = \sum_j r_j w_{ij}, \tag{1}$$

where r_j is the firing rate of a neuron j with a connection to neuron i, and w_{ij} is a variable which describes the strength of the connection from neuron j to neuron i.

The output firing r of a neuron i is a function of the input from the recurrent connections (h_i) and external input(e_i). With the function

$$r_i = f(h_i + e_i) \tag{2}$$

defined as the activation function. The activation function must be nonlinear (usually taken to be sinusoidal) to prevent positive feedback along the collaterals to cause the network to become unstable (E. T. Rolls, 2008).

1.2.1 Attractor network architecture

Neural networks can be classified based into different basic architectures that depends on the way the synaptic connections are arranged in the network. Neural networks can be thought of as a directed graph with N nodes, which represent neurons, and C edges, which represent the synaptic connections. Treves and Rolls have described two attributes that can be used to classify networks (E. T. Rolls and A. Treves, 1998). One attribute is the preferred direction of information flow, either recurrent or feedforward. The other attribute is the degree to which there is recurrent connectivity, or dilution, in the network. The recurrent connectivity of an attractor network is defined as the average number of connections per neuron from neurons in the network divided by the total number of neurons in the network. The value of this parameter can therefore take values in the range of $1/N$ for a fully diluted network to 1 for a fully connected network.

An attractor network has the output of each individual neuron feedback into the system along *recurrent collaterals*, see Figure 4. In order to model the propagation along the recurrent collaterals, we introduce the discrete time variable t. At each time step t the output of every neuron is used as input at time $t+1$. For example, at time $t = 0$, given an input e_i, a network will produce firing in the ensemble of neurons assigned to $\mathbf{e_i}$, while the rest will remain silent. I refer to the output firing of the neurons at a time by the rate vector $\mathbf{r_t}$. In the case I consider here, we take $\mathbf{r_0} = \mathbf{e_i}$. At each subsequent time step the network's state will be determined by strength of the recurrent collaterals as well as external input. I denote these recurrent collaterals as a $N \times N$ weight matrix $\mathbf{W}$, where w_{ij} is the weight between input unit i and output unit j, and N is the number of neurons in the network. Neuronal firing $\mathbf{r} = \{r_1, r_2, \ldots, r_N\}$ produces recurrent activation $\mathbf{h} = \{h_1, h_2, \ldots, h_N\}$ along the synapses through the function

$$h = \mathbf{r}\mathbf{W}.$$

Population sparseness, α, is important parameter in neural networks that measures the overall activation of the network. This parameter is used describe the encoding of memory patterns used to train the network. For instance, a low sparseness could be used to describe a pattern where only a few neurons are firing given a particular stimulus. Using data measured from populations of neurons in the real brain, Franco et al. (2007) found the population sparseness had an average value of 0.77. Population sparseness is defined as:

$$\alpha = \frac{(\sum_i^N \frac{y_i}{N})^2}{\sum_i^N \frac{y_i^2}{N}}$$

where y_i is the mean firing rate of neuron i.

One of the first comparisons between attractor networks and statistical mechanics was given by Little (1974). Later, in the 1980s and 1990s, attractor net-

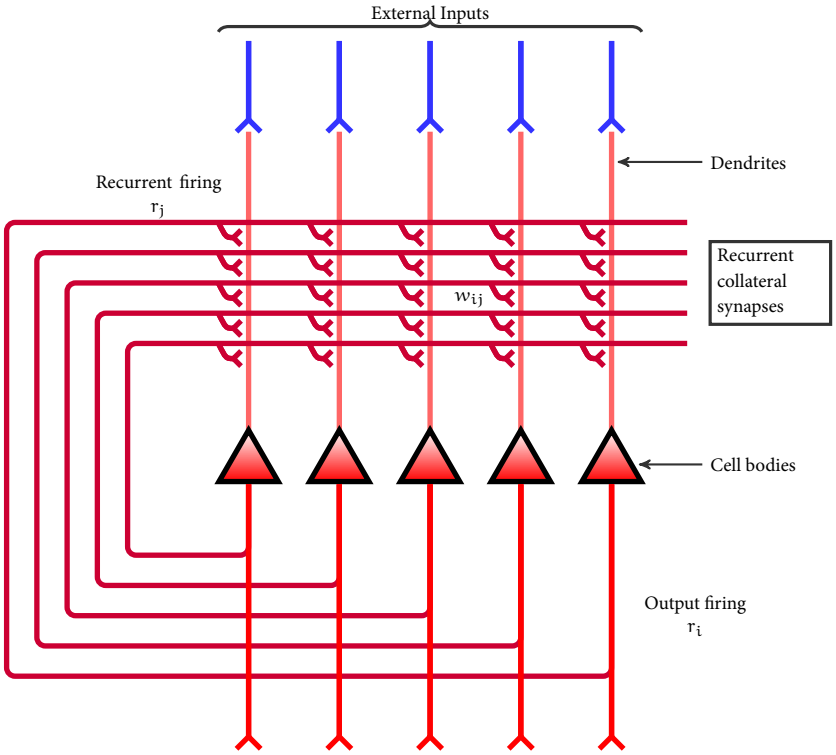

Figure 4: Connection diagram of a typical attractor network. External stimulus (in blue) is presented to each neuron at the cell body (red triangles), causing it to fire at rate r_i. The presence of external stimulus causes feedback into the network through the recurrent collaterls as described by the synaptic weight matrix **W**. The output firing will tend to settle into a steady pattern.

works with McCulloch-Pitts type neurons were often compared to spin glasses and other physical systems by Hopfield and others (Amit, 1989; Derrida, Gardner, and Zippelius, 1987; Gutfreund, 1990; Hopfield, 1982; Zippelius, 1993). It was this work that lead to rigorous analyses using both deterministic and stochastic dynamics. The techniques used in the analysis of the standard attractor network models assume that connections are reciprocal and symmetric in weight. If we adopt this set of assumptions we can use mean-field statistics to approximate free energy and mutual information in the network (E. T. Rolls and A. Treves, 1998). The approach used is related to Boltzmann's theories of statistical mechanics, which seeks to describe the macroscopic features of a system by averaging over the microscopic interactions (Lebowitz, 1993). Mean field equations are a very useful tool in the study of oscillation in these network; for it frees us from concerning ourselves with microscopic details (Gerstner and Kistler, 2002).

The following application of a mean-field approach applied to the neuron model I have just described is adapted from Gerstner and Kistler (2002). In this example, we consider a population of N McCulloch-Pitts neurons that are time dependent. We are interested in the behavior of the network in the steady state as time approaches infinity, $T \to \infty$. We know that a neuron's activation will be

a function of its synaptic input at any given time. Equation 1 is modified so that a neuron's input is dependent on the other neurons' activation in the previous timestep.

$$h_i(t) = \sum_j^N r_j(t-1) w_{ij}, \tag{3}$$

In this example, the synaptic weights are taken to be excitatory and inhibitory in nature, and independent and identically distributed (i.i.d.) with probabilities given by

$$\begin{aligned} Pr[w_{ij} = 1] &= \frac{C_{exc}}{N} \\ Pr[w_{ij} = -1] &= \frac{C_{inh}}{N} \end{aligned} \tag{4}$$

Where C_{exc} and C_{inh} represent the number of each type of synapse that the neuron recieves.

A neuron will fire given that its post synaptic potential exceeds a firing threshold, these dynamics are given by

$$r_i(t) = \Theta[h_i(t) - \theta_i)],$$

where θ_i is the firing threshold, and $\Theta[n]$ is the discrete Heavyside step function.

The network is initialized with a random pattern of activity,

$$r_i(t_0) \in \{0, 1\}, \text{ with probability } r_i(t_0) = 1 = a_0,$$

where a_0 represents the percentage of neurons that are active initially. We can then calculate the firing in the subsequent time step $\mathbf{r}(\mathbf{t_1})$ by the deterministic dynamics of the system.

A neuron's probability of being active in time step $t = 1$ if it receives input greater that its firing threshold. This is given by a sum over the probabilities of its synaptic inputs.

$$a_1 = a_0 \sum_{k=\theta_i}^{N} \sum_{l=0}^{k-\theta_i} Pr[L = l] Pr[K = k], \tag{5}$$

where K and L are random variables of the synaptic weights with distributions given by Equation 4. In this equation, the outer sum is a sum over the chances of a neuron having a number of excitatory synapses greater than its threshold, θ_i, and the inner sum is a sum over the chances that a neuron does not have enough inhibitory synapses to decrease its activation below its threshold.

Because K and L are i.i.d. we may use a binomial distribution to calculate the joint probabilities given in Equation 5.

$$a_1 = \sum_{k=\theta_i}^{N} \sum_{l=0}^{k-\theta_i} \binom{N}{k} (a_0 C_{exc} N^{-1})^k (1 - a_0 C_{exc} N^{-1})^{N-k} \binom{N}{l} (a_0 C_{inh} N^{-1})^l (1 - a_0 C_{inh} N^{-1})^{N-l}. \tag{6}$$

For $C_{exc} \ll N$ and $C_{inh} \ll N$, the binomial distribution above is approximated by a Poisson distribution. Therefore, the probability than an input to a neuron will exceed its firing threshold is given by

$$a_1 = \sum_{k=\theta_i}^{N} \sum_{l=0}^{k-\theta_i} \frac{(a_0^{k+l} C_{exc}^k C_{inh}^l)}{k!l!} e^{-a_0 (C_{exc} + C_{exc})}. \tag{7}$$

This result can be generalized over all time steps through this recurrence relationship to find the steady state behavior of this network, for details consult Gerstner and Kistler (2002). A computer simulation of such a network is shown in Figure 5.

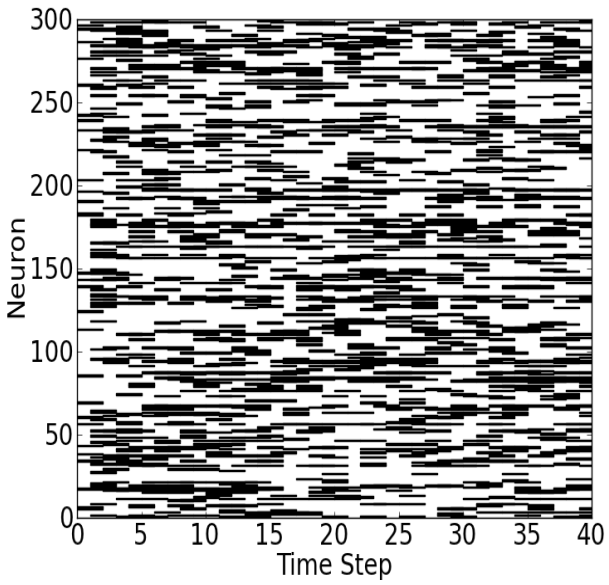

Figure 5: Firing of a recurrent McCulloch-Pitts neural network, $C_{exc} = 0.05$, $C_{inh} = 0.1$, $\theta_i = 1$.

1.3 HOPFIELD NETWORKS

A well known example of an attractor network is the Hopfield network (Hopfield, 2007), named after its inventor John Hopfield. In his famous 1982 paper, Hopfield described how an attractor network could function as a content addressable memory system from the standpoint of dynamical systems theory. Hopfield networks were then used as a model network across many different fields, and was heavily analyzed with methods from statistical physics due to a direct mapping with the well understood Ising model (Amit, Gutfreund, and Sompolinsky, 1985).

I have so far assumed that each neuron in the network is updated synchronous at each time step. The Hopfield network lifts this assumption, and the update rule to each neuron may behave asynchronously, as one would assume in the real brain Amit (1989). When we randomly select the neurons to update at each time Hopfield network behave like a stochastic dynamical system (Rojas, 1996). The neurons first described in Hopfield nets were binary threshold units, i.e. neurons can either take on a state 1 or 0. State 1 corresponds to the neuron firing at its maximum rate, denoted $r_i = 1$, and state 0 corresponds to the neuron not firing. A neuron i in the network has the threshold binary activation function:

$$r_i = \begin{cases} 1 & \text{if } \sum_j w_{ij} r_j > \theta_i \\ 0 & \text{otherwise} \end{cases} \tag{8}$$

with $\theta_i = 0$ being the threshold for neuron i.

I have said that attractor networks function to encode patterns of neural activations. In order to do this the network must undergo learning. The patterns we wish to store in an attractor network are represented by a vector of rates of length N, denoted here $\mathbf{e}^p = \{e_i^p, \ldots, e_N^p\}$. Our goal is after presentation of a fragment of an encoded pattern along the network's external inputs to have the firing of the network eventually reaching some stable firing pattern. We can then compare the firing of the network in this final state with the learned patterns. In the Hopfield model patterns are learned by the network through synaptic modification in accordance with Hebb's rule,

$$\begin{aligned} w_{ij} &= \tfrac{1}{N} \sum_p^P e_i^p e_j^p \text{ where } i \neq j \\ w_{ij} &= 0, \text{ where } i = j, \end{aligned} \tag{9}$$

where P is the number of patterns we wish to store. All patterns can be stored in one iteration of presenting each pattern to the network, calculating the activation, and updating the synaptic weights using Equation 9; this is a process called one-shot Hebbian learning. Proper application of this algorithm causes a network to learn the broad statistical structure of the inputs (O'Reilly, 1998), making it suited to preform well with a set of input vectors with uniformly distributed values.

The appeal of Hebb's rule as applied to biological systems is that it is a local learning rule, is dependent only on the firing of the presynaptic and postsynap-

tic neurons which share the weight. Hebb's rule is commonly interpreted to say that a change in the synaptic weight between two connected neurons is a function of the weighted product of their firing rates.

$$\Delta w_{ij} = k r_i r_j, \tag{10}$$

and Equation 9 extends this rule across a vector of patterns.

The network performs recall operations through a dynamical update of state. There are procedures for both updating a Hopfield network sequentially (asynchronously) or parallel (synchronously). In the sequential case the update of the network is done by first choosing a neuron i at random; and then if $\sum_j r_i w_{ij} + e_i > \theta_i$ then set $r_i = 1$, otherwise set $r_i = 0$.

One of Hopfield's major breakthroughs was the definition of an energy landscape, with basins of attraction, of the different possible states of the memory system. In recall, partial cues are presented to the network by setting each neuron's external input. This starts the network firing in a state which lies inside a basin of attraction. The system will then settle down into a state that corresponds to a stored pattern through the updating procedure. A Hopfield network is designed to store and retrieve a number of patters up to a certain critical value, after which the network will catastrophically fail (Kanter and Sompolinsky, 1987; E. T. Rolls and A. Treves, 1998). This critical value, $\alpha_c \equiv p/N$, is dependent on the type of pattern stored, the connectivity of the network, and the sparseness. Some authors have found that for Hopfield networks $\alpha_c \approx 0.14$ (Crisanti, Amit, and Gutfreund, 1986). Using other methods, multiple other authors have analyzed the standard Hopfield model, and they have found that α_c (with all stored memories being recallable) asymptotes at $N/(4\log(N))$ memories (Feng and Tirozzi, 1997; McEliece et al., 1987).

The spareness of the memory patterns is a major factor determining the storage capacity of the network. Training the network with patterns of low spareness will increase the amount of patterns that can be stored (E. T. Rolls and A. Treves, 1998). Intuitively, this increased storage capacity can be interpreted as a result of having less overlap of the same neurons firing in two different patterns because there are less neurons firing over all. Treves and Rolls 1998 described the storage capacity α_c in terms of the parameters of connectivity and sparseness:

$$p_{max} \sim \frac{C}{a \ln(\frac{1}{a})} k \tag{11}$$

where k is a constant around $0.2 - 0.3$.

These basins of attraction, which are local minima of an energy function, correspond to steady state values of the system. In these steady states, the firing of the neurons is the same as the stored memory patterns. The energy landscape of a Hopfield network is defined by the function

$$E = -1/2 \sum_{i}^{N} \sum_{j}^{N} w_{ij} r_i r_j - \sum_{i}^{N} r_i e_i \tag{12}$$

The tendency of the Hopfield network to settle and stay in one particular basin, from the set of possible basins defined by the energy landscape, means that it is classified as a point attractor in the dynamical systems taxonomy of attractor networks. This taxonomy includes stable point, line, and ring attractors; and unstable cyclic, and chaotic attractors (Eliasmith, 2007).

The energy landscape shows how pattern completion and the memory recall can occur under different conditions. With this formulation Hopfield shed tremendous light on the question of how many memories an attractor network can store.

Up to this point I have only considered binary representations for the neurons. Neurons in the brain fire with continuously variability. Continuous firing rates were analyzed by Hopfield (1984). He replaced the binary neurons in his original network which neurons which continuously increased in activity when exposed to greater input. The firing rate of these neurons were bound on both sides by a minimum, usually 0, and maximum firing rate. Hopfield also modeled a lag in the synaptic current reaching the soma after the behavior of real neurons.

In graded pattern representations, neurons can fire at many different discrete rates. For example, one step up from a binary representation would be a ternary representation. In a ternary representation the neuron can either not fire, fire at a low rate, or fire at a highly rate. Using a high graded pattern representation of the memories will not change the storage capacity of the network from using a lower representation. Theoretical analysis and simulation results show that such a network is able to store a similar number of patterns using graded patterns of composed of 10 and 50 graded rates (E. T. Rolls et al., 1997a; A. Treves and E. T. Rolls, 1991). The performance of the network will vary with the type of pattern used for training and recall. Simulation results show that recall performance of an attractor network trained with patterns of neurons that can fire at 10 different rates is markedly worse than the same network trained with binary patterns (E. T. Rolls et al., 1997b).

In this chapter I have summarized attractor models and their application to brain function. It will be used as a basis to understand more complex spiking neural network models, where we will replace the neuron's firing rate variables with an explicit calculation of a neuron's membrane potential and a spike generation mechanism.

2 SPIKING NEURAL NETWORK MODELS

Biologically accurate mathematical descriptions of neurons first appeared in earnest with the seminal work of Hodgkin and Huxley. Hodgkin and Huxley mathematically modeled the squid giant axon using dynamics that accounted for the concentration of ions inside and outside the neuron membrane. The ions flow in and out of the membrane through dynamics dependent on biologically plausible gating variables. For the time, the model was extraordinarily detailed with respect to the functioning of ion channels, and 60 years after their 1952 paper the Hodgkin-Huxley (HH) neuron model is still in use (D. Noble, Garny, and P. J. Noble, 2012). The Hodgkin-Huxley model is very good at capturing the type of behavior measured from actual neurons, yet it has a relatively high computational demand, compared to other non-spatial spiking neuron models. Often, in the past, the model has only been effective in smaller network simulations (Izhikevich, 2004). More recently, advanced library integration techniques have been developed, that can simulate HH neural networks with a computational efficiency comparable to using a simpler spiking neuron model, without sacrificing the rich dynamics of a HH network (Sun et al., 2009).

I will first describe the need for more detailed models than the artificial neuron described in the preceding chapter. Neurons in the brain have a difference in electrical charge between the extracellular region and the intracellular region. This is known as a neuron's *membrane potential*. This is due to a carefully managed balance of electrically charged ions across the cell's lipid bilayer. An equation that can describe the equilibrium or resting potential of neurons was first devised by Walther Nernst (Stock and Orna, 1989). Later, Goldman (1943) mathematically described how ionic current will behave when the current is not equal to the resting potential. Crucially these dynamics must be understood to model neurons that capture realistic spiking behavior using detailed ion dynamics, such as Hodgkin-Huxley type neurons. However, neuroscientist have been interested in the different levels of abstraction at which one can model neurons and still approximate more realistic behavior (Herz et al., 2006). I consider here models that exist at the level of abstract ion dynamics, but detailed in the behavior of the membrane potential. This makes them more detailed than the type of dynamics used by the artificial neuron models described in chapter 1. This level of detail is well suited for studying very large populations of neurons, in excess of 100,000, where the individual timings of spikes play a role. Neurons with spiking dynamics are also used to study spike timing dependent plasticity (STDP) (Bi and Poo, 1998; Caporale and Dan, 2008), effects of spike related stochasticity (Amit and Brunel, 1997b), and neural coding (Gütig and Sompolinsky, 2006).

There are now a multitude of tools and packages to simulate spiking neuron networks under a number of strategies (Brette, Rudolph, et al., 2007). Spiking neural networks are usually simulated on a computer through one of two different approaches. The first is a time-driven simulation, which involves numerically integrating the ordinary differential equations which describe each neu-

ron using a standard method such the Euler or Runge-Kutta method. This approach is easy to implement, but suffers from errors introduced by numerical integration, and is computationally expensive in that every neuron in a network must be updated at every timestep. To correct for the error a small integration timestep must be chosen, resulting in a speed/accuracy trade off. Another more sophisticated approach is the event-driven method. Using this approach the network is updated in the following three steps: 1) analytically determine the time of the soonest spike in the network, 2) advances the network to that time value and analytically determines each neurons new potential at the new time step, 3) propagate the PSP from the neuron that just fired, and repeat. This approach results in faster simulations (Cessac and Viéville, 2008), and it depends on synaptic interaction terms being analytically tractable; however, approximations for conductance based synapses have been proposed (Rudolph and Destexhe, 2006). Stewart and Bair (2009) developed a promising new method for simulation based on the Parker-Sochacki method and presented results of increased speed/accuracy payoff. Modern graphics processing units, one can simulate a network of 55,000 spiking neurons at real time speeds (Nowotny, 2011), cluster based simulations of neuron networks have been preformed with almost half a billion synapses (Izhikevich and Edelman, 2008).

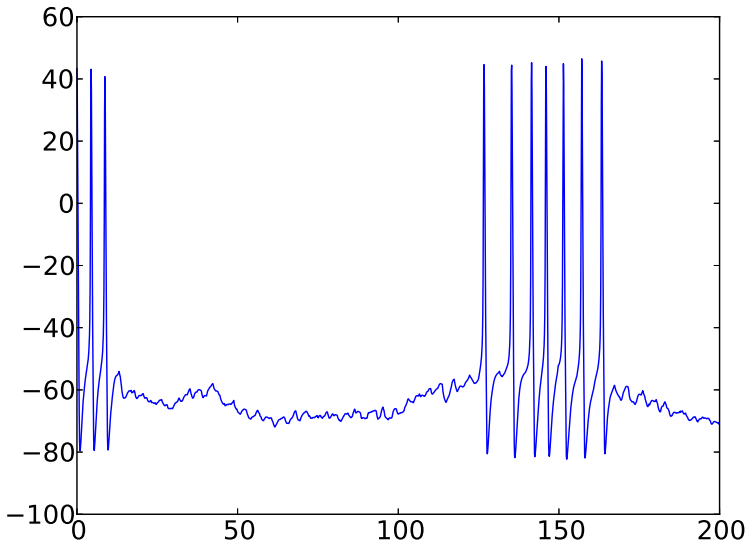

Figure 6: Simulation of Hodgkin-Huxley type neuron using exponential Euler integration. Single neuron recording taken from a 4000 neuron network of excitatory and inhibitory neurons. Parameters taken from (Brette, Rudolph, et al., 2007).

We can choose less detailed neuron models for their computational speed, and sometimes their greater analytical tractability. One such model is the leaky integrate and fire (IF) neuron model; it is an early point (non-spatial) neuron model, and it was first formulated by Lapicque in 1907 (Lapicque, 1907). Even though it is a simple model, it has endured many years and is still in use today

(L. F. Abbott, 1999; Brunel and Rossum, 2007). The simple dynamics used by this model is adequate only at describing the subthreshold behavior of a neuron's membrane potential, because the action potential is not explicitly modeled. Other extensions to the IF model exist, including the exponential IF model (Fourcaud-Trocmé et al., 2003), quadratic IF model (Brunel and Latham, 2003), adaptive exponential IF model (Brette and Gerstner, 2005), and resonate and fire model (Izhikevich, 2001). Given these other options, Izhikevich (2004) states that the leaky IF model is a poor choice when it comes to biological realism, because it lacks key features such "phasic spiking, bursting of any kind, rebound responses, threshold variability, bistability of attractors, or autonomous chaotic dynamics."

IF dynamics (Burkitt, 2006; Knight, 2000) describe the membrane potential of neurons. We can choose biologically realistic constants to obtain firing rates that are comparable to experimental measurements of actual neural activity. IF neurons integrate synaptic current into a membrane potential, and then fire when the membrane potential reaches a voltage threshold. The equation that governs the membrane potential of a neuron V_i is given by

$$C_m \frac{dV_i(t)}{dt} = -g_m(V_i(t) - V_L) - I_{syn}(t), \tag{13}$$

where C_m is the membrane capacitance, g_m is the leak conductance, V_L is the leak reversal potential, and I_{syn} is the total synaptic input. A spike is produced by a neuron when its membrane potential exceeds a threshold $V_{thr} = -50$ mV and its membrane potential is reset to a value $V_{reset} = -55$ mV. Neurons are held at V_{reset} for a refractory period τ_{rp} immediately following a spike.

Neurons in the brain do not receive constant input current. One of the early elaborations of the non-leaky IF model to account for stochastic input was given by G. L. Gerstein and Mandelbrot (1964), later extended by Stein (1965) to the leaky version of the model, and reviewed by Wilbur and Rinzel (1982). Here, the variation of a neuron's membrane potential away from equilibrium is governed by the stochastic set of presynaptic spikes that the neuron receives. In such a regime, we let the membrane receive synaptic input that be described by a Poisson process. Each event in the Poisson process corresponds to a presynaptic spike arriving at the neuron. On the arrival of a event the neuron receives a depolarizing "kick" to its membrane potential, as shown in Figure 7.

The stochastic input to a neuron is usually modeled as a set of delta functions that represent the shot noise of presynaptic input. IF neurons are one compartment models with presynaptic spiking having a direct effect on the membrane through a postsynaptic activation function. Burkitt (2006) outlines common synaptic types are used to represented the activation function *current synapses* or *conductance based synapses*. Current synapses provide a linear post synaptic potential (PSP) that does not depend on the membrane potential of the post synaptic neuron, while conductance based synapses provide a nonlinear PSP that depends on the difference between the membrane potential and its reversal potential. Typical models link a perceptual decision to the activity of a subpopulation of neurons (Braun and Mattia, 2010).

The Gaussian approximation of the membrane potential for an integrate and fire neuron a very useful mathematical formulation. This is because a sum of delta functions is very difficult to handle mathematically, even more so when

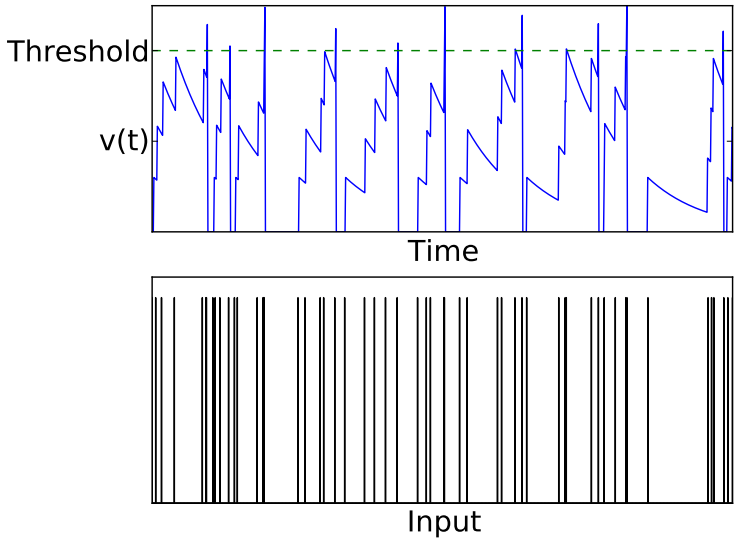

Figure 7: Effect of stochastic spiking input on a neuron's membrane potential. Top: A neuron's membrane potential is increased towards the firing threshold for every presynaptic spike it receives (bottom).

extended to population dynamics. The approximations has been described by Gerstner and Kistler (2002) and Burkitt and Clark (2000). In this model one ignores the firing threshold and instead considers the unrestricted path of the membrane potential. This notion can be extended to work out the firing rate of a neurons by calculating the moments of the input. Amit and Brunel (1997b) used Gaussian approximation to obtain steady state dynamics of spontaneous (low firing rate) neuron activity, which has paved the way for the majority of the work conducted in this thesis.

Another useful analytical tool for population dynamics is the Fokker-Plank formalism, which describes the distribution of membrane potentials across time (Brunel, 2000; Brunel and Hakim, 1999). This approach was shown to be flexible enough to be applied to conductance based synapses (Richardson, 2004). The model that forms the basis of this thesis has been extensively studied using the Fokker-Plank formalism. First work by Brunel, Sergi, et al. (1998) provided an expression for the frequency of the IF neuron. Later Brunel and X.-J. Wang (2001) described the activity of four populations of neurons by a system of four coupled nonlinear equations. A bifurcation analysis of the parameters describing the different populations yielded the bistable model which is described by the rest of this chapter.

2.1 AN INTEGRATE-AND-FIRE ATTRACTOR NEURONAL NETWORK MODEL OF DECISION-MAKING: METHODS USED THROUGHOUT THE THESIS

In this section I will present the methods used throughout the rest of the thesis. The probabilistic decision-making network I use throughout this thesis is in the mold of a spiking neuronal network model with a mean-field equivalent (X.-J. Wang, 2002). I set the network to operate with parameters determined by the mean-field analysis that ensure that the spontaneous firing rate state is stable even when the decision-cues are applied, so that it is only the noise that provokes a transition to a high firing rate attractor state, allowing the effects of the noise to be clearly measured (Deco and E. T. Rolls, 2006; E. T. Rolls and Deco, 2010).

What follows in this section is the description of the model. Its application to decision-making is first presented in chapter 3; however, I will mention a few aspects of biological function that this model does capture at the end of the section.

The fully connected network consists of separate populations of excitatory and inhibitory neurons as shown in Figure 8. Two sub-populations of the excitatory neurons are referred to as decision pools, 'D1' and 'D2'. The decision pools each encode a decision to one of the stimuli, and receive as decision-related inputs λ_1 and λ_2. The remaining excitatory neurons are called the 'non-Specific' neurons, and do not respond to the decision-making stimuli used, but do allow a given sparseness of the representation of the decision-attractors to be achieved. (These neurons might in the brain respond to different stimuli, decisions, or memories.) A description of the network follows.

The network consists of N neurons, with $N_E = 0.8N$ excitatory neurons, and $N_I = 0.2N$ inhibitory neurons. The two decision pools are equal size sub-populations with the proportion of the excitatory neurons in a decision pool, or the sparseness of the representation with binary encoding, $f = 0.1$. The neuron pools are non-overlapping, meaning that the neurons in each pool belong to one pool only.

We structure the network by establishing the strength of interactions between pools to take values that could occur through a process of associative long-term potentiation (LTP) and long-term depression (LTD). Neurons that respond to the same stimulus, or in other words ones that are in the same decision pool, will have stronger connections. The connection strength between neurons will be weaker if they respond to different stimuli. The synaptic weights are set effectively by the pre-synaptic and post-synaptic firing rate reflecting associative connectivity (E. T. Rolls, 2008). In the representation case neurons in the same decision pool are connected to each other with a strong average weight w_+, and are connected to neurons in the other excitatory pools with a weak average weight w_-. All other synaptic weights are set to unity. Using a mean-field analysis which applies to the firing rate distribution case (Deco and E. T. Rolls, 2006), we chose w_+ to be near 2.1, and w_- to be near 0.877 to achieve a stable spontaneous state (in the absence of noise) even when the decision cues

were being applied, and stable high firing rate decision states. In particular, $w_- = \frac{0.8-f_{S1}w_+}{0.8-f_{S1}}$ (Brunel and X.-J. Wang, 2001; Deco and E. T. Rolls, 2006; Loh, E. T. Rolls, and Deco, 2007a; X.-J. Wang, 2002).

The synaptic current is conductance based, and the flow of current into each neuron is described in terms of neurotransmitter components. The four families of receptors used are GABA, NMDA, $AMPA_{rec}$, and $AMPA_{ext}$. The neurotransmitters released from a presynaptic excitatory neuron act through $AMPA_{rec}$ and NMDA receptors, while inhibitory neurons activate ion channels through GABA receptors. Each neuron in the network has $C_{ext} = 800$ external synapses that deliver input information and background spontaneous firing from other parts of the brain to the $AMPA_{ext}$ synapses. Each neuron receives via each of these 800 synapses external inputs a spike train modeled by a Poisson process with rate 3.0 Hz, making the total external input 2,400 Hz per neuron.

The current at each synapse is produced by synaptically activated ion channels that alter their conductances with particular time constants and that depend on the membrane potential of the neuron and the reversal potential of the currents that pass through each ion channel. These currents are summed to describe the form of the PSPs at the neuron's cell body. AMPA is modeled as a fast receptor, and NMDA as a slow receptor. Synaptic current flowing into a neuron is given by the set of ordinary differential equations

$$I_{syn}(t) = I_{GABA}(t) + I_{NMDA}(t) + I_{AMPA,rec}(t) + I_{AMPA,ext}(t) \quad (14)$$

with currents described by

$$I_{AMPA,ext}(t) = g_{AMPA,ext}(V(t) - V_E) \sum_j^{C_{ext}} s_j^{AMPA,ext}(t) \quad (15)$$

$$I_{AMPA,rec}(t) = g_{AMPA,rec}(V(t) - V_E) \sum_j^{C_E} w_j s_j^{AMPA,rec}(t) \quad (16)$$

$$I_{NMDA,rec}(t) = \frac{g_{NMDA,rec}(V(t) - V_E)}{(1 + e^{-0.062V(t)})/3.57} \sum_j^{C_E} w_j s_j^{NMDA}(t) \quad (17)$$

$$I_{GABA,rec}(t) = g_{GABA}(V(t) - V_I) \sum_j^{C_I} s_j^{GABA}(t), \quad (18)$$

where V_E and V_I are reversal potentials for excitatory and inhibitory PSPs, the g terms represent synaptic conductances, s_j are the fractions of open synaptically activated ion channels at synapse j, and weights w_j represent the structure of the synaptic connections. The divisor in the NMDA current term, with two constants and voltage dependent term, are from the original definition of the model (Brunel and X.-J. Wang, 2001). The subscripts $_{ext}$ and $_{rec}$ signify whether the synaptic current is originating from the external input or from the recurrent connections.

Post-synaptic potentials are generated by the opening of channels triggered by the action potential of the presynaptic neuron. As mentioned above, the dy-

namics of these channels are described by the gating variables s_j. The dynamics of these variables are given by

$$\frac{ds_j^{AMPA}(t)}{dt} = -\frac{s_j^{AMPA}(t)}{\tau_{AMPA}} + \sum_k \delta(t - t_j^k)$$
$$\frac{ds_j^{NMDA}(t)}{dt} = -\frac{s_j^{NMDA}(t)}{\tau_{NMDA,decay}} + \alpha x_j(t)(1 - s_j^{NMDA}(t))$$
$$\frac{dx_j(t)}{dt} = -\frac{x_j(t)}{\tau_{NMDA,rise}} + \sum_k \delta(t - t_j^k)$$
$$\frac{ds_j^{GABA}(t)}{dt} = -\frac{s_j^{GABA}(t)}{\tau_{GABA}} + \sum_k \delta(t - t_j^k)$$

where the sums over k represent a sum over spikes formulated as δ-Peaks ($\delta(t)$) emitted by presynaptic neuron j at time t_j^k.

The constants used in the simulations are shown in Table 1.

Global constants		
$V_L = -70$ mV	$V_{thr} = -50$ mV	$V_{reset} = -55$ mV
$V_I = -70$ mV	$V_E = 0$ mV	$\alpha = 0.5\text{ms}^{-1}$
Inhibitory neuron constants		
$C_m = 0.2$ nF	$g_m = 20$ nS	$\tau_{rp} = 1$ ms
$\tau_m = 10$ ms	$g_{AMPA,ext} = 1.62$ nS	$g_{AMPA,rec} = 0.162$ nS
$g_{NMDA} = 0.516$ nS	$g_{GABA} = 1.946$ nS	$\tau_{AMPA} = 2$ ms
$\tau_{NMDA,decay} = 100$ ms	$\tau_{NMDA,rise} = 2$ ms	$\tau_{GABA} = 10$ ms
Excitatory neuron constants		
$C_m = 0.5$ nF	$g_m = 25$ nS	$\tau_{rp} = 2$ ms
$\tau_m = 20$ ms	$g_{AMPA,ext} = 2.08$ nS	$g_{AMPA,rec} = 0.208$ nS
$g_{NMDA} = 0.654$ nS	$g_{GABA} = 2.5$ nS	$\tau_{AMPA} = 2$ ms
$\tau_{NMDA,decay} = 100$ ms	$\tau_{NMDA,rise} = 2$ ms	$\tau_{GABA} = 10$ ms

Table 1: The default parameter set used in the integrate-and-fire simulations

The population sparseness a of a representation is the proportion of neurons active to represent any one stimulus or decision in the set. The sparseness can be generalized to non-binary representations as shown in Equation 19.

$$a = \frac{(\sum_i^{N_E} r_i)^2}{\sum_i^{N_E} r_i^2}, \tag{19}$$

where r_i is the firing rate, over a time period, measured for neuron i in the population of N_E excitatory neurons in the network (Franco et al., 2007; E. T. Rolls, 2008; E. T. Rolls and A. Treves, 1990; A. Treves and E. T. Rolls, 1991).

We note that this is the sparseness of the representation measured for any one stimulus over the population of excitatory neurons (Franco et al., 2007; E. T. Rolls, 2008). For the sparseness values shown in this thesis, the population sparseness on each trial was calculated using the time-averaged firing rate of all excitatory neurons, and then this population sparseness was averaged across trials.

The network was simulated numerically using a second order Runge-Kutta algorithm step with an integration step $dt = 0.02$ ms for a time period of 4 seconds. First there was a 2 s baseline period of spontaneous activity in which λ_i = 3.0 Hz for all external synapses onto every neuron in pool i, where the pools were inhibitory, decision-making pool 1, decision-making pool 2, and the non-specific excitatory pool. There was then a 2 s decision period in which the decision stimuli were applied by increasing the firing rates for the 800 external input synapses on each of the neurons in the two decision pools so that the mean of λ_1 and of $\lambda_2 = 3.04$ Hz per synapse (an extra 32 Hz per neuron, given the 800 external synapses onto each neuron). During the decision period, the noise in the network, and the increased firing rate bias applied as a decision cue to each decision pool of neurons, causes one of the decision populations of neurons to jump to a high firing rate attractor state with the assistance of the positive feedback in the recurrent collaterals, and this high firing inhibits through the inhibitory interneurons the other decision population of neurons. There is thus a single winning population on each trial, and which of the two populations wins on a particular trial is determined by the statistical fluctuations in the firing rates of the neurons in each decision population, and the difference in the two inputs λ_1 and λ_2, i.e. $\Delta\lambda$. In the simulations I describe, unless otherwise stated, $\Delta\lambda^{syn} = 0.008$ Hz per synapse. This corresponds to a firing rate of 3.044 Hz per synapse being applied as λ_1 and 3.036 Hz per synapse being applied as λ_2 as the external inputs to the two decision-making spools during the decision-making period. I refer to the quantity $\Delta\lambda$ to be the sum of this value over a neuron's 800 synapses, $\Delta\lambda = 800\Delta\lambda_i^{syn} = 6.4$ Hz for the default case.

The differences in firing rates (3.044 Hz and 3.036 Hz) of individual presynaptic neurons does seem very small. However, another way to look at this situation is through a method suggested by X.-J. Wang (2002) in his definition of a similar model. In our model $\lambda_i = 3.0$ Hz is the baseline per synapse input to each neuron, which can be thought of as a non-preferential input, because we are just on the edge of the decision boundary. This leaves $\lambda_1^{cue} = 0.044$ Hz and $\lambda_2^{cue} = 0.036$ Hz as the two signal inputs to each pool (possibly from preferential MT neurons). By using Wang's formulation for motion strength, c', we compared the relative strength of the two signals. In our case $c' = (\lambda_1^{cue} - \lambda_2^{cue})/(\lambda_1^{cue} + \lambda_2^{cue}) = 10.0\%$, which is a very plausible value to be making a decision at.

To obtain an Weber fraction (Deco and E. T. Rolls, 2006) for these quantities, we take the ratio of $\Delta\lambda$ over the average input to each neuron, $\Delta\lambda/(\frac{\lambda_1+\lambda_2}{2}800)$, where λ_i is the external input per synapse to a neuron in pool i, and there are 800 synapses per neuron. With $\Delta\lambda = 6.4$ Hz, the Weber fraction, $= 6.4/2432 = 0.0027$.

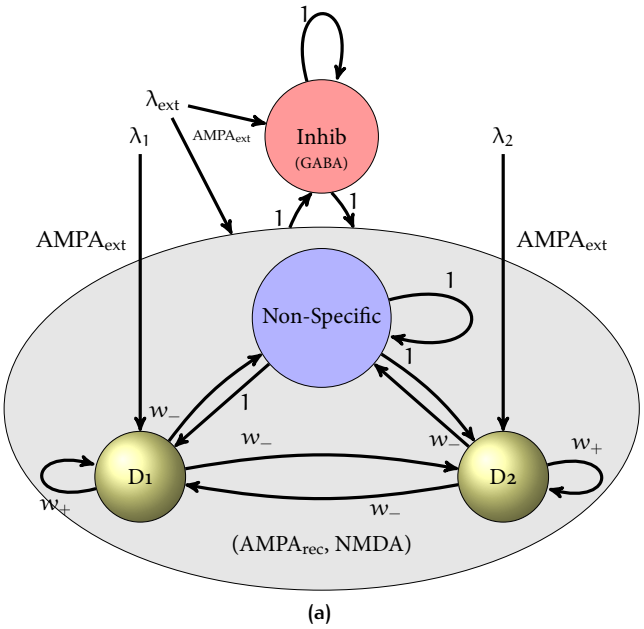

(a)

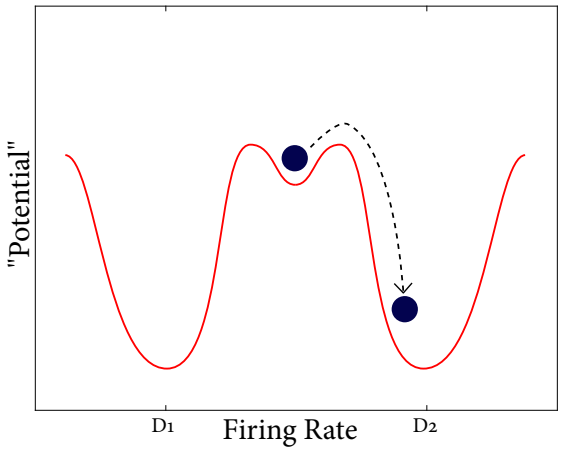

(b)

Figure 8: (a) The architecture of the probabilistic decision-making spiking neural network. The single attractor network has pools, "D1" and "D2", of excitatory neurons which encode the decision response. One of these pools becomes active when a decision is made. The remaining population of excitatory neurons are "non-specific", and there is also a population of inhibitory neurons. Pools D1 and D2 receive decisions cues λ_1 and λ_2 which reflects an external stimulus. All neuron are driven by Poisson set of input spikes λ_{ext} representing activity from other neurons in the brain. Stochastic fluctuations in the network mean that the attractor to which the system settles is determined by (b) a multistable 'effective energy landscape' for decision-making with stable states shown as low 'potential' basins. Before cues are applied to the network, the spontaneous firing rate state is stable (there is not enough 'energy' to overcome the peak barrier). When cues are applied, the additional input provokes a stochastic transition from the low firing rate spontaneous state S into the high firing rate decision attractor state D1 or D2. The greater the decision cues are, the easier it will be for the system to climb the energy barrier. Thus, the reaction time of the system will be shorter for stronger cues. An difference between λ_1 and λ_2 will skew the landscape, making one decision more likely than the other.

This model captures some key biologically features of decision-making, described in section 1.1, that occurs in the process of choosing between two or more alternate choices. In order to arrive at a decision the brain often has to combine information from sensory systems and other sources of information in the brain. When tasked with a decision the brain accumulates sensory evidence over time. This is supported experimentally by studies that show an increase in the firing rates of neurons in the lateral intraparietal area that correlates with an animal's performance in a two input decision task (Schall, 2003; M. Shadlen, K. Britten, et al., 1996; M. Shadlen and W. Newsome, 2001). The evidence here suggests that decision-making that occurs in the face of uncertain input is probabilistic and is governed by the relative strengths of the two inputs (X.-J. Wang, 2008). Further experimental evidence shows that, in subjects given a two alternative forced-choice task, there is a speed-accuracy tradeoff that occurs in the decision-making areas of the brain(Bogacz, Wagenmakers, et al., 2010).

The reasons for using this particular integrate-and-fire spiking attractor network model are that this is an established model with a mean-field equivalent allowing mathematical analysis; that many studies of short-term memory, decision-making and attention have been performed with this model which captures many aspects of experimental data (in a number of cases because, for example, NMDA receptors are included); and that it captures many aspects of cortical dynamics well (Brunel and X.-J. Wang, 2001; Buehlmann and Deco, 2008; Deco and E. T. Rolls, 2005, 2006; Loh, E. T. Rolls, and Deco, 2007a; E. T. Rolls and Deco, 2010; E. T. Rolls, Grabenhorst, and Deco, 2010a,b; E. T. Rolls, Loh, and Deco, 2008; Smerieri, E. T. Rolls, and Feng, 2010; X.-J. Wang, 2002, 2008).

In the absence of a decision state, neurons in the brain show a spontaneous pre-cue state with Poisson-like firing statistics (Compte et al., 2003). The action potentials are generated in a way in which the spikes for a given mean firing rate occur at times that are essentially random (apart from a small effect of the refractory period), with a coefficient of variation of the interspike interval distribution (CV) near 1.0 (E. T. Rolls and Deco, 2010; Softky and Koch, 1993). The sources of the noise include quantal transmitter release, and noise in ion channel openings (Faisal, Selen, and Wolpert, 2008). The membrane potential is often held close to the firing threshold, and then small changes in the inputs and the noise in the neuronal operations cause spikes to be emitted at almost random times for a given mean firing rate. Spiking neuronal networks with balanced inhibition and excitation currents and associatively modified recurrent synaptic connections can be shown to possess a stable attractor state where neuron spiking is approximately Poisson too (Amit and Brunel, 1997a; Miller and X.-J. Wang, 2006). The noise caused by the variability of individual neuron spiking which then affects other neurons in the network can play an important role in the function of such recurrent attractor networks, by causing for example an otherwise stable network to jump into a decision state (Deco and E. T. Rolls, 2006; E. T. Rolls and Deco, 2010).

If such an attractor network is provided with two or more inputs, as illustrated in Figure 8a and b, each biasing an attractor, then this forms a biased competition model of decision-making in which a high firing rate of one of the possible attractor states represents a decision (Deco and E. T. Rolls, 2006; X.-J. Wang, 2002, 2008). The noise in the operation of the system makes the decision-making process non-deterministic, with the system choosing one of

the attractor states with a probability that depends on the relative strengths of the different input biases λ_1, λ_2 (Deco and E. T. Rolls, 2006; X.-J. Wang, 2002). The randomness or stochasticity in the operation of the system can be advantageous, not only by providing a basis for probabilistic decision-making in which each decision will be sampled in a way that depends on the relative strengths of the inputs, but also in memory recall which by being probabilistic allows different memories to be recalled from occasion to occasion, helping with creative thought processes. The theory of stochastic resonance (Benzi, Sutera, and Vulpiani, 1999; Gammaitoni et al., 1998) explains that some particular dynamical systems with external periodic forces will perform better in the presence of noise, and it has subsequently been applied to neural systems (McDonnell and D. Abbott, 2009; E. T. Rolls and Deco, 2010), perhaps in too broad of a context. McDonnell and Ward (2011) coins a new term, 'stochastic facilitation', in which noise and signal are less specified than in stochastic resonance theory, which acknowledges the very important role of noise in biological systems, without disturbing the original framework created by Benzi. The role of noise is still an open question, but, as I have said above, noise grants some performance advantages.

Noise provides a basis for probabilistic decision-making in which each decision will be sampled in a way that depends on the relative strengths of the inputs. It is adaptive in memory recall which by being probabilistic allows different memories to be recalled from occasion to occasion, helping with creative thought processes. The stochasticity is also useful in signal detection which can become more sensitive than a fixed threshold system in the process known as stochastic resonance (E. T. Rolls and Deco, 2010). I note that the less neurophysiologically detailed DDMs of decision-making involve linear accumulation of noisy inputs until some threshold is reached (J. Palmer, Huk, and M. N. Shadlen, 2005; Ratcliff and McKoon, 2008; Smith and Ratcliff, 2004; Usher and McClelland, 2001). Both DDMs and spiking neuron models of decision-making can account for the same experimental evidence, and it has been found that the Wang's 2002 model is a special case of the Usher-McClelland 2001 model (Bogacz, Wagenmakers, et al., 2010). These and other models can describe decision time distributions and related phenomena (Bogacz, Wagenmakers, et al., 2010; Braun and Mattia, 2010; Bressloff, 2010; R. H. Carpenter, Reddi, and Anderson, 2009; Gigante et al., 2009; Miller, 2006; Ratcliff, Zandt, and McKoon, 1999; Sakai, Okamoto, and Fukai, 2006; Wong and Huk, 2008; Wong and X. Wang, 2006) and some aspects of experimentally investigated decision-making (J. M. Beck et al., 2008; Ditterich, 2006; Miller and Katz, 2010; Resulaj et al., 2009; Roitman and M. N. Shadlen, 2002; Wong, Huk, et al., 2007). This section 2.1, thus described the methods that apply to most of the simulations described in this thesis. Each chapter contains additional details as they are pertinent to the particular work of that chapter.

Part II

Main Results

3 NOISE IN ATTRACTOR NETWORKS IN THE BRAIN PRODUCED BY GRADED FIRING RATE REPRESENTATIONS

Many processes in the brain are influenced by the noise or variability of neuronal spike firing (Deco, E. Rolls, and Romo, 2009; Faisal, Selen, and Wolpert, 2008; E. T. Rolls and Deco, 2010).

For these advantageous stochastic processes to be realized in the brain, the amount of noise must be significant. One factor that affects the amount of noise is the number of neurons in the fully connected network. As the number of neurons approaches infinity, the noise term of the recurrent synaptic input decreases to zero, and the mathematically convenient mean-field approximation holds, allowing many properties of the system to be calculated analytically (Brunel and X.-J. Wang, 2001; Deco and E. T. Rolls, 2006; E. T. Rolls and Deco, 2010; X.-J. Wang, 2002). Using the integrate-and-fire attractor network described in section 2.1, it has been shown that the stochastic fluctuations in a finite-sized system are still a significant influence to produce probabilistic decision-making with networks with 4096 neurons and 4096 synapses per neuron (Deco and E. T. Rolls, 2006). This is biologically relevant in that neocortical neurons are likely to have in this order 4,000–9,000 of recurrent collateral excitatory connections from other pyramidal cells (Abeles, 1991; Braitenberg and Schütz, 1991; Elston et al., 2006; E. T. Rolls, 2008).

Another factor that may influence the noise is the distribution of the firing rates of the population of neurons. In most analyses of integrate-and-fire attractor neuronal networks, a binary distribution of the firing rates of the neuronal populations is used, partly because this is consistent with the mean-field approximation that allows analytic calculation (Brody, Romo, and Kepecs, 2003; Brunel and X.-J. Wang, 2001; Deco and E. T. Rolls, 2006; E. T. Rolls and Deco, 2010; X.-J. Wang, 2002), and partly because the code is simpler and more efficient. With a binary distribution, a proportion of the neurons has the same high rate, and the remainder have a low rate. The sparseness of the representation can then be defined as the proportion of neurons with a high rate, that is, the proportion of the neurons in any one of the attractors stored in the network (E. T. Rolls, 2008; E. T. Rolls and A. Treves, 1998; A. Treves and E. T. Rolls, 1991). However, representations in the brain are not binary, with one or a number of neurons with the same high firing rate for any one stimulus, and the remainder of the neurons with a low spontaneous rate of firing. Instead representations provided by populations of neurons in the brain are often graded with firing rates in which for each stimulus or event a few neurons fire fast, and more and

more neurons fire with lower rates (E. T. Rolls, 2008). This has been found for representations of visual stimuli in the inferior temporal visual cortex (Baddeley et al., 1997; E. T. Rolls and M. J. Tovee, 1995; E. T. Rolls, A. Treves, M. Tovee, et al., 1997) and the primary visual cortex (Baddeley et al., 1997); of olfactory stimuli in the orbitofrontal cortex (E. T. Rolls, H. D. Critchley, and A. Treves, 1996); of taste and oral texture stimuli in the primary taste cortex (Verhagen, Kadohisa, and E. T. Rolls, 2004), orbitofrontal cortex (E. T. Rolls, H. Critchley, et al., 2010; E. T. Rolls, Verhagen, and Kadohisa, 2003) and amygdala (Kadohisa, E. T. Rolls, and Verhagen, 2005a,b); and of spatial view in the primate hippocampus (E. T. Rolls, A. Treves, Robertson, et al., 1998). The firing rate probability distribution of each neuron to a set of stimuli is often exponential (or gamma if there is higher spontaneous activity) (Baddeley et al., 1997; Franco et al., 2007; S. Treves A. P. et al., 1999), as shown in (b). Across a population of neurons, the probability distribution of the firing rates for any one stimulus is also close to exponential (Franco et al., 2007; S. Treves A. P. et al., 1999). The graded nature of the firing rates of a population of inferior temporal neurons to one stimulus from a set of 20 stimuli is illustrated in (a) (Franco et al., 2007; E. T. Rolls, 2008).

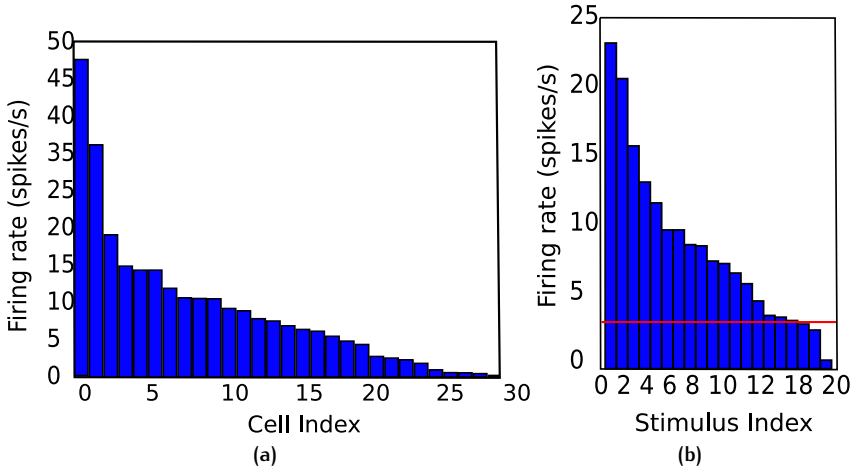

Figure 9: Neuron recordings from primates show selectivity that results in graded firing rates. (a) The firing rates of a population of inferior temporal cortex neurons to one stimulus from a set of 20 face and non-face stimuli. (b) Firing rate of a inferior temporal neuron to 20 different stimuli. The horizontal line indicates the spontaneuos firing rate of the neuron. Figures adapted from Franco et al. (2007).

The important question that then arises is how the noise present in a graded population firing rate representation, as frequently found in the brain, compares with the binary firing rate representations. In this chapter we investigate this by developing new integrate-and-fire simulations of neuronal networks that allow graded, close to exponential as found in the brain, representations to be used, and then measuring the time taken to reach a decision, which measures the noise-influenced escape time from the spontaneous state, as illustrated in Figure 8b (E. T. Rolls and Deco, 2010). We perform this investigation in a system in which the spontaneous state, even when the decision cues are being applied, is

stable, so that it is only noise that provokes an escape from the spontaneous state to a high firing rate attractor state. We are careful to control the sparseness of the graded representation, to allow direct comparison with the binary representation. We show that there is more noise with graded as compared with binary representations, draw out the implications for understanding noise, decision-making, and related phenomena in the brain. The implications include the fact that, given that graded representations are more noisy than binary representations, spiking-related stochastic dynamics will continue to be a principle of brain function that makes a contribution even up to realistically large neuronal networks as found in the brain, with in the order of thousands of recurrent collateral synapses onto each neuron (E. T. Rolls and Deco, 2010).

3.1 METHODS

For the results presented in this chapter we made use of the simulation framework presented in section 2.1. In our initial simulations, the network contained $N = 500$ neurons, with $N_E = 0.8N$ excitatory neurons, and $N_I = 0.2N$ inhibitory neurons. The two decision pools are equal size sub-populations with the proportion of the excitatory neurons in a decision pool, or the sparseness of the representation with binary encoding, $f = 0.1$, resulting in the number of neurons in a decision pool $N_E f = 40$.

3.1.1 Graded weight patterns

In an attractor network, the synaptic weights of the recurrent connections are set by an associative (or Hebbian) synaptic modification rule. This learning is assumed to take place outside of our simulation, and is a simple justification for choosing an initial value of recurrent weight strength which forms the attractor architecture. To achieve this for the firing rate distributions investigated, we imposed binary and graded firing rates on the network by selecting the distribution of the recurrent synaptic weights in each of the two decision pools. To achieve a binary firing pattern all the weights within a decision pool were set uniformly to the same value w_+ .

Graded firing patterns were achieved by inverse transform sampling (Devroye, 1986) for a random variable, representing the desired firing rate of a neuron, that obeys a cumulative distribution function using methods taken from E. T. Rolls, Treves, Foster, and Perez-Vicente (1997a).

This CDF function takes the form,

$$P(X \leqslant r) = \begin{cases} 1 - \frac{4}{3}a\lambda e^{-2r_i} & \text{for } r_i \in R, i > 0 \\ 1 - \sum\limits_{r_i \in R : i \neq 0}^{N} P(X \leqslant r_i) & \text{for } r_0 \in R \end{cases} \tag{20}$$

where, $R = \{r_0, r_1 \ldots, r_N\}$ is a discrete set of possible firing rates for a neuron with the first element $r_0 = 0$, a is the sparseness of the pattern defined in Equation 19, N is the number of discrete firing rates, i.e. the pattern depth or the number of elements in R, and X is a random variable over the sample space

R. The result of evaluating Equation 20, first the top part and then the bottom part which is dependent on the top, is shown in Figure 10b.

In simulations we use $a = 0.1$ to correspond to the fraction of excitatory neurons that are in a single decision pool.

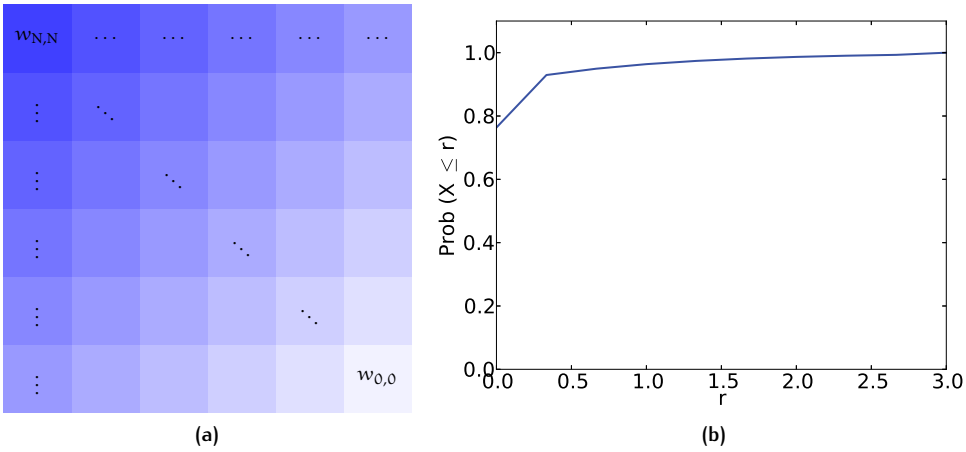

Figure 10: (b)Visualization of how the graded weight matrix could appear with 5 discretized firing levels. Darker colours correspond to stronger weights. Scale is for illustration purposes only, and the distribution was nonlinear in the actual simulations. (b) The CDF used to sample firing rates, from Equation 20, parameterized in accord with our simulations.

We chose 10 equal-spaced discretized levels to evaluate the distribution ($R = \{0, \frac{1}{3} - r_*, \frac{2}{3} - r_*, \ldots, 3 - r_*\}$). r_* and λ are chosen so that first and second moments of the firing rate distribution are equal to the sparseness, i.e. $< r > = < r^2 > = a$; $\lambda \approx 0.738$, $r_* \approx 0.0002$.

All neurons in a decision pool receive the same input in all simulations, so their firing rates were set to be higher and lower from each other by setting different recurrent synaptic weight strengths. A weight matrix $W = \{w_{1,1}, \ldots, w_{1,fN_E}, w_{2,1}, \ldots, w_{fN_E,fN_E}\}$ was constructed by first sampling a desired firing rate for each neuron, r_i^n, where i is the neuron number in this case, using Equation 20 and a uniformly distributed random number, u, in the range $[0, 1)$. Upon sampling u using a pseudo-random number generator on the computer, r_i^n was selected to equal r such that $P(X \leqslant r) = u$. After determining a firing rate for each neuron using this method, each element in the weight matrix was set such that $w_{ij} = \nu_{shift} + \nu_{spread}(\frac{r_i^n + r_j^n}{2} w_+)$. ν_{shift} and ν_{spread} are two free parameters used to fine control the firing activity of the network. This method produced a weight matrix similar to the one illustrated in Figure 10.

3.2 RESULTS

The operation of the system is illustrated for a single trial in Figure 11 which shows that for both the binary case and the graded case the neurons in the winning pool have an average firing rate greater than 25 Hz.

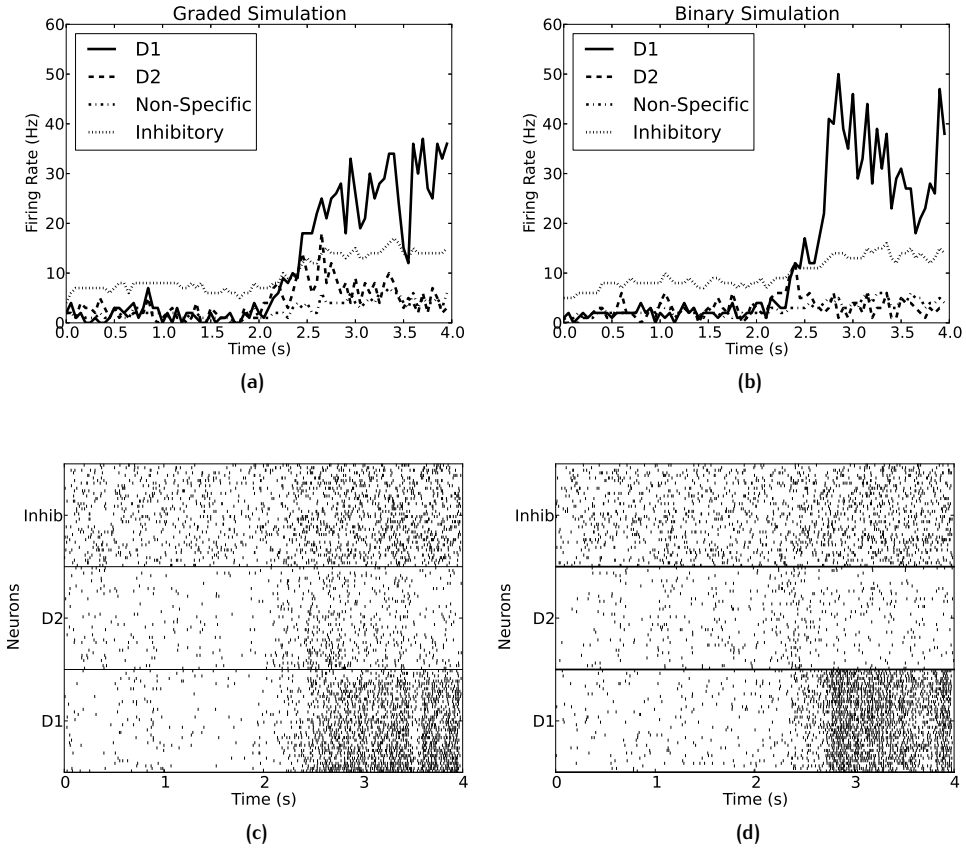

Figure 11: Example of the average firing rates for the different pools on a single trial for (a) the graded firing rate simulations and (b) the binary firing rate simulations. (c) and (d): the rastergrams for the corresponding trial, with each row of the rastergram providing the spike times for one of 40 neurons in each pool. In the case of the graded simulation, the neurons with the higher firing rates are plotted in the lower rows for each population of neurons.

3.2.1 Firing rate distribution

Figure 12a and b shows for the graded (a) and binary (b) simulations the firing rates achieved by the weight matrix we selected. The firing rates were measured in the last 1 s of the simulation $t = 3$–4s. The distribution of firing rates for the binary case has low variance, with nearly identical mean firing rates for each of the individual neurons in the winning pool. In contrast, the graded simulations show more variation in the distribution, which has an exponential-like shape.

The exponential-like shape occurs in both the spontaneous and decision states, but is more pronounced in the decision state. The parameters were set to achieve this set of graded firing rates, rather than a perfectly exponential distribution, because we wished to ensure that the mean firing rate and sparseness of the representation were similar in the binary and graded cases, while at the same time having clearly graded firing rates for the graded simulations so that the effects of graded vs binary firing rate distributions could be measured under conditions where the mean rate, and the sparseness, were essentially identical.

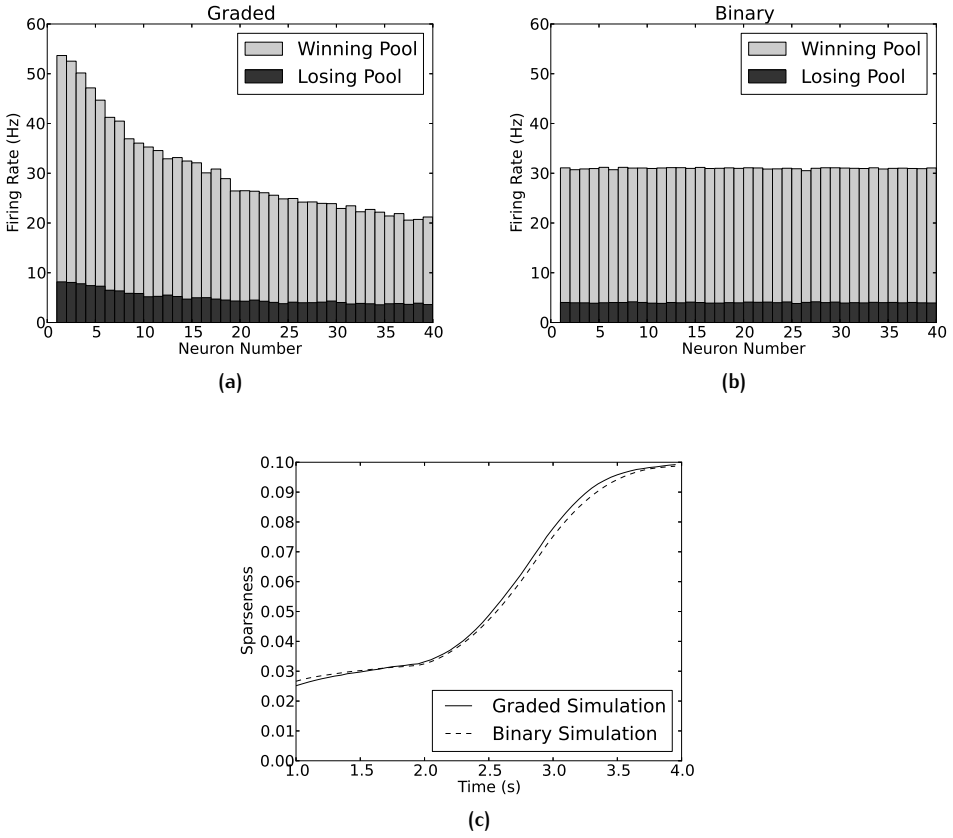

Figure 12: The mean firing rate of individual neurons in the winning and losing pools across 1000 simulation trials measured from the final 1 s of the simulation for the graded case (a) and the binary case (b). Neurons are sorted in descending order of the firing rate r_i. (c) The sparseness of the representation calculated using Equation 19 across all 400 excitatory neurons in 50 ms temporal windows. The sparsenesses were very similar for the binary and graded cases.

Further evidence on the nature of the graded and binary firing rate representations that were obtained is provided in the firing rate probability distributions shown in Figure 13. These are shown for the winning pool measured from the final 1s of the simulations for the graded case Figure 13a and binary case b. The mean firing rates for the graded case (a) were 30.3 spikes/s and for the binary case were 31.0 spikes/s, showing that the parameters for the recurrent weights

had been selected to make the firing rates very similar in these two cases. This was an aim, as higher firing rates can reflect increased excitation in the network which could decrease decision times. However, as was an aim, the standard deviation of the firing rate probability distribution was higher for the graded case (10.7 Hz) than for the binary case (4.9 Hz).

As the sparseness of the representation might influence the noise in the network and the measured decision time (with sparse representations with small values of a expected to be more noisy), we were careful to ensure that the sparseness of the representation for the binary and graded cases were similar. (They were set by the choice of the recurrent synaptic weights in the two decision populations, which is the distribution that produced the graded firing rates.) The sparseness measured using Equation 19 from both sets of simulations was similar, as shown in Figure 12c. The sparseness values were averaged over 1000 simulation trials, and were calculated with time windows of 50 ms. The increase of sparseness from the time at which the decision cues were applied ($t = 2$ s) reflects the fact that one of the decision pools became active after this time. The final steady state value with one of the pools in its winning attractor state is close to the theoretical value of 0.1, due to there being 40 neurons in each decision pool in a population of 400 excitatory neurons.

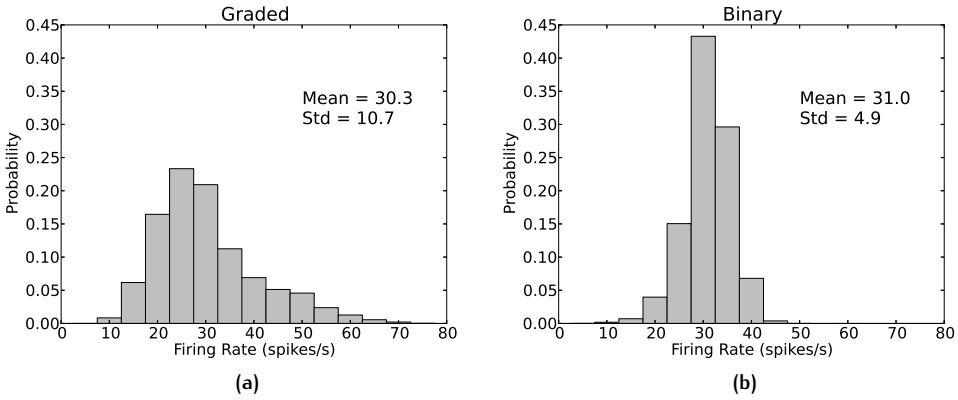

Figure 13: Firing rate probability distributions of the winning pool measured from the final 1 s of the simulations for the graded case (a) and binary case (b).

3.2.2 Decision time

An important measure of the noise in the system is the escape time of the system after the decision cues are applied from the spontaneous state to a decision state. Increased noise will decrease the escape time, and thus the decision or reaction time, as illustrated in Figure 8b. $\Delta\lambda$ was 0 for these simulations.

To address the amount of noise in the system with graded vs binary firing rate representations, we show in Figure 14 the decision times of the network with graded (a) and binary (b) representations. The decision (or reaction) time was measured by the time it took from the time at which the decision cues were applied ($t = 2$ s) when the network was in the spontaneous firing rate baseline

state for one of the decision pools to fire 25 Hz higher than the other one for 150 ms. The important result is that the graded firing patterns produce significantly ($p < 0.0001$) faster reaction times ($\approx$ 90 ms), than binary patterns (Figure 14a and b). The mean reaction time was 882 ms for the binary firing rate representations, and 791 ms for the graded representations. Further analysis showed that these decision times became significantly shorter ($p < 0.05$) for the graded compared to the binary representation with on average 541 trials.

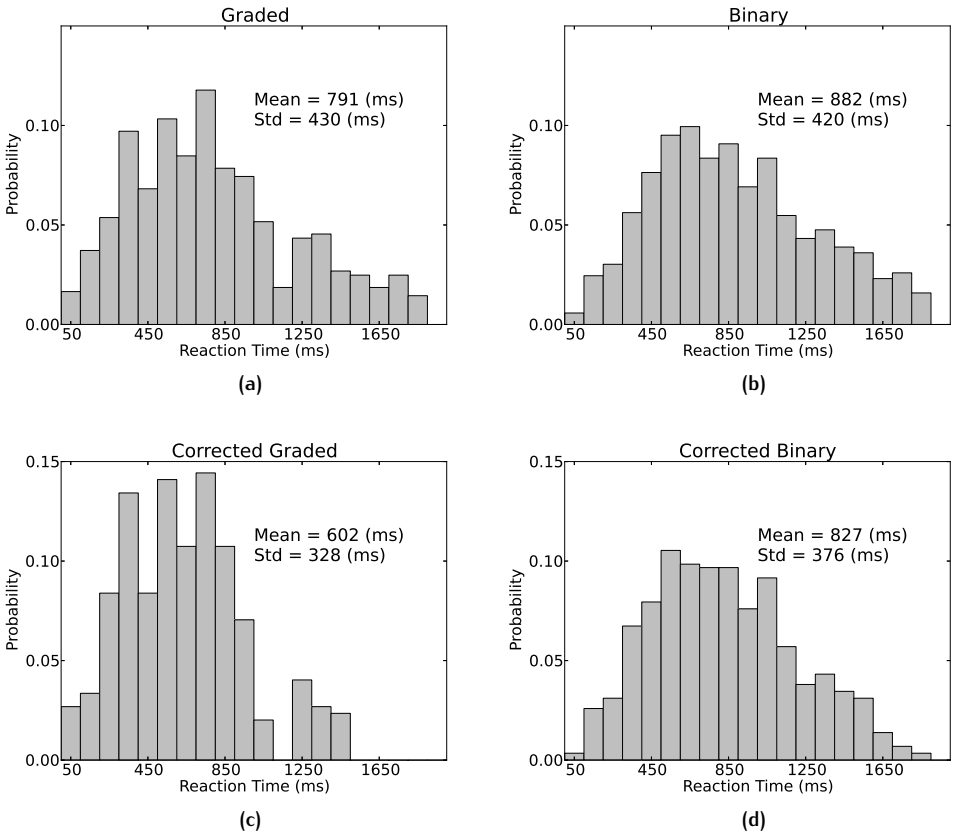

Figure 14: Histograms of reaction times for 1000 graded (a) and binary (b) firing rate distribution simulations. The criterion for a reaction time was that the average firing rate of one decision pool should be 25 Hz higher than that of the other decision pool for three consecutive 50 ms periods. (c) and (d) show corrected reaction time distributions created by subtracting a firing rate distribution with no applied decision cues. $p < 0.0002$ for (a) vs (b), and for (c) vs (d) using Kolmogorov-Smirnoff tests, t-tests, and Mann-Whitney U tests of the two distributions.

The faster decision times for the graded firing rate distributions (Figure 14a,b) were found when the mean firing rates when in the attractor, and the sparseness of the representation, were carefully matched in the graded and binary simulations. We further showed that it was not a faster firing rate for the graded simulations that accounted for the faster reaction times for the graded firing rate distribution by performing a whole series of further simulations (each with

1000 trials) in which the parameters of the recurrent synaptic weights between the neurons in a decision pool were systematically varied to obtain reaction times for the graded and binary firing rate distribution cases that bracketed each other. It is clear (Figure 15a) that while increases of w_+ that increased the firing rates when in the winning attractor did decrease the mean reaction time of the decision-making process, for any given mean firing rate of the neurons in the winning attractor, the decision times were faster for the graded than for the binary firing rate distributions. The faster reaction times for the graded than for the binary firing rate distributions are statistically significant and robust across different firing rates of the winning pool (Figure 15a).

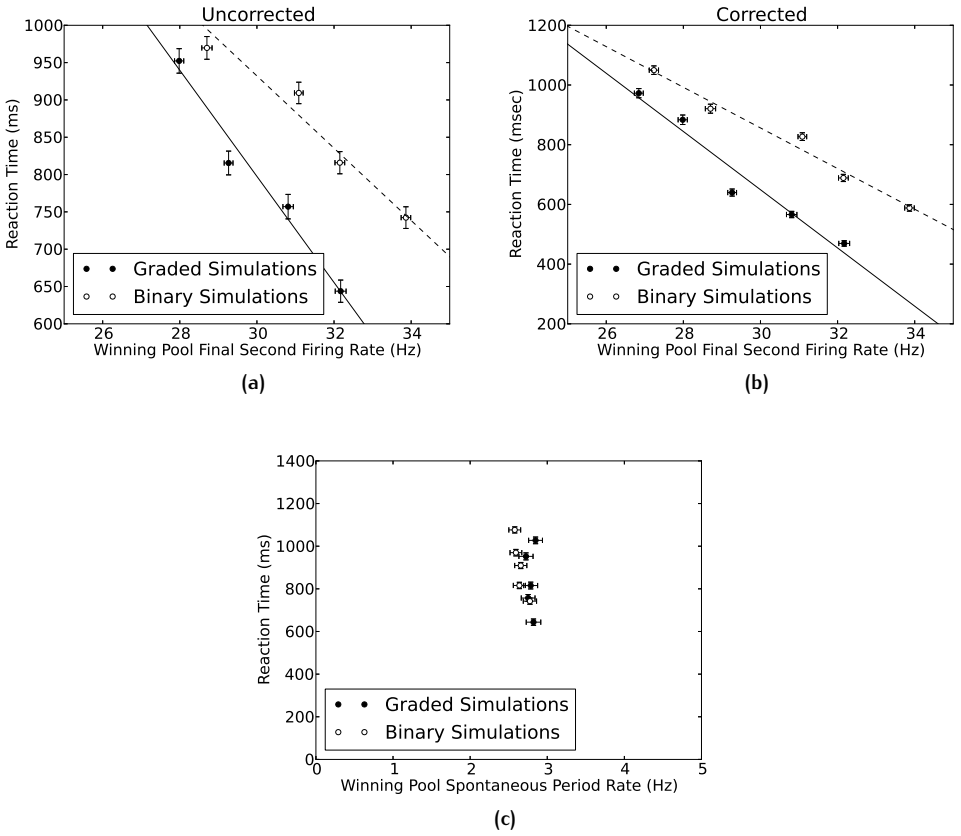

Figure 15: (a) Decision times of 1000 simulations for each point with a shifted w_+ parameter and thus different firing rates for the winning pool in the final second, for the graded and binary firing rate distribution cases. (a) The same as (b) except that distributions corrected for premature decisions were used (see text). The error bars signify the estimated standard error of the firing rate and reaction time. (c) The same plot as (a) except that the firing rate is measured during the spontaneous period.

Further evidence on this follows. The graded firing rate distribution simulations tended to have a higher firing rate for the winning pool when simulations were run across distributions with the same average synaptic weight between the neurons in a decision pool. We chose $\nu_{\text{shift}} = 2.078$ and $\nu_{\text{spread}} = 0.9$ to

find a winning firing rate and sparseness that were close for both distributions for the results illustrated in Figure 14a, and b. The average firing rates for these values of the parameters are shown in Figure 18. The similar firing rates for the winning pools during the spontaneous baseline and decision periods are shown.

As analyzed in subsection 3.2.4 simulations with graded compared to binary firing rate distributions showed an alteration in their stability when in the spontaneous firing rate state before the decision cues were applied. A contribution to the decreased reaction times could be that the graded simulations destabilized not due to the applied cues, but rather became unstable in the baseline spontaneous firing rate in the period before the decision cues were applied. For example, in 1000 trials we ran with a network size $N = 500$, on 149 trials the firing jumped into or towards a decision state early, by t=2 s, in the binary case. This has been described previously for similar parameters of the system (Loh, E. T. Rolls, and Deco, 2007a,b; E. T. Rolls, Loh, Deco, and Winterer, 2008). We excluded from the decision time analysis those trials that transited into or towards a decision state before the decision cues were applied at $t = 2$ s. The criterion was that trials were excluded if the mean rate of a decision pool exceeded 10 spikes/s in the half second before the decision cues were applied. What we did find in the present simulations was that with the graded firing rate simulations, there were more trials, 270, in which the spontaneous state was unstable, in that there was a noise-provoked transition into a decision state before the decision cues were applied at $t = 2$ s. To correct for this possible effect we subtracted a reaction time distribution without the application of decision cues from the distribution with decision cues. Simulations were repeated with the same parameters, except that no cues were applied. The distribution of the reaction times of these 'no cues' simulations was computed. The 'corrected distributions' were computed by subtracting the number of times the 'no cues' simulation reacted in a given period from the number of times the simulation reacted in the same period in the 'with cues' simulations. This provided a reaction time distribution that is corrected for the possibility of simulation trials jumping purely from the baseline spontaneous rate to a high firing rate state. When this correction is applied, we still observed that the reaction times are faster for the graded than for the binary firing rate distribution cases, as shown in Figure 14c,d and Figure 15b. However, caution should be used when interpreting the significance of these corrected distributions, as they just control against any strange destabilizing behavior. Our simulation results showed that they were mainly well behaved and flat with respect to time.

In summary, faster decision times are found with graded than with binary firing rate distributions, and this is not likely to be due to any increase in firing rate during the spontaneous period, nor is it due to faster firing rates during the decision-making period.

So far, the results presented have been for a network of size $N = 500$ neurons in the network. To investigate whether the decision times remain shorter for the graded than the binary firing rate distributions as the network becomes larger, an important issue as networks in the cerebral cortex typically have in the order of thousands of recurrent collateral synaptic connections onto each neuron (E. T. Rolls, 2008), we performed further simulations with larger N. Figure 17a shows that for each size of network up to $N = 4000$, the decision time is shorter for the graded than for the binary firing rate distribution cases. The performance in

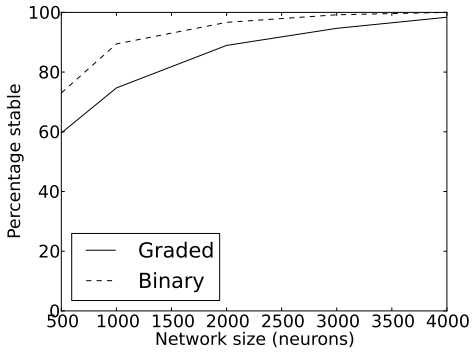

(a)

Figure 16: The percentage of trials on which the spontaneous state was stable for the graded and the binary firing rate distribution cases for networks of different size N, the total number of neurons in the network.

terms of the percentage correct was similar for the graded and binary cases for different network sizes, as shown in Figure 17b, so there is no penalty in terms of decision accuracy of the faster decision times found with networks with graded than with binary firing rate distributions. An important aspect of this result is that the larger networks are quite stable in the spontaneous period (as shown in Figure 16), and this is further evidence that instability of the spontaneous state is not crucial to the faster decision times of the networks with graded than with binary firing rate distributions. (For example, with $N = 4000$, 98% of the trials in the graded case were stable in the spontaneous period (and were excluded from the analysis), and we still found faster reaction times when the decision cues were applied for the graded firing rate distributions, as shown in Figure 17a.)

3.2.3 Performance during decision-making with $\Delta\lambda \neq 0$

So far we have shown results mainly for $\Delta\lambda = 0$, that is when the inputs during the decision-making period to D1 and D2 are equal. The performance of the network is close to the expected 50% correct, that is D1 wins on approximately 50% of the trials, and D2 on approximately 50% of the trials. However, the evidence for the two decisions is often not equal, and in this section we consider whether when running with $\Delta\lambda > 0$, different effects occur. For example, if the graded system is more excitable and responds faster than the binary system, there might be a speed-accuracy tradeoff of the type investigated for many decades in psychology (Beamish et al., 2006). It would be of interest if for example the graded system with its faster decision times was less accurate (in terms of percentage correct), though also interesting if it maintained its accuracy even when the reaction times were faster.

Figure 17a shows that for different sizes of network up to $N = 4000$, the decision time is shorter for the graded than for the binary firing rate distribution cases with $\Delta\lambda = 16$. The performance in terms of the percentage correct was

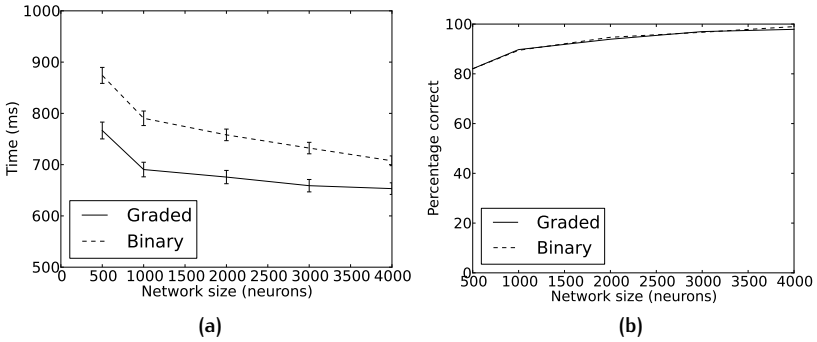

Figure 17: (a) Decision times of 500 simulations for networks of different size N, the number of neurons in the network, for the graded and binary firing rate distribution cases. The means and standard deviations are shown. (b) The percentage correct for networks of different size N, the number of neurons in the network, for the graded and binary firing rate distribution cases. $\Delta\lambda$ was 16 for these simulations.

similar for the graded and binary cases for different network sizes, as shown in Figure 17b, so there is no penalty in terms of decision accuracy of the faster decision times found with networks with graded than with binary firing rate distributions.

3.2.4 Stability of the spontaneous state

Noise and the positive feedback in this system can cause the network to jump into a decision state from the spontaneous state even before the decision cues are applied (at $t = 2$ s in our simulations). We analyzed the stability for the graded vs binary firing rate distribution cases by measuring the percentage of trials on which the binary and graded firing rate simulations transited into or towards a high firing rate decision state before the decision cues were applied at $t = 2$ s. The parameters for the binary simulation had been set with the mean-field analysis so that the mean spontaneous firing rate should be 3 spikes/s. The criterion for instability of the spontaneous state was that the mean rate of either decision pool exceeded 5 spikes/s in the 250 ms before the decision cues were applied. Figure 16 shows the percentage of trials on which the spontaneous state was stable for the graded and the binary firing rate distribution cases for networks of different size N, the total number of neurons in the network. As expected, the larger in terms of N the network becomes, the more stable the network becomes, as the finite size of the network becomes less of a factor. (In the mean-field case, or with an infinite number of neurons in the spiking simulations, the recurrent synaptic input noise effects would diminish to zero.) Figure 16 shows that the network with the graded firing rate distribution is for each value of N less stable in the spontaneous period than the network with the binary firing rate distribution.

This effect was not accounted for by any increase in the mean spontaneous firing rates of the decision pool neurons in the graded firing rate distribution

case, which remained at a mean value of approximately 3Hz as shown in Figure 18 (unless a noise-provoked transition occurred) because w_- was decreased to compensate for any increase in w_+ by using the procedure described previously (Brunel and X.-J. Wang, 2001; Deco and E. T. Rolls, 2006; Loh, E. T. Rolls, and Deco, 2007a; E. T. Rolls and Deco, 2010; X.-J. Wang, 2002). Indeed, the results in Figure 15c show that the firing rate during the spontaneous period does not respond to changes in the w_+ parameter because it is compensated for by changes in the w_- parameter. These results are consistent with the mean-field theory developed by (Brunel and X.-J. Wang, 2001), who set up a system in which changes in w_+ will only change the firing rates during the decision state, not during the spontaneous state. Moreover, the sparseness of the representation was the same for the graded and binary firing rate distribution cases.

The results on stability during the spontaneous state thus provide further evidence that the network with graded firing rate distributions is more noisy than the network with binary firing rate distributions for the decision pools, even when the mean rates and sparsenesses are the same.

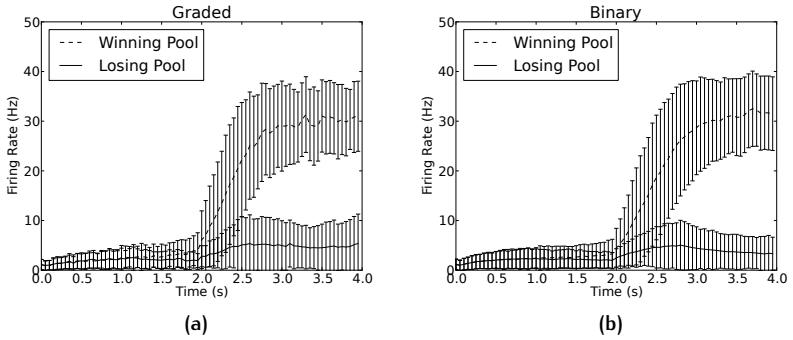

Figure 18: Mean firing rates over 1000 trials for the winning and losing pools in graded (a) and binary (b) firing rate distributions. The decision cues were turned on at $t = 2$ s. The error bars show the standard deviations. The winning pool is chosen to be the pool with average firing rate 10 Hz greater than the competing pool in the last 1 s of the simulation.

3.2.5 Noise in the system: the variance of the firing rates of the neurons

Another measure of the noise in the system is the variance of the firing rates of the neurons in a decision pool during decision-making. If some of the neurons in a pool have more variance, that pool may be more likely to cross a bifurcation from the spontaneous firing rate state and to enter a decision state without any decision cue, or to make a decision after the decision cues have been applied more rapidly (cf. Figure 8). Figure 19 shows the distribution for the 40 neurons in decision pool 1 of the variance across trials of the firing rate in the spontaneous period ($t = 1.5$–2 s) for a network of size $N = 500$ for the graded (a) and binary (b) cases. The variance is that for each neuron across trials of the firing rates measured in a 50 ms bin during the spontaneous period with > 550

trials with stable spontaneous firing rates using the criterion described above. The average variance for each neuron over 10 bins from t = 1.5–2.0 s is indicated. The variance distribution reaches higher values for some neurons with the graded than with the binary distribution, and this is just consistent with the approximately Poisson firing of the neurons (with which the variance = the mean), and the fact that the firing rate distribution shows some neurons with relatively high firing rates (up to 4 spikes/s) with the graded representation in the pre-cue period, as shown in Figure 19c and d. We emphasize that the mean firing rates and variances are very similar for the binary and graded cases: it is the distributions that are different, as shown in Figure 19. The concept here is that for the graded representation the subset of neurons with higher than average variance (and firing rates) contribute especially strongly to the noise (i.e. variation, fluctuation) in the system that promotes diffusion (Marti et al., 2008) across the barrier in the energy landscape (Figure 8), and that the effect of these neurons is helped by their stronger than average connection weights to other neurons within their decision pool, which enable statistical fluctuations in their rates to be felt especially strongly by the other neurons in the same decision attractor.

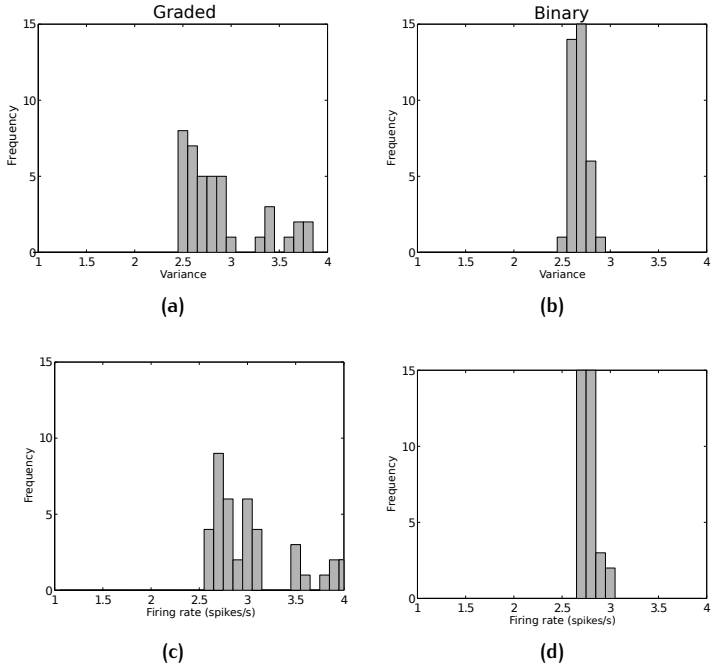

Figure 19: The distribution of the variance across trials of the firing rates in pool 1 during the spontaneous period (t = 1.5–2.0 s) for a network of size N = 500 for the graded (a) and binary (b) cases. The variance across trials of each neuron is that of the firing rates measured in 50 ms bins. The data was taken from the > 550 trials with stable spontaneous firing that passed the criterion described in the text. The average variance for each neuron over the 10 bins from t = 1.5–2.0 s is shown. Firing rate probability distributions for the spontaneous firing rate during the same period for the graded (c) and binary (d) cases.

3.2.6 Spectral analysis of decision pool power spectra

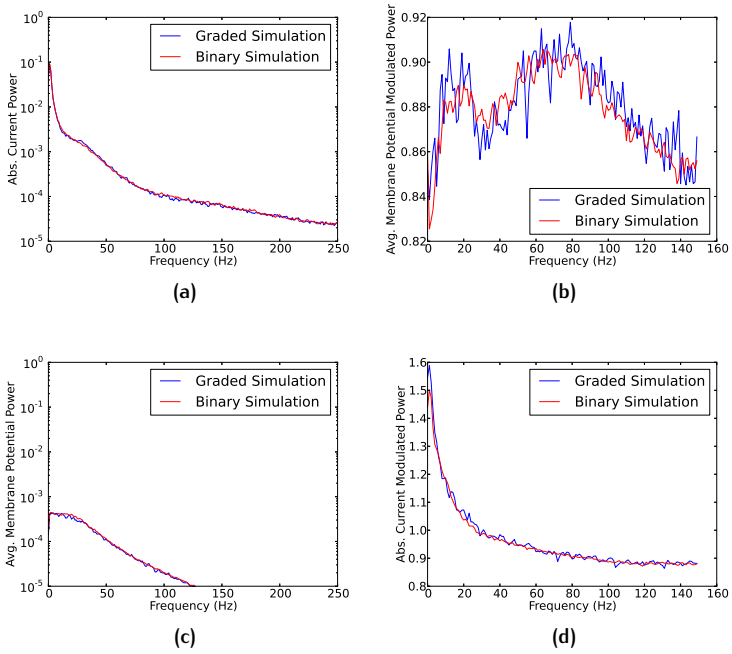

Figure 20: Power spectral densities and modulated power spectral densities for the winning pool. (a) PSD of the LFP averaged across trials of the decision period. (b) Modulated PSD, same as (a). (c) Decision period PSD averaged across trials of the average membrane potential in a pool. (d) Modulated PSD, same as (c).

We investigated the power spectra of the system to see if stronger oscillations of the Local Field Potential (LFP) and average membrane potential of the winning pool could contribute to decreased reaction times in graded simulations. Recent work have found that a spiking balanced neural network is able to generate LFPs similar to those obtained from the primary visual cortex (Mazzoni et al., 2008). In order to construct LFP recording we took the absolute sum of all of the synaptic currents to replicate the work of Mazzoni et al. (2008). In our case the additional presence of slow activating NMDA current reduced most activity in the gamma 60 Hz range. We took the data for each trial and high pass filtered it at 1 Hz with a 4th order digital butterworth filter. Multiple Slepian data tapers with a bandwidth of 4 Hz were applied. This approach has the advantage of eliminating bias in frequency domain for each trial, and allows for an average of the Power Spectral Densities (PSDs) over many trials. The measurement periods in the spontaneous period are 1,000–1,500 ms, and in the decision state period 3,500–4,000 ms. The results are shown in Figure 20.

Figure 20a shows that graded and binary PSD of the LFP during the decision period have similar means between the graded and binary case. The variability of the PSD is slightly higher in the graded case. The modulated PSD of LFP, which is how the PSD changes from spontaneous to stimulus period, is shown

in Figure 20b. Here the graded shows a higher response in low frequency bands, and the binary case has a greater response in the 30–50 Hz band. Overall, higher variability points to a greater level of noise in the system in the graded case.

In Figure 20c the decision period PSD of the membrane potential is plotted. As in the LFP case, the mean power is similar, with perhaps the binary case having more power in low frequency bands, and the graded case having greater variability. The modulated PSD of the membrane potential, Figure 20d shows that the graded case has a higher very low frequency response to the stimuli than the binary, along with greater variability.

3.2.7 Noise with graded representations in larger networks

As spiking attractor networks are increased in size, the statistical fluctuations caused by the close to Poisson spiking times of the neurons become smaller, until with an infinite number of neurons the noise term of the synaptic input becomes 0 (E. T. Rolls and Deco, 2010). It has been shown that in practice, measures of the noise such as the decision (escaping) time do decrease as the number of neurons is increased to 4,000, but that there is still noise due to the spiking fluctuations with this size of network, in which $C = N_E = 3{,}200$ (Deco and E. T. Rolls, 2006; E. T. Rolls, Grabenhorst, and Deco, 2010a,b). However, the number of connections C for the recurrent collateral synapses which provide for the attractor dynamics is in the order of 9,000 in the neocortex, and 12,000 in the CA3 neurons in the hippocampus (E. T. Rolls, 2008). To check that the findings in the present chapter apply in principle to these larger networks, we were able to perform further simulations with as many as 8,000 neurons in the network, which then had $N_E = 6{,}400$ excitatory neurons, and 6,400 recurrent collateral synapses onto each excitatory neuron.

We simulated scaled up networks with 8,000 neurons, and therefore 320 neurons in each specific decision population. With w_+ left at 2.1 as in the earlier simulations, the decision times were faster with the graded (mean 947 ms) than with the binary (mean 1,073 ms) firing rate distributions ($p < 10^{-7}$ with 320 trials). Thus graded firing rate distributions do introduce more noise into the system than binary firing rate distributions, even with large networks that are the same order as the size of networks found in the cerebral cortex. Further analysis showed that these decision times became significantly shorter ($p < 0.05$) for the graded compared to the binary representation with on average 21 trials.

With $w_+ = 2.1$ and 8,000 neurons, the spontaneous state was much more stable, and indeed there were no unstable trials in the spontaneous period for the graded and for the binary representations. To test whether the graded distribution was inherently more unstable in the spontaneous state even at this large size of network, we ran further simulations with 8,000 neurons, but with $w_+ = 2.25$ to promote more instability. This revealed more instability with the graded (only 87% stable) than with the binary firing rate representations (97% stable, $p < 0.02$).

3.3 DISCUSSION

In integrate-and-fire simulations of an attractor decision-making network, we have shown that the noise is greater for a graded than for a binary firing rate distribution of the populations of neurons. The noise effect was measured by faster escape times from the spontaneous firing rate state when the decision cues are applied, and this corresponds to faster decision or reaction times (Figure 14, Figure 15 and Figure 17).

The greater effect of the noise with the graded firing rate distributions was also measured as greater instability of the spontaneous firing rate state before any decision cues were applied (Figure 16), that is by more noise-provoked transitions from the spontaneous state which was shown to be a stable state in the mean-field analysis in which there is no noise. The conclusion is that spiking-related noise stochastic dynamics will continue to be a principle of cortical computation that influences processes such as decision-making, signal detection, short-term memory, and memory recall even with the quite large networks found in the cerebral cortex (E. T. Rolls and Deco, 2010), if the greater noise evident with graded firing rate distributions is taken into account.

These effects were found even when the firing rates and the sparseness of the representations were carefully equated across the graded and binary firing rate distribution conditions (e.g. Figure 15).

The results support the hypothesis that increased noise with the graded firing rate distributions is responsible for the decreased decision or reaction times. Conceptually, one can think that with graded firing rate distributions, a small number of neurons are made more important through their stronger weights and higher firing rates, noting that the variance of a Poisson process is equal to its mean. The influence of the few most highly firing neurons through their particularly strong synaptic weights on other neurons will have the effect of increasing the statistical fluctuations, which will be dominated by the relatively small number of highly firing neurons, and their possibly strong effects on a few other neurons with particularly strong synaptic weights from those highly firing neurons. Effectively the few strongly firing neurons in an attractor with their extra-strong couplings mean that a relatively few neurons dominate the statistical fluctuations, which are large because with the graded firing rate distributions a few neurons have extra high firing rates and extra-strong couplings to each other. In a sense, we can think of the graded firing rate distribution as providing a more sparse representation, with fewer neurons highly active when in a high firing rate attractor state, with the small number of highly active neurons promoting greater statistical fluctuations due to the finite size effect operating with smaller numbers. We note that in an attractor network, prototypical of the design of the neocortex and the hippocampal CA3 region (E. T. Rolls, 2008), in which the synaptic weights of the recurrent connections are set up by an associative (Hebbian) synaptic modification rule (e.g. Equation 10), graded firing rates will always be associated with graded recurrent synaptic weights, and so both can contribute to the effects produced on the noise in the network.

More formally, we can consider the currents injected into a neuron as consisting of a synaptically weighted sum of the input Poisson firing rate to each synapse. For a weighted sum of Poisson inputs, the contribution to the variance is more significant from the weight (proportional to its square) than from the

rate of the Poisson process (proportional to the value itself). Hence, for two input currents with identical mean, with one from the weighted summation of Poisson processes, and the other from the simple summation of Poisson processes, we should expect that the weighted sum in general would have a larger variance.

More precisely, let us consider two synaptic inputs I_1 and I_2

$$I_1(t) = \sum_{i=1}^{K} w_+ N_i(t),$$
$$I_2(t) = \sum_{i=1}^{K} w_i \bar{N}_i(t)$$

where K is the numbers of synapses, $N_i(t)$ in the binary case is a Poisson process with firing rate λ (a Poisson process counts the number of spikes after time t) and weight w_+, and in the graded case $\bar{N}_i(t)$ is another Poisson process with firing rate λ_i with weight w_i. The means of these two types of input are

$$EI_1(t) = Kw_+\lambda t \equiv EI_2(t) = \sum_{i}^{K} w_i\lambda_i t.$$

This yields

$$w_+\lambda = \frac{\sum_i^K w_i\lambda_i}{K}. \tag{21}$$

For simplicity, and it is the actual case in our simulations here, we further assume that $\lambda_i = aw_i, \lambda = aw_+$, where a is a positive scaling number. Hence (Equation 21) turns out to be

$$w_+ = \sqrt{\frac{\sum_i^K w_i^2}{K}}.$$

The variances of the two synaptic inputs are

$$var(I_1(t)) = Kw_+^2\lambda t;$$
$$var(I_2(t)) = \sum_{i}^{K} w_i^2\lambda_i t$$

respectively. We can seen that in general the second term above, $var(I_2(t))$, is larger than the first, $var(I_1(t))$, since

$$var(I_1(t)) = Kw_+^2\lambda t$$

$$
\begin{aligned}
&= tKa{w_+}^3 = tKa\left\{\frac{\sum_i^K w_i^2}{K}\right\}^{3/2} \\
&\leqslant tKa\frac{\sum_i^K (w_i^2)^{3/2}}{K} \\
&= tKa\frac{\sum_i^K w_i^3}{K} \\
&= tK\frac{\sum_i^K w_i^2 \lambda_i}{K} \\
&= var(I_2(t)). \qquad (22)
\end{aligned}
$$

The inequality above is due to Jensen's inequality which states that for any convex function ϕ, $\phi\left(\frac{\sum w_i^2}{K}\right) \leqslant \frac{\sum \phi(w_i^2)}{K}$. In our case $\phi(x) = x^{3/2}$. Thus the weighted sum of Poisson processes has greater variance than the sum of Poisson processes when the expected means are equal. Accordingly we would expect more variance of the currents injected into neurons with a graded firing rate and weight distribution than with the binary firing rate and weight distribution when the injected currents are the same. This analysis is supported by our finding that the variance of the NMDA currents injected into each neuron of pools 1 and 2 in the spontaneous period was greater in the graded than the binary case (300 vs 254, $p < 10^{-10}$), whereas the means were similar (48.3 vs 48.4 nA).

We emphasize that the mean firing rates and mean variances of the decision populations of neurons are very similar for the binary and graded cases: it is the distributions that are different, as shown in Figure 19. The concept here is that for the graded representation the subset of neurons with higher than average variance (and firing rates) contribute especially strongly to the noise (i.e. variation, fluctuation) in the system that promotes diffusion (Marti et al., 2008) across the barrier in the energy landscape (Figure 8), and that the effect of these neurons is helped by their stronger than average connection weights to other neurons within their decision pool, which enable statistical fluctuations in their rates to be felt especially strongly by the other neurons in the same decision attractor.

To clarify, the descent into the decision attractor basin first has to overcome the energy barrier that keeps the system in the spontaneous stable state (Figure 8b). Greater variation in the system will mean that this transition is more likely to happen quickly. This is due to the fact that many coincident spikes are needed to overcome this energy barrier. Increased noise means that we are more likely to observe the right set of coincident spikes occurring earlier.

The work described here shows that a potentially useful property of the graded firing rate representations found in the brain (Franco et al., 2007; E. T. Rolls, 2008) is the faster decision times found than with binary firing rate distributions. Given that attractor networks in the cortex have to be large, with thousands of recurrent collateral synapses onto each neuron, as this is the leading factor that determines the number of different memories that can be stored and correctly retrieved (E. T. Rolls, 2008; E. T. Rolls and A. Treves, 1998; A. Treves and E. T. Rolls, 1991), the graded firing rate distributions may enable the finite size statistical fluctuations to still influence the processing, and indeed make

the processing faster than it would be with binary firing rate distributions. This speed is important, for recurrent collateral processing may be useful at every stage of each sensory hierarchy of cortical processing, yet there may be time for only 20–25 ms of processing at each cortical stage of the hierarchy (Panzeri, Biella, et al., 1996; Panzeri, E. T. Rolls, et al., 2001; E. T. Rolls, 2003, 2008; E. T. Rolls, M. J. Tovee, and Panzeri, 1999). The functions to which the noisy graded firing rates contribute in cortical attractor networks include memory recall, probabilistic decision-making, the facilitation of perceptual detection by stochastic resonance, creative thought, disengagement of attention, and an element of unpredictability of behaviour that can be advantageous (E. T. Rolls and Deco, 2010).

The framework used here can be extended very naturally to account for the probabilistic decisions taken when there are multiple, that is more than two, choices. One such extension models choices between continuous variables in a continuous or line attractor network (Furman and X.-J. Wang, 2008; Liu and X.-J. Wang, 2008) to account for the responses of lateral intraparietal cortex neurons in a 4-choice random dot motion decision task (A. K. Churchland, Kiani, and M. N. Shadlen, 2008). In another approach, a network with multiple discrete attractors (Albantakis and Deco, 2009) can account well for the same data. The effects described in the current chapter, that the greater spiking-related noise of graded than of binary representations can reduce the stability, and increase the speed of decision-making, will apply directly to the discrete attractor scenario, in which greater noise will decrease the escape time from one state to another in the energy landscape (Figure 8b) (E. T. Rolls and Deco, 2010). These results are consistent with other computational frameworks about how the brain makes decisions. For instance, some drift diffusion models contain an implicit energy barrier corresponding to a leak term that slows decision-making (Bogacz, Brown, et al., 2006; Gold and M. N. Shadlen, 2001).

The graded nature of the firing rate representations in the cortex may of course be adaptive for other reasons than the speed of processing, which might be an added benefit if there are other reasons for graded firing rate representations. If the number of spikes recorded in a fixed time window is taken to be constrained by a fixed maximum rate, one can try to interpret the distribution observed in terms of optimal information transmission (Shannon, 1948), by making the additional assumption that the coding is noiseless. An exponential distribution, which maximizes entropy (and hence information transmission for noiseless codes) is the most efficient in terms of energy consumption if its mean takes an optimal value that is a decreasing function of the relative metabolic cost of emitting a spike (Levy and Baxter, 1996). This argument would favour sparser coding schemes the more energy expensive neuronal firing is (relative to rest). Although the tail of actual firing rate distributions is often approximately exponential (Baddeley et al., 1997; Franco et al., 2007; E. T. Rolls, A. Treves, M. Tovee, et al., 1997), the maximum entropy argument cannot apply as such, because noise is present and the noise level varies as a function of the rate, which makes entropy maximization different from information maximization. Moreover, a mode at low but non-zero rate, which is often observed (Franco et al., 2007; E. T. Rolls, 2008; E. T. Rolls, A. Treves, M. Tovee, et al., 1997) is inconsistent with the energy efficiency hypothesis.

In conclusion, we have investigated the effects of graded firing patterns in a recurrent spiking neural network attractor model of decision-making. The graded patterns we produced in the numerical simulations took a similar form to those found neurophysiologically. The main finding is that the transition time to an attractor state, or reaction time, is decreased when neurons fire with the more biologically realistic graded firing rates across the neuronal populations. One advantage of these graded firing rate representations is that they provide a sparse distributed representation with independence of the information provided by each neuron, allowing for the useful properties in associative networks of generalization, completion, and graceful degradation (E. T. Rolls, 2008; E. T. Rolls and A. Treves, 2011). It has been argued elsewhere (Levy and Baxter, 1996) that graded firing rates may also maximize information transmission for a given mean rate of firing, and therefore energy consumption, given that high average firing rates require more metabolic expenditure. [However, an alternative account of the graded distributions is that they arise with integrate-and-fire neurons with slow fluctuations in the inputs (reflecting different stimuli) and fast fluctuations in the inputs (reflecting for example trial-by-trial variability in the response to a given stimulus, to which the effects of the spiking-related, close to Poisson, high entropy, fluctuations in the number of spikes in a short time window analyzed in this chapter could contribute) (S. Treves A. P. et al., 1999). The long tail of graded firing rate probability distributions may also be required for cost efficiency (Polavieja, 2002).] The results described here show that an additional useful property of the graded representations found in the brain is that they may increase the speed of decisions, reducing the time required for many processes such as memory recall as well as more conventionally understood decision-making (E. T. Rolls and Deco, 2010).

We emphasize that it is important to understand the effects of noise in networks in the brain, and its implications for the stability of neuronal networks in the brain. For example, a stochastic neurodynamical approach to schizophrenia holds that there is less stability of cortical attractor networks involved in short-term memory and attention due to reduced functioning of the glutamate system, which decreases the firing rates of neurons in the prefrontal cortex, and therefore, given the spiking-related noise that is present, the depth of the basins of attraction. This it is suggested contributes to the cognitive changes in schizophrenia, which include impaired short-term memory and attention (Loh, E. T. Rolls, and Deco, 2007a; E. T. Rolls and Deco, 2011; E. T. Rolls, Loh, Deco, and Winterer, 2008). In another example, a stochastic neurodynamical approach to obsessive compulsive disorder holds that there is overstability in some networks in prefrontal cortex and connected areas due to hyperglutamatergia (E. T. Rolls, 2011; E. T. Rolls, Loh, and Deco, 2008). In both these cases, and also in normal brain function in relation to decision-making, memory recall, etc, it is important to know to what extent noise contributed by randomness in the spiking times of individual neurons for a given mean rate contributes to stochastic effects found in the brain which affect decision-making, stability, and which may if the stability is disturbed contribute to neuropsychiatric disorders. In this context, the findings described in this chapter are important for understanding normal and disordered brain function. In particular, a very interesting implication of the findings described here is that there is more noise with the graded representations found in the brain (see (E. T. Rolls, 2008) Appendix 3 on information en-

coding in the brain) than with binary firing rate distributions (which are often used in simulations, because they are amenable to mean-field analyses (Deco and E. T. Rolls, 2006; X.-J. Wang, 2002)). Thus when noise is found to be a significant factor in the operation of integrate-and-fire decision-making networks with binary firing rates up to sizes that have been tested of 4,096 neurons each with 4,096 synapses per neuron, then it is likely that with graded firing rates, spiking-related noise will continue to be a factor in the operation of cortical circuitry even up to the larger numbers of recurrent collateral synapses onto each neuron. For example, in the cerebral cortex there are typically in the order of 9,000 recurrent collateral synapses onto onto each cortical pyramidal cell, from a total of in the order of 18,000 synapses (Abeles, 1991; E. T. Rolls, 2008).

4 CORTICAL ATTRACTOR NETWORK DYNAMICS WITH DILUTED CONNECTIVITY

In this chapter we investigate the effects of dilution of the connectivity on the noise in the network. In integrate-and-fire simulations, it is convenient to analyze the performance with full connectivity. Reasons for this include the fact that there is then a mean-field equivalent, and that the simulations are easier to code and run much faster with full connectivity. Mean-field theory can hold for networks with random diluted connectivity (Amit and Brunel, 1997a; Brunel, 2000; Brunel and Hakim, 1999; Renart, Brunel, and X.-J. Wang, 2004), with the assumption that the network is so diluted that neurons are not likely to have reciprocal connections. With asymmetric diluted connectivity, the application of approaches using energy minima applied to symmetric fully connected networks (Hopfield, 1982) no longer hold formally. Extensions of the approach do show that networks with diluted connectivity trained with an associative rule are still likely to perform with many of the same properties as a fully connected network (Bovier and Gayrard, 1992; Perez Castillo and Skantzos, 2004; E. T. Rolls and A. Treves, 1998; E. T. Rolls et al., 1997a; A. Treves, 1991; A. Treves and E. T. Rolls, 1991). For example, with diluted connectivity, the number of patterns that can be stored and recalled correctly is still determined mainly by the number of connections onto each neuron received from the other excitatory neurons in the network (Bovier and Gayrard, 1992; Perez Castillo and Skantzos, 2004; E. T. Rolls and A. Treves, 1998; E. T. Rolls et al., 1997a; A. Treves, 1991; A. Treves and E. T. Rolls, 1991).

The attractor networks that are theorized to be in the neocortex and the hippocampus have diluted connectivity. An estimate for the rat hippocampus is 4% (12,000 connections C per CA3 neuron, and 300,000 CA3 neurons). An estimate for neocortex might be 10% [For the neocortex, assuming 10,000 recurrent collaterals per pyramidal cell, that the density of pyramidal cells is 30,000 / mm^3 (E. T. Rolls, 2008), that the radius of the recurrent collaterals is 1 mm, and that we are dealing with the superficial (or deep) layers of the cortex with a depth of approximately 1 mm, the connectivity between the superficial (or deep) pyramidal cells would be approximately 10%.] What impact does this diluted connectivity have on the dynamics of the operation of cortical networks? Does it make the decision or memory recall times slower, due to a potentially longer path for every neuron to reach every other neuron functionally? If so, how much slower? Does the diluted connectivity make the diluted networks more or less stable, both in terms of spiking noise-provoked jumps from the spontaneous state to a high firing rate state; and when in a high firing rate state implementing a short-term memory, out of that state? We study this in networks in which we keep the number of excitatory recurrent collateral connections to a neuron constant, for this is the leading factor in determining the memory capacity of the network, that is the number of memories that can be stored

and successfully retrieved (E. T. Rolls, 2008; E. T. Rolls and A. Treves, 1998; A. Treves, 1991). We assume that the brain is designed to make the capacity as large as possible, and that in the order of 10,000 recurrent collateral connections per neuron is about as high as can easily be produced biologically. The finite-size noise is influenced by the number of neurons N in a fully connected network where $N = C$, the number of recurrent collateral synapses per neuron (E. T. Rolls and Deco, 2010). In a diluted network, it may be N which influences the finite-size noise, and this is one issue we investigate.

We investigate these issues in networks with 800 recurrent collateral synapses per neuron, comparing networks with dilutions of 0.25 and 0.1 with networks with full connectivity.

4.1 METHODS

For the results presented in this chapter we extend the simulation framework presented in section 2.1 in a different manner than the previous chapter. In our fully connected network simulations, the network contained $N = 1000$ neurons, with $N_E = 0.8N$ excitatory neurons, and $N_I = 0.2N$ inhibitory neurons. The two decision pools are equal size sub-populations with the proportion of the excitatory neurons in a decision pool, or the sparseness of the representation with binary encoding, $f = 0.1$, resulting in the number of neurons in a decision pool $N_E f = 80$. The neuron pools are non-overlapping, meaning that the neurons in each pool belong to one pool only.

The synaptic weights are set to be binary, i.e. neurons in the same decision pool are connected to each other with a strong average weight w_+, and are connected to neurons in the other excitatory pools with a weak average weight w_-. All other synaptic weights are set to unity. The diluted network we studied operated in a very similar scenario to the previous chapters. We note that mean-field analyses of networks with highly diluted connectivity have been described previously (Brunel, 2000; A. Treves and E. T. Rolls, 1991).

4.1.1 Diluted connectivity

In the full connectivity case, see Figure 21a, the network contains N neurons. The two decision pools are equal size sub-populations with the proportion of the excitatory neurons in a decision pool, or the sparseness of the representation with binary encoding, $f = 0.1$, resulting in the number of neurons in a decision pool $N_E f$. The neuron pools are non-overlapping, meaning that the neurons in each pool belong to one pool only. In the investigations described here, we chose to set the number of excitatory recurrent collateral connections C per neuron to 80 in a decision-making pool, the number in a standard fully connected network with $N_E = 800$ excitatory neurons, as with a network this size there is still with a standard set of parameters some instability of the spontaneous firing rate state, so that stability can be investigated. The number of non-specific excitatory neurons in this network with $N = 1000$ is 640. These neurons simulate the effects of noise from other networks in the system than those involved in the decision-making. The sparseness of the representation,

the proportion of excitatory neurons with high activity when an attractor wins, is $80/800 = 0.1$ for the fully connected network. Given that there were two decision pools each with 80 neurons in the fully connected network, there were 80 connections onto each neuron from each decision pool.

In setting up the diluted connectivity, we aimed to keep the total number of excitatory synapses devoted to the recurrent collateral synapses fixed, as this is likely to be a biological parameter that can not be increased without limit, and that number was 800, as noted above. The number of synapses for each decision (or specific) pool was also maintained at the default value for this size of network, 80 synapses per neuron. We kept the number of inhibitory neurons constant at 200 for this size of network. To dilute the connectivity within each specific decision-making pool of neurons to 0.25, we increased the number of neurons in each specific pool from 80 in the fully connected case to 320 in the diluted case, as shown in Figure 21b. The 80 synapses onto each neuron were randomly chosen from the 320 neurons in each decision pool to achieve a dilution of the connectivity in each decision pool of 0.25.

This meant that the population sparseness was 0.25 (320 neurons / 1,280 excitatory neurons for the representation for each specific decision-making pool for the dilution to 0.25 case. Considering each synaptic weight vector on each excitatory neuron, the number of synapses for a specific decision-making pool (e.g. pool 1) was 800, and of these 80 were intrapool synapses for decision 1, so the sparseness of a representation seen by each neuron for decision 1 was held constant at $80/800 = 0.1$, independently of the degree of dilution (The same was true for the other decision pool, pool 2). Given that there were two decision pools each with 80 synapses per neuron in a decision pool, there were 80 connections onto each neuron from each decision pool just as in the fully connected case above. The numbers are summarized in Table 2. The decision cues were presented to the network in the same way regardless of dilution: each neuron in the decision pool received additional input, i.e. input representations were not sparse. In all cases, the number of non-specific neurons, i.e. those not in a specific decision-making pool, was kept constant at 640. The total number of excitatory neurons in each network is shown by N_E in Table 2.

The above values for the parameters were for connectivity diluted to 0.25. We also ran further simulations with the connectivity diluted to 0.1, as shown in Figure 21c. The parameters in this case were as shown in Table 2. In the Connectivity column, the value 1 refers to full connectivity, and the value 0.25 to a network with the connectivity diluted to 0.25 using an algorithm which ensured that for each of the 80 synapses on a neuron for a given decision-making pool, the neuron in the decision pool to which to connect was chosen randomly, with no double connections allowed to a neuron.

Connectivity	C	$C_{fromDpool}$	N_{Dpool}	N_E	Sparseness a
1	800	80	80	800	0.1
0.25	800	80	320	1280	0.25
0.1	800	80	800	2240	0.357

Table 2: Parameters for the full and diluted connectivity simulations: C, the number of excitatory connections received by an excitatory neuron; $C_{fromDpool}$, the number of excitatory connections received from each decision-making pool; N_{Dpool}, the number of excitatory neurons in a decision-making pool; N_E, the total number of excitatory neurons in the simulations, in which the number of nonspecific neurons was 640; a, the population sparseness of the representation, the proportion of excitatory neurons active for any one decision.

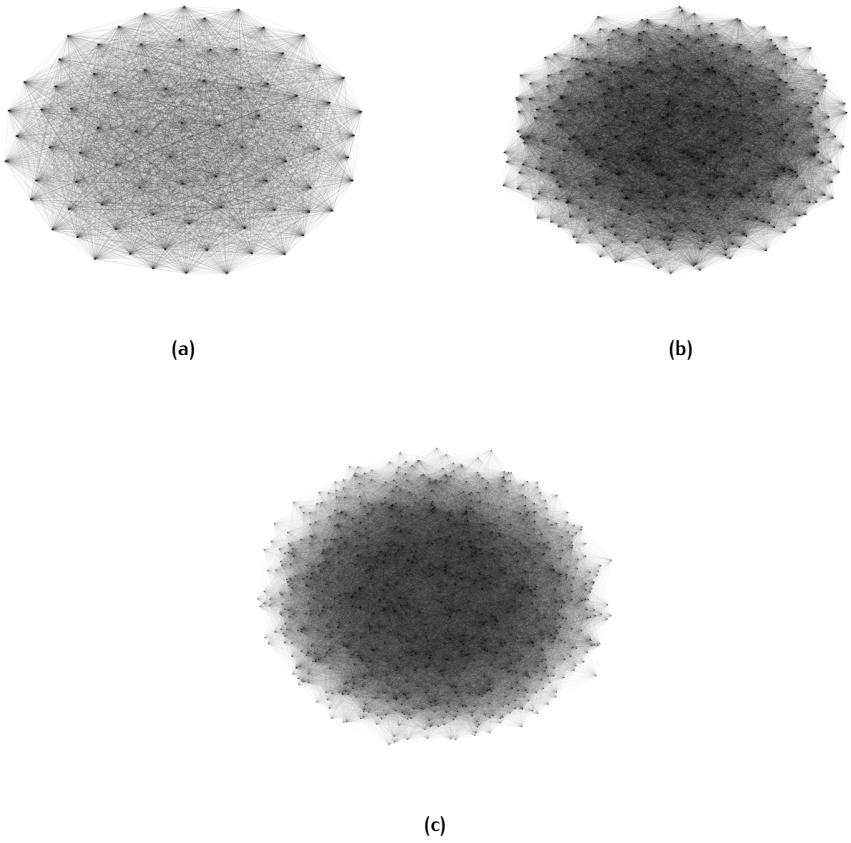

Figure 21: Visualization of the network connectivity in decision pools for (a) full connectivity, (b) 0.25 diluted connectivity, and (c) 0.1 diluted connectivity. Nodes correspond to neurons, and edges represent a synaptic connection.

4.2 RESULTS

As before, decision-making was investigated in the integrate-and-fire neuronal attractor network model of cortical decision-making mechanisms illustrated in Figure 8 and described in section 2.1 and section 4.1. Again as before, the decision-making was probabilistic because of the stochastic fluctuations produced by the almost random (Poisson) firing times for a given mean firing rate of the neurons in the network (E. T. Rolls and Deco, 2010). Figure 22 shows that we had achieved changes, in the networks with connections between the neurons diluted to 0.25 or 0.1, that did not affect the mean firing rates of the decision populations of neurons. The first 2 s of the simulation are spontaneous firing before the decision cues are applied starting at $t = 2{,}000$ ms. The firing rates of the neurons in the winning decision-making pool or population of neurons are shown. The losing population maintained its activity close to the spontaneous level of firing during the decision period from $t = 2{,}000$–$4{,}000$ ms. The performance of the network with a diluted connectivity $= 0.25$ is described in subsection 4.2.1– subsection 4.2.4, and with dilution $= 0.1$ in subsection 4.2.5.

4.2.1 Decision time

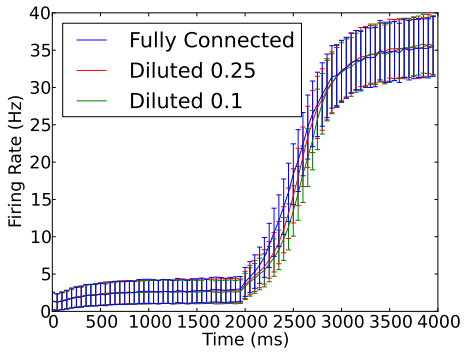

Figure 22: Mean firing rates over 1,200 trials for the winning pool in fully connected networks and with networks with connectivity diluted to 0.25 and to 0.1. The first 2 s is the period of spontaneous firing before the decision cues were applied at time 2 s. The winning pool is chosen to be the pool with average firing rate 10 Hz greater than the competing pool in the last 1 s of the simulation. The small differences in mean rate at the decision time after $t = 2$ s are due to the small increase in the decision times with dilution.

With diluted connectivity, it is possible that the attractor network might settle more slowly towards a decision attractor state, due to the longer time that it might take any ongoing changes to reach all neurons, and because the connections are no longer symmetric between pairs of neurons. With the method of diluting the connectivity, reciprocal connections were present only by chance; but if present the weights would be equally strong due to the Hebbian learning. Indeed, analytically with asymmetric diluted connectivity, there is no longer an

energy minimum of the type defined by (Hopfield, 1982), though it has been shown that such a network still has many of the same properties, including storage capacity, completion, etc (A. Treves, 1991; A. Treves and E. T. Rolls, 1991). However, the dynamics of the settling into the attractor has not been investigated previously.

The decision time distributions for the fully connected network and the networks with dilutions of 0.25 are shown in Figure 23. We found that the decision times were a little slower, approximately 50 ms slower, with diluted than with complete connectivity (952 ms for the diluted case vs 894 ms for the fully connected case, $p < 0.0002$). Factors that influence the shape of the distribution are considered in the Discussion.

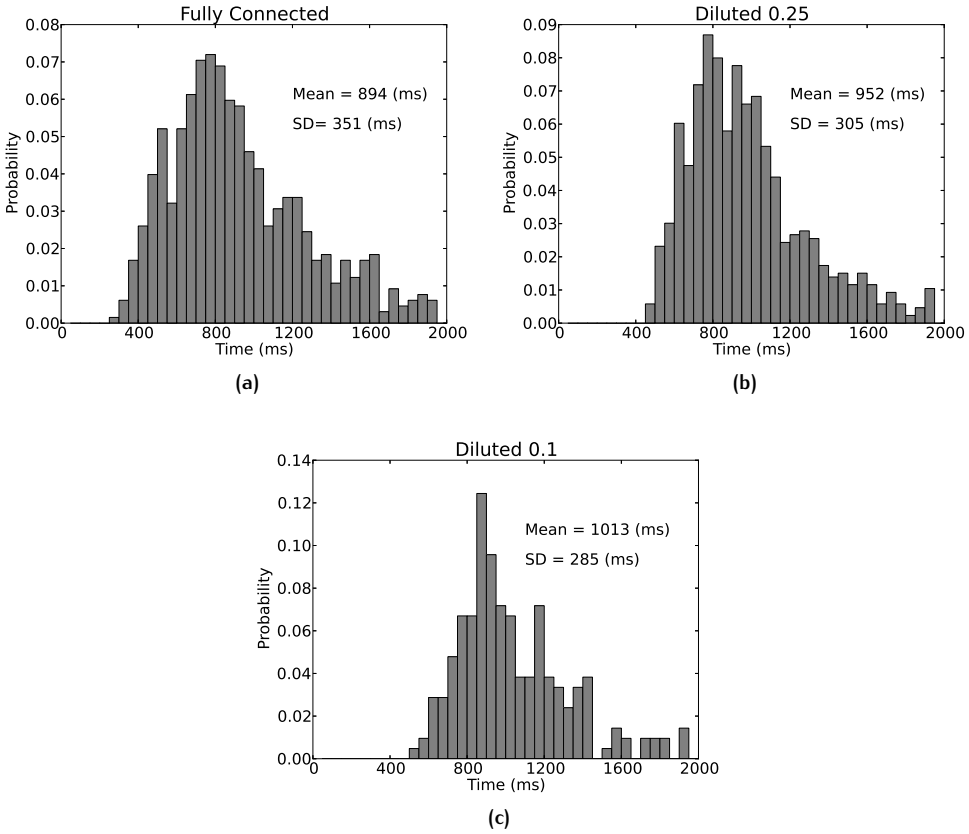

Figure 23: Histograms of decision times for 1,200 trials with (a) full, (b) 0.25 diluted connectivity, and (c) 0.1 diluted connectivity. $p < 0.0002$ for (a) vs (b) using Kolmogorov-Smirnoff tests, t-tests, and Mann-Whitney U tests of the two distributions. The smaller standard deviations of the decision times with dilution are consistent with less noise in the diluted networks.

4.2.2 Decision accuracy

The accuracy of the correct decisions (with $\Delta\lambda = 6.4$) was 64.3% in the fully connected case and 75.7% in the 0.25 diluted case. This was calculated over 1,200 trials apart from those that were rejected from the analysis due to instability of the spontaneous state (that is, instability in the 2 s period before the decision cues were applied). The greater accuracy in the diluted case is probably related to the fact that there were more neurons in the attractor for each decision pool: 320 neurons for the 0.25 dilution case, and 80 for the fully connected case.

4.2.3 Stability of the spontaneous state

Noise and the positive feedback in this system can cause the network to jump into a decision state from the spontaneous state even before the decision cues are applied (at $t = 2$ s in our simulations). We analyzed the stability for the diluted vs complete connectivity cases by measuring the percentage of trials on which these simulations transited into or towards a high firing rate decision state before the decision cues were applied at $t = 2$ s. The parameters for the fully connected simulation had been set with the mean-field analysis so that the mean spontaneous firing rate should be 3 spikes/s. The criterion for instability of the spontaneous state was that the mean rate of either decision pool exceeded 5 spikes/s in the 250 ms before the decision cues were applied.

It was found that the stability of the spontaneous state was increased (keeping the number of connections per neuron constant) in the diluted connectivity networks compared to the fully connected case, as shown in Figure 24.

This effect was not accounted for by any difference in the mean spontaneous firing rates of the decision pool neurons in the diluted vs fully connected cases, which remained at a mean value of approximately 3 Hz, as shown in Figure 22.

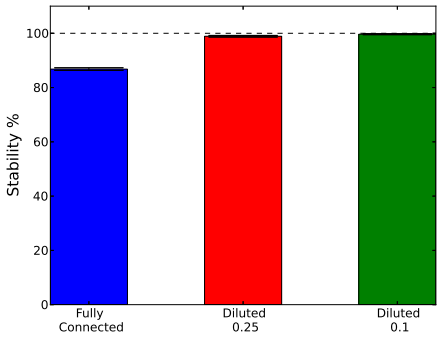

Figure 24: Stability of the spontaneous firing state before the decision cues are applied. The percentage of stable trials is shown for networks with full connectivity, and with dilutions to connectivities of 0.25 and 0.1. The network size was as shown in Table 2. The error bars (barely visible) are the standard deviations. There was a significant difference between the fully connected and 0.25 dilution cases ($p < 0.0001$, chi-square test, number of trials 5,000).

4.2.4 Sparseness

The sparseness of the representation was measured during the last 0.5 s period of the simulation in which the network was firing stably in one of the attractors. The sparseness a calculated with Equation 19 was 0.39 for the fully connected network and 0.43 for the network with connectivity diluted to 0.25. It is just the small amount of spontaneous firing in the non-selective and losing pools of approximately 3–10 spikes/s that makes these values a little higher than the value that would be obtained with a binarized firing rate. If the rates below 15 spikes/s were set to zero to exclude spontaneous activity (producing a measure that might be called the sparseness of the population response, where response = firing rate − spontaneous rate cf. E. T. Rolls and M. J. Tovee (1995)) the sparseness values from the simulations were then very close to the expected values shown in Table 2, namely 0.10 for the fully connected case for which the expected value was 0.1, and 0.25 for the network with 0.25 dilution for which the expected sparseness value was 0.25.

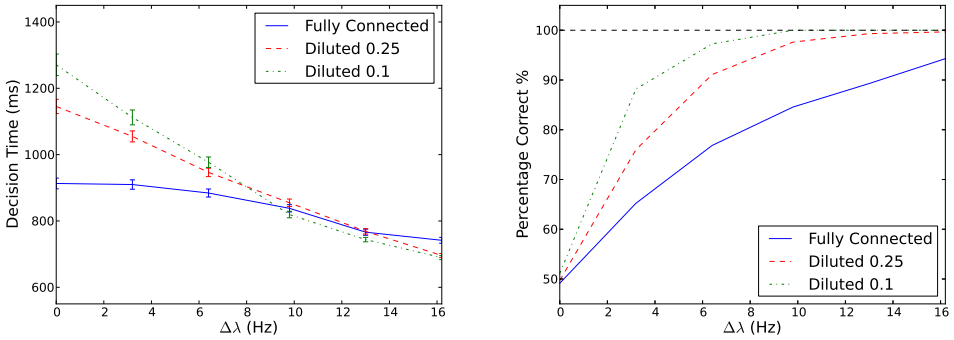

Figure 25: (a) Decision time as a function of $\Delta\lambda$ for networks with full connectivity, and with dilutions to connectivities of 0.25 and 0.1. The standard errors are shown calculated across 600 trials. (b) Percentage correct as a function of $\Delta\lambda$ for networks with full connectivity, and with dilutions to connectivities of 0.25 and 0.1. The network size was C = 1,600 synapses per neuron, with the other parameters $C_{fromDpool}$, N_{Dpool} shown in Table 2 also doubled.

4.2.5 Performance with connectivity diluted to 0.1

We repeated the investigations just described with a greater level of dilution, 0.1, as this is the value of an estimate of the dilution in the neocortex (0.1), and closer to an estimate of the dilution in the CA3 recurrent collateral connections of the hippocampus (0.04). The size of the network was 2,240 excitatory neurons, with 80 connections within each excitatory decision pool, and 800 neurons in each excitatory pool (see Table 2). The stability of the spontaneous state was even greater (see Figure 24). The spontaneous rate was 2.14 spikes/s (measured in the time period 1–2 s which is the last 1 s of the spontaneous period), and the

rate when in the decision attractor was 33.6 spikes/s. (On incorrect trials the mean rate was 1.91 spikes/s.) (For the fully connected simulation, the mean spontaneous firing rate in the spontaneous period was 2.28 spikes/s).

We found that the decision times were a little slower, approximately 145 ms slower, with connectivity diluted to 0.1 than with complete connectivity (1,013 ms with 0.1 dilution vs 894 ms for the fully connected network, $p < 10^{-7}$, Figure 23). The decision time was also slower for the 0.1 level of dilution (1,013 ms) than for the 0.25 level of dilution (952 ms, $p = 0.001$). The smaller standard deviations of the decision times with dilution of 0.1 are also consistent with less noise in the diluted networks.

The accuracy of the correct decisions (with $\Delta\lambda = 6.4$ Hz) was 64.3% in the fully connected case and 90.3% in the 0.1 diluted case. This was calculated over 351 trials in the diluted case. The greater accuracy in the diluted case is probably related to the fact that there were more neurons in the attractor for each decision pool: 800 neurons for the diluted case, and 80 for the fully connected case. The accuracy was intermediate for the 0.25 dilution case (75.7%).

The implication is that an advantage of diluted connectivity (if it is implemented by increasing the number of neurons in a network, as in the brain, while keeping the number of connections C onto each neuron constant), is that the diluted connectivity case will, with more neurons, be more stable with fewer fluctuations of the type illustrated in the fully connected network in the spontaneous firing rate period. The relevance of this is that the spontaneous firing rate period is the state when the decision cues are applied, and the state from which a decision is taken.

The decrease in all networks in the Fano factor from approximately 1.0 during the spontaneous period of firing to a value of approximately 0.45 after the decision has been taken and the system is in a high firing rate state for one of the decision attractor pools is considered in the Discussion.

4.2.6 Performance as a function of the input bias $\Delta\lambda$

The results presented so far have been with $\Delta\lambda = 6.4$ Hz. We now explore the effect of different values of $\Delta\lambda$ in diluted networks. Decision times as a function of $\Delta\lambda$ for networks with full connectivity, and with dilutions to connectivities of 0.25 and 0.1, are shown in Figure 25a. (The network size was twice that of previous simulations, partly to explore these effects with much larger networks. C was 1,600 synapses per neuron, with the other parameters $C_{\text{fromDpool}}$, N_{Dpool} and N_E shown in Table 2 altered accordingly. Thus the number of neurons within a decision pool N_{Dpool} for a connectivity of 0.1 was 1,600 neurons for the simulations shown in Figure 25a.) Figure 25a shows that with low values for the bias $\Delta\lambda$ the fully connected network was fastest, with slower decision times for greater dilutions. A reason for the longer decision times with diluted connectivity is the slower percolation of the effects of activity in any given neuron to all neurons in the population with diluted connectivity. At higher values of $\Delta\lambda$ (10 Hz and above) the bias $\Delta\lambda$ is sufficiently strong in pushing the network towards a decision that the effects of the dilution and percolation effects become no longer relevant to the decision time.

Figure 25b shows the percentage correct as a function of $\Delta\lambda$ for networks with full connectivity, and with dilutions to connectivities of 0.25 and 0.1. The

percentage correct at most values of $\Delta\lambda$ is better for the diluted networks than for the fully connected network. The interpretation is that there is less noise within a decision pool as the number of neurons in the decision pool increases, in this case from 160 neurons in the fully connected case to 640 neurons with 0.25 dilution and 1,600 neurons with 0.1 dilution.

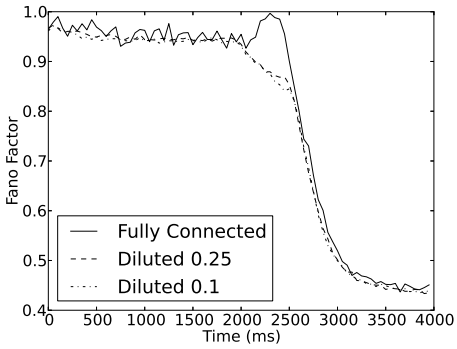

Figure 26: The Fano factors for the fully connected network and for the networks with diluted connectivity of 0.25 and 0.1. The Fano factor for the neurons in the winning pool is shown, where the Fano factor was defined as the variance across trials / the mean firing rate across trials for the time windows of 50 ms. The small increase in the Fano factor at the time of the decision in the fully connected case is related to the differences in the decision times on different trials. The decision cues were presented at $t = 2.0$ s.

4.2.7 Noise in the system: the Fano factor

Another measure of the noise in the system is the variance of the firing rates of the neurons in a decision pool during decision-making. If the firing of the neurons in a pool has more variance, that pool may be more likely to cross a bifurcation from the spontaneous firing rate state and to enter a decision state without any decision cue, or to make a decision more rapidly after the decision cues have been applied (cf. Figure 8).

Figure 26 shows the Fano factor for the neurons in the winning pool, where the Fano factor was defined as the variance across trials / the mean firing rate across trials using time windows of 50 ms. Although the Fano factors are in general similar for the 0.25 diluted and full connectivity cases, there is more variability in the Fano factor in the different 50 ms time windows in Figure 26 in the pre-decision cue spontaneous firing period from 0–2 s in the fully connected compared to the diluted connectivity cases. An implication is that with the Fano factor, and the variance, being calculated over 320 neurons in the diluted case compared to 80 neurons in the full connectivity case, there are more statistical fluctuations, at least in different time windows, in the case with fewer neurons in a decision pool, the fully connected case.

In addition, the elevation in the Fano factor at the time that the decision is taken in the fully connected case is related to the fact that on some trials the

decision is fast, and on others slower, so that on some trials the rate is higher, and on others still low, soon after the decision cues are applied. This greater variability in the decision time with the fully connected network is very consistent with the other evidence that there is greater noise in the fully connected than the diluted network, so that the variability in the decision times is greater in the fully connected case. Further factors involved are discussed elsewhere (A. K. Churchland, Kiani, Chaudhuri, et al., 2011; Renart, Moreno-Bote, et al., 2007).

The implication is that an advantage of diluted connectivity (if it is implemented by increasing the number of neurons in a network, as in the brain, while keeping the number of connections C onto each neuron constant), is that the diluted connectivity case will, with more neurons, be more stable with fewer fluctuations of the type illustrated in the fully connected network in the spontaneous firing rate period. The relevance of this is that the spontaneous firing rate period is the state when the decision cues are applied, and the state from which a decision is taken. This smaller stochastic fluctuation with the diluted connectivity appears to be an adaptive situation for the brain, in that too much noise can lead to instability of cortical systems, and associated disorders such as epilepsy, and neuropsychiatric disorders such as schizophrenia 2007a; 2005, 2011; 2010; 2008.

The decrease in all networks in the Fano factor from approximately 1.0 during the spontaneous period of firing to a value of approximately 0.45 after the decision has been taken and the system is in a high firing rate state for one of the decision attractor pools is considered in the Discussion.

The Fano factor with 0.1 dilution shown in Figure 26 was similar to that of the 0.25 diluted case, and different in the ways described above from the fully connected case.

4.2.8 Noise in the system: within-trial variability

To assess the variability of the firing within a trial, as a measure of the internal noise in the system, we calculated the coefficient of variation of the firing in the last 1 s of the spontaneous period, using 50 ms bins each containing the number of spikes from a single neuron. This coefficient of variation was then averaged across all the neurons for each trial, and then the mean value across trials was calculated (ensuring that only trials with stability maintained throughout the spontaneous period were included) to ensure that the estimated coefficient of variation was reliable. The CV measures the variability in the firing of single neurons on individual trials, and is a useful measure of the noise in the system. The CV was ≈ 2.44 (± 0.010 se) for the diluted network, and ≈ 2.46 (± 0.016 se) ($p < 0.05$) for the fully connected case, for the spontaneous, that is, pre-cue period. There was thus less stochasticity in the diluted network than in the fully connected network. This was related to the larger number of excitatory neurons in the diluted connectivity, and was found even though the number of connections onto each neuron was identical in the diluted and fully connected networks. This finding is consistent with the finding that there was more stability in the diluted networks in the spontaneous period, in that with less noise, there was less tendency to jump because of the noise to a high firing rate attractor state.

We also measured the CV in the period when the networks had fallen into a high firing rate decision attractor.

For the final 1 s period the same calculations showed that the CV was 0.17 for the diluted network, and 0.28 for the fully connected case, again indicating less noise in the diluted network.

4.3 DISCUSSION

In integrate-and-fire simulations of an attractor decision-making network, we have shown that the noise is smaller for diluted connectivity than for full connectivity. This was shown by the greater stability in the spontaneous period of the diluted simulations, and by the slower decision times with diluted than with full connectivity (Figure 23 and Figure 24). The slower decision times in the diluted case reflect less noise, as it is the noise that with the parameters chosen is required for the network to escape from the spontaneous state into a decision state. Further evidence is that the Fano factor, reflecting the trial by trial variation in the firing rate, was more steady for the diluted network as a function of time within a trial (that is in the different 50 ms bins in each trial), as shown in Figure 26. Further, the measure of the within-trial variability of the firing rate, the coefficient of variation, was also smaller for the diluted than for the fully connected network, reflecting less noise in the diluted network. Moreover, the accuracy of the decisions was also greater with the diluted network, reflecting fewer noise-induced errors. The finding that for more diluted networks performance but also decision time both increase can be described as a speed-accuracy trade-off due to a reduction of the noise.

The exact distribution of the decision times shown in Figure 23 is not a focus of the results presented here. Others have described part of a mechanism by which the decision time distribution is affected by error trials, and indeed may be longer for error compared to correct trials (E. T. Rolls, Grabenhorst, and Deco, 2010b). This models effects that are found in human performance (Vickers and Packer, 1982), especially with difficult decisions, (Luce, 1986; Welford, 1980), and that have been modelled (R. H. Carpenter, Reddi, and Anderson, 2009; Moreno-Bote, 2010; E. T. Rolls, Grabenhorst, and Deco, 2010b). There are a number of reasons why errors can occur, which affect decision times and their distributions, including a failure to maintain attention, distraction, etc, and the decision times on such trials might be short or long. Slower reaction times on error trials are usually observed in humans when there is no time pressure, while with time pressure the pattern is the opposite (Ratcliff and Rouder, 1998).

These results were obtained in a regime where the number of excitatory recurrent collateral connections per neuron was held constant (at 80 synapses for the neurons in each of the two specific pools, and a total of 800 synapses on each neuron). The reason that this number was held constant is that this is the leading term in the capacity of attractor networks (E. T. Rolls and A. Treves, 1998; A. Treves, 1991), and this is a crucial factor that affects the biological utility of attractor networks in the brain (E. T. Rolls, 2008, 2010). The interesting finding presented here is that when forming diluted connectivity by increasing the number of neurons in the network, one obtains greater stability of the network against erroneous transitions into high firing rate states, and the result

may be that attractor networks can more easily be used up to capacity (set by the number of recurrent synapses per neuron) when they have diluted connectivity, because they are more stable, i.e. less noisy.

Our hypotheses for how diluted connectivity decreases the statistical fluctuations, the noise, in an attractor network are as follows. First, it is known that in a fully connected network, the noise decreases according approximately to the square root of the number of neurons in the network (Deco and E. T. Rolls, 2006; Mattia and Del Giudice, 2002, 2004; E. T. Rolls and Deco, 2010). As the number of neurons approaches infinity, the recurrent synaptic input noise approaches zero, and this is the mean-field limit. The concept is that as more and more independent Poisson processes reflecting the spike times of different neurons contribute to the mean value, the mean value shows smaller and smaller statistical fluctuations. And in an integrate-and-fire attractor network, the small fluctuations in the firing of each neuron in the whole large population with its global inhibition will result in the noise, the statistical fluctuations, being received by any one neuron through its synapses being small. This effect operates in our diluted connectivity network, in that as the dilution increases, so the number of neurons in a selective population or pool increases (as C, the number of recurrent connections per neuron, is held constant). Second, any correlation of the firing of the neurons in an integrate-and-fire attractor network that is related to the noise (Moreno-Bote and Parga, 2006; Renart, Moreno-Bote, et al., 2007) is fed back by the recurrent collaterals, and effectively amplified. This amplification of noise-related effects will be reduced by diluted connectivity, because the dilution will tend to reduce the correlation between the neuronal firing felt by a receiving neuron. It is this effect that enables diluted attractor networks to show a somewhat higher memory capacity (the number of patterns that can be stored and correctly retrieved) than fully connected networks, as has been shown by E. T. Rolls and A. Treves (1998); A. Treves and E. T. Rolls (1991).

We note that memory systems with a large capacity are likely to be selected for in evolution, so that animals and humans can remember for example many separate events, places, episodic memories, facts, etc (E. T. Rolls, 2008). We believe that neurons set the number of recurrent excitatory synapses to be rather large, up to 12,000 in the rat CA3 hippocampal network for example (E. T. Rolls, 2010; A. Treves and E. T. Rolls, 1994a), so that the memory capacity is as large as possible. It may be that with the precision of neurons, it is difficult to utilize more than approximately 20,000 recurrent excitatory connections onto each neuron. In this situation, we argue, diluted networks in the brain are built to keep the number of synapses per neuron high, and this means that the dilution must be obtained by increasing the number of neurons in the network. This has the advantageous effect of increasing the stability of the network, and increasing its accuracy in the face of spiking-induced noise, while making the decision times only a little slower.

In addition to an effect of dilution of connectivity in increasing the stability of attractor networks as described here, there may be other advantages to dilution of connectivity in the cerebral cortex. One is that in competitive neuronal networks, which appear to be being used in the cerebral cortex to build new representations (E. T. Rolls, 2008), the diluted connectivity in the feedforward synaptic connections may help to stabilize the 'feature analyzer' properties of the neurons that are built, by enabling each neuron to learn to respond to a

subset of the possible input feature combinations (E. T. Rolls, 2008). This may help to break the symmetry, and may be being used in the entorhinal grid cell to hippocampal place cell transform (E. T. Rolls, Stringer, and Elliot, 2006). In a fully connected competitive network there is also for example the potential problem that if the inputs are gradually drifting or changing over time, the output neurons may gradually change the feature combinations to which they respond (G. A. Carpenter, 1997; Hertz, Krogh, and R. G. Palmer, 1991; E. T. Rolls, 2008). Dilution in the connectivity is likely we suggest to help minimize such drift effects, and to keep the outputs provided by cortical competitive networks constant.

It was also of interest that in the diluted case, the accuracy of the decisions was higher. The reason for this is that with less noise in diluted networks, there are fewer errors induced by the spiking-related noise producing decision transitions against the bias $\Delta\lambda$ providing the evidence for the decision (E. T. Rolls, Grabenhorst, and Deco, 2010a,b). This is another advantage of the diluted connectivity (in the condition that the number of synapses to other neurons in the same decision pool is kept constant).

An advantage of the diluted connectivity is that it can increase the storage capacity of autoassociation (attractor) networks (when the sparseness of the representation is not very low, when the advantage disappears) (A. Treves and E. T. Rolls, 1991). Another advantage of diluted connectivity is that it reduces the probability of multiple synaptic connections between pairs of neurons, which can greatly degrade the memory capacity of autoassociation networks (E. T. Rolls and A. Treves, 2011).

We emphasize that the mean firing rates of the decision populations of neurons are very similar for the fully connected and diluted cases (Figure 22). We found more within-trial variation in the spontaneous period (measured by the CV described above) in the fully connected than in the diluted case, which again is consistent with less noise in the diluted connectivity case. Further, there was less variability in the final decision period in the firing rate in the fully connected case, as shown by the somewhat lower Fano factor in the diluted than in the fully connected case from $t = 3$–4 s. We checked the basis for the effect, and found that the variance was higher in the diluted than in the fully connected case. The implication is that another advantage of dilution in the connectivity is that once in an attractor, which might be used to implement short-term memory, the memory is more stable in the diluted connectivity case.

The decrease in the Fano factor of the firing rates shown in Figure 26 as the simulation moves from spontaneous firing in the period $t = 0$–$2{,}000$ ms, where the Fano factor is close to 1, to lower values when the network is being driven by inputs, is also found experimentally with neuronal activity in a number of different cortical areas (M. M. Churchland et al., 2010). Our simulation thus provides an account in an integrate-and-fire attractor decision-making network of the decrease in the variability of neuronal activity recorded in the brain as a decision is being reached (M. M. Churchland et al., 2010). It is also of interest that the coefficient of variation of the interspike interval distribution of a neuron on each trial was lower than would be expected of close to Poisson firing when the network was in a high firing rate attractor state. One factor that may contribute to the high variability in the Fano factor of the firing rate in the spontaneous period is that statistical fluctuations can be great when the numbers of spikes involved are

low, as occurs with spontaneous activity (E. T. Rolls and Deco, 2010). This may help produce the variability that is reflected in a Fano factor close to 1. Another factor may be that the NMDA receptors are less engaged at low (spontaneous) firing rates than at high firing rates. A consequence of this may be that when operating with spontaneous activity, there is effectively more of a single, and short, excitatory time constant, that of the AMPA receptors (5–10 ms), which is close to the short time constant of the inhibitory system (in the order of 5 ms). With higher rates and more strong driving of the neurons, a greater proportion of NMDA receptor activation may increase the time constant of the system, but also introduce a long excitatory time constant to add to a short excitatory time constant, and this may produce less variability of the spiking (cf. X.-J. Wang (1999)). It is of interest that we found in addition that the Fano factor for the winning population of neurons is lower when $\Delta\lambda$ is larger, when the system is being driven into high firing rate states by strong inputs. The CV may also decrease in the high firing rate attractor state (Renart, Moreno-Bote, et al., 2007). We note that the somewhat higher values of the Fano factor found with neurons in cortical areas (M. M. Churchland et al., 2010) than those described here may be accounted for by noise that is additional to the internal spiking-related noise generated by the neurons within the network, that is if there is in addition noise in the external inputs to the network, produced for example by different amounts of arousal, attention, motivation, and signal on different trials.

To summarize this chapter, we have investigated the effects on the dynamics of dilution of connectivity in a recurrent spiking neural network attractor model of decision-making, which applies also to memory recall. We showed that diluted connectivity (for the same number of connections per neuron and thus memory capacity) increases the stability and accuracy of the network as there is less noise in the diluted network, with little cost in increased decision times. We emphasize that it is important to understand the effects of noise in networks in the brain, and its implications for the stability of neuronal networks in the brain.

5 COMMUNICATION BEFORE COHERENCE

5.1 INTRODUCTION

Gamma band synchronization has been found in many cortical areas and in a variety of tasks. It has been studied most extensively in the visual cortex of cats and monkeys (Fries, Reynolds, et al., 2001; Fries, Womelsdorf, et al., 2008; Gray et al., 1989; Womelsdorf, Fries, et al., 2006; Womelsdorf, Schoffelen, et al., 2007). Several authors have proposed that these synchronizations influence the interactions among neuronal groups (Salinas and Sejnowski, 2001; Varela et al., 2001), a hypothesis referred to as Communication through Coherence (CTC) (Fries, 2005, 2009; Wildie and Shanahan, 2011). The theory is based on the the notion that oscillations in a neuronal population create small periods of time where input from another area of the brain will produce a greater reaction. Therefore, information flow is goverend by the relative phase of oscillations between different populations. In effect this theory states that neuronal populations only exchange information when oscillating in phase, and visa versa.

Buehlmann and Deco (2010) set up a test of the hypothesis by setting up two of the model, integrate-and-fire, neuronal networks described in section 2.1. The first network could connect to the second by forward connections to the second, and, to model the situation in the cerebral neocortex, there were also backprojections, typically set to be one third of the value of the forward connections. They were able to induce gamma oscillations in the range of 50–70 Hz in both networks by increasing the conductance of the short time constant (2 ms) AMPA receptor activated channels relative to the long time constant (100 ms) NMDA receptor activated channels.

In the present investigation, we set up a different experiment in which an external stimulus applied to one of two decision-making neuronal populations or pools of neurons could encourage the first network to take a decision, in which one decision pool reached a high rate. We then measured how the decisions taken by the second network depended on how strong the connections were from the first to the second network. In this way, we were able to measure the information transmission, using Shannon information theory, (Cover and Thomas, 1991; E. T. Rolls and A. Treves, 2011) to assess what information was transmitted from the first to the second network, and also the percentage correct performance of the same network. We were able to measure how this depended on whether there were oscillations in both of the networks, and we were also able to measure whether the transmitted information depended on or was influenced by whether the networks were coherent, and were phase-locked into synchrony. We were able to do this by not only measuring the neuronal spiking, but also by measuring the currents in the neurons, which provides a surrogate measure of the local field potentials, which are believed to be generated by these currents (Mazzoni et al., 2008).

5.2 METHODS

5.2.1 Two network experiment design

The network model consists of two parts (Figure 27). Network 1 (N1) is an attractor decision-making network that receives an external input λ_1 at $t = 1000$ ms that makes decision neuronal population or pool 1 (N1D1) win with a latency of approximately 500 ms. Pool N1D1 is connected to Net 2 decision pool 1 (N2D1) with forward connections w_f and backward connections w_b. w_b was set to be 1/3 of the value of w_f because this ratio was found to be effective in enhancing coherent oscillations by (Buehlmann and Deco, 2010). Both Net 1 and Net 2 were set up to have gamma oscillations by increasing the g_{AMPA} / g_{NMDA} factor to a low value of 0.12 (The short time constant of the AMPA receptors promotes oscillations, which are normally weak or absent at the normal ratio of NMDA to AMPA that we use as shown in Table 1 (Buehlmann and Deco, 2010; E. T. Rolls and Deco, 2010).)

The plan of the investigations was to increase the values of the connecting weights (w_f and w_b) between N1D1 and N2D1 from 0 upwards, to determine when N2D1 started to take the correct decision, and to examine how extensive measures of coherence, phase, and synchrony between the two networks were related to the amount of information transmitted, to the percent correct of Net 2, and of the latency of the decision in Net 2. The communication through coherence (CTC) hypothesis holds that communication is facilitated by coherence. The communication between Net 1 and Net 2 was being measured in these investigations by the information transmitted between the networks, by the percent correct of the second network, and by the latency of a correct response in Net 2. The advantage to testing this by simulation is that we have precise control over all the parameters that influence the operation of the system, and we can measure all the properties of the system. The aim is to show whether in this precise situation information transmission is facilitated by coherence. Whatever is found with the network is likely to be important in understanding effects measured in the brain. To make the results relevant to understanding cortical function, the model we investigate is an integrate-and-fire model with spiking neurons and dynamically modelled synaptic conductances, as described in detail in section 2.1.

Each network remains fully connected and has recurrent collateral synapses within Net 1 and Net 2 that are separate. Net 1 and Net 2 have separate populations of inhibitory neurons to ensure that the networks can oscillate separately if the weights w_f and w_j are zero.

Gamma oscillations in a network with excitatory and inhibitory neurons are generated through a pyramidal-interneuron feedback loop (Brunel and X.-J. Wang, 2003; Hansel, Mato, et al., 2001; Traub, Jefferys, and Whittington, 1997). Pyramidal neurons excite interneurons, and inter-neurons in turn send inhibition back on pyramidal cells. The population frequency is determined by the sum of excitatory and inhibitory lags. The recurrent excitatory connections tend to decrease the oscillation frequency (as compared to only excitatory-inhibitory and inhibitory-excitatory connections) as they tend to prolong the positive phase in each cycle. In our network we can therefore generate and control the oscillations in the gamma frequency band by adjusting the AMPA and NMDA con-

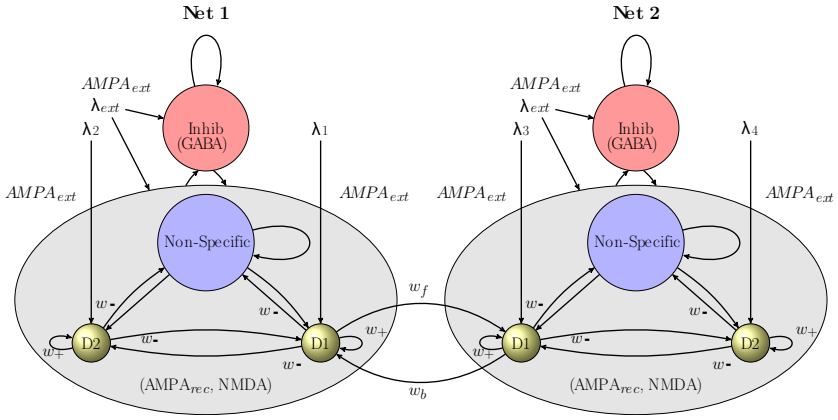

Figure 27: Schematic representation of the network. The network consists of two connected attractor decision-making nets, Net 1 and Net 2. There are feedforward (w_f) and feedback (w_b) connections between Net 1 and Net 2. Inputs are applied to Net 1 λ_1 and λ_2, which takes a decision with Net 1 decision pool 1 (N1D1) winning. Through the connections (w_f) Net 2 pool D1 is encouraged to win the competition in Net 2. The network allows information transmission from Net 1 to influence the decision made by Net 2 to be investigated, to determine how it is influenced by the connection strength (w_f) and whether there are oscillations in both Nets 1 and 2, which may be coherent or not. There are external inputs (λ_{ext}) to simulate the spontaneous activity being received from other neurons in the system. Each decision pool has strong recurrent connections (w_+) to enable the pool to act as part of an attractor decision-making net. The strengths of the other synapses are shown, and are described in the text.

ductances. For example, increasing the g_{AMPA} and decreasing g_{NMDA} shifts the balance in the network towards fast excitation (AMPA) and slow inhibition (GABA) and thus increases the gamma frequency band oscillations. The base conductances in our network are varied according to the following rule: $g_{NMDA} = g_{NMDA} - \beta g_{NMDA}$ and $g_{AMPA} = g_{AMPA} + 10\beta g_{AMPA}$. We refer to the parameter β as the g_{AMPA} / g_{NMDA} modification ratio. The factor 10 stems from the fact that near the firing threshold, the ratio of NMDA:AMPA components becomes 10 in terms of charge entry, as stated in (Brunel and X.-J. Wang, 2001). Therefore, in order not to change the spontaneous state, a decrease in g_{NMDA} is compensated by a tenfold increase in g_{AMPA}. All recurrent conductances (both inhibitory and excitatory) are changed according to this rule. Both Net 1 and Net 2 were set up to have gamma oscillations by reducing β to a low value of 0.1, from the normal default values for the g_{AMPA} and g_{NMDA} conductances shown in Table 1, as this reduction has been shown to produce good gamma oscillations in this network (Buehlmann and Deco, 2010). We refer to the default conductances shown in Table 1 as the NMDA case, and to the $\beta = 0.1$ case where the g_{AMPA} is doubled and the g_{NMDA} is reduced to 0.9 of the values shown in Table 1. Parameters that took different values than default are shown in Table 3. In our simulations, each Net contained $N = 1000$ neurons.

5.2.2 Analyses

Spectral analyses

We performed spectral analyses as described by Bendat and Piersol (2010) to analyze the oscillations and possible synchrony in the network. The analyses are described using their notation, and were implemented in MATLAB (version 2010a) using the cpsd function with the default values for the windowing and data sections to ensure that reliable averaged estimates were obtained on single trials. We do not showˆsymbols in the following to simplify the notation, as these averages were always used.) The number of points in the FFT was set for the analyses described to 256, and we checked carefully that the magnitudes and phases obtained were not altered if smaller values of 128 or 64 were used. The data for each analysis consisted of 512 ms of LFP data with 1 ms spacing. The data were obtained on each trial in a time period that started 12 ms before the decision in Net 2, unless otherwise stated (as oscillations were not present in Net 2 before this time, and this time was when the decision was being made). The finding that gamma oscillations are not present during spontaneous firing, and only start in Net 2 when the neurons increase their firing rates, is illustrated by the single trial type of analysis shown in Figure 30. Yet when the Net 2 D1 neurons selectively increase their firing rates, the decision has effectively been taken, that is the bifurcation has been crossed. This is one of the implications of the investigations described here: great care has to be taken using single trial analyses with neurophysiological data to measure exactly when the gamma oscillations start, and also when any synchrony starts that may be present, in relation to the time of the decision or more generally of the information transmission. e The value for LFP used is the sum of the absolute values of synaptic currents, a simple and effective method to generate realistic LFP recordings in excitatory and inhibitory networks (Mazzoni et al., 2008).

We computed the Power Spectral Density (PSD) ($G_x(f)$ for Net 1 D1, and $G_y(f)$) for the winning pool in Net 2. We computed the Cross-Spectral Density ($G_{xy}(f) = C_{xy}(f) - jQ_{xy}(f)$, where the real part $C_{xy}(f)$ is the coincident spectral density function, and the imaginary part $Q_{xy}(f)$ is the quadrature spectral density function. In the graphs we plot the magnitude of the cross-spectral density (CSM), $|G_{xy}(f)|$, as

$$|G_{xy}(f)| = \sqrt{C_{xy}^2(f) + Q_{xy}^2(f)} \tag{23}$$

and the phase as

$$\theta_{xy}(f) = \tan^{-1}\left[\frac{Qxy(f)}{C_{xy}(f)}\right]. \tag{24}$$

We note that synchrony is a state in which there is a fixed phase in the activity of the two systems (e.g. neural populations), that is when they are phase-locked. (The phase-locking need not be at zero phase.)

The coherence was calculated as

$$\gamma_{xy}^2 = \frac{|G_{xy}(f)|^2}{G_x(f)G_y(f)}. \tag{25}$$

This makes it clear that one can define an unnormalized coherence measure as the square of the magnitude of the CPSD, i.e. as $|G_{xy}(f)|^2$.

The above analyses provided the quantitative data for the conclusions reached. However, to visualize the timecourse of the spectral changes within a trial, to help determine the time within a trial in which to perform the spectral analyses just described, we also utilized Slepian multi-taper methods for spectrograms (i.e. spectral estimation as a function of time) (Fries, Womelsdorf, et al., 2008; Mazzoni et al., 2008). We used an optimal family of orthogonal tapers given by the discrete prolate spheroid sequences (Slepian functions) as described elsewhere (Fries, Womelsdorf, et al., 2008; Mazzoni et al., 2008), building on the MATLAB implementation of Partha Mitra modified by Ken Harris[1]. The length of the moving window was 256 ms. Examples are shown in Figure 30.

Spike-triggered average, STA; and cross Spike-triggered average, cross STA

We calculated the spike-triggered average (STA) of the local field potential (LFP) within a network, as this is found neurophysiologically to be a sensitive measure of oscillations. We also calculated the cross spike triggered average (cross STA) between for example the spikes in Net 1 D1 and the LFP in Net 2 D1, as the cross STA is a sensitive measure of synchrony between neuronal populations (Gregoriou et al., 2009).

STAs were calculated by averaging LFP segments $\pm$50 ms around every recorded spike. This was calculated in the same 512 ms timewindow used for the spectral analyses. To display more clearly the average relative phase of spikes, the STA was smoothed with a 5-point smooth. The cross STA was calculated in an analogous way. The surrogate for the LFP was the sum of the absolute values of the AMPA and GABA currents into a neuron in the pool being considered (averaged across all the neurons in the pool), as the LFPs are thought to reflect currents such as these. (We checked that the conclusions were not affected if the absolute values of the NMDA currents were included as well.)

The neuronal firing rates for each neuronal population were calculated as the average across a population of the firing rate in 50 ms sliding bins.

Mutual information analyses

The information transmission from Net 1 (pool N1D1) to Net 2 (pool N2D1) was measured by the Shannon mutual information. In the simulations where we have an attractor state reached in Net 2 (measured by the firing rates being 10 spikes/s higher in one of the decision pools than the other in a 500 ms period starting at the time when the firing rates diverged in N2D1 and N2D2), we can measure the mutual information between the stimulus s applied to Net 1, and the attractor state reached in Net 2, which we denote as s'. In Net 1, the attractor that wins (pool D1 or D2) was set to be D1 by setting input stimulus λ_1 to 3.11 and λ_2 to 2.99 Hz per external synapse (at the end of the spontaneous firing period in which both had been 3.00 Hz per external synapse), where there are $N_{ext} = 800$ synapses per neuron). For Net 2, information transmission is good

1 Made available under the GNU GPL at `http://osiris.rutgers.edu/BuzsakiHP/Downloads/downloads.html`

when N2D1 enters a high firing rate attractor state $s' = 1$ when s is 1. We measure the mutual information between the input stimuli s and the state reached in Net 2, s'.

In more detail, we constructed symbol vectors for each net if $\mathbf{s}$ and $\mathbf{s}'$, where each entry in the vector was 1 if pool D1 won a trial, and 0 otherwise. In other words, each element s, and s' are random variables which obey a probability distribution over the sample space $\{0, 1\}$. The information entropy for such a vector is equivalent to the binary entropy function:

$$H_b(s) = -p(s)\log_2 p(s) - p(1-s)\log_2 p(1-s) \tag{26}$$

where $p(s)$ is the probability of a N1D1 winning trial, which we can approximate by analyzing the trial data from simulations. In the analyses presented in this chapter we set this probability to be $p(s = 0) \equiv p(s = 1) \equiv 0.5$ by modifying the pool index for the winning pool in Net 1 and also the corresponding pool in Net 2 to study a situation with a maximum entropy of one bit. We know from information theory that entropy describes the amount of uncertainty in a signal, and the maximum uncertainty of a binary entropy function is one bit.

The conditional entropy of Net 2 the same corresponding pool activate as Net 1 is defined in standard information theory terms as

$$H(s|s') = \sum_{j\in s}\sum_{i\in s'} p(s_j, s'_i)\log_2 \frac{p(s_j)}{p(s_j, s'_i)}, \tag{27}$$

where $p(s'_1) \equiv p(s' = 1)$ ($p(s'_0) \equiv p(s' = 0)$) is the probability of a Net 1 successfully (unsuccessfully) communicating with Net 2, by the same decision pool number activating. In our analysis, we measured the firing rates for the decision pools in Net 2 in the 500 ms period of $t = 1{,}500 - -2{,}000$ ms on each trial, and compared it to the winning rate in Net 1. The probability of s' was then calculated from frequency that successful communication occurred. Conditional entropy describes how much uncertainty is in a signal, given that we know the value of another signal. Here we apply these values to calculate the mutual information, which in our case describes how much knowing the state of Net 1 refines our guess of Net 2's decision.

$$I(s, s') = H(s) - H(s|s') = 1 - \sum_{j\in s}\sum_{i\in s'} p(s_j, s'_i)\log_2 \frac{p(s_j)}{p(s_j), p(s'_i)} \tag{28}$$

This equation has the following properties: if s and s' are the same random variable, i.e if information is always transmitted, their conditional entropy will be equal to zero, and the mutual information will be equal to one; if on the other hand s and s' are both independent the mutual information will be equal to zero. We calculated the mutual information from simulation vectors $\mathbf{s}$ and $\mathbf{s}'$ using MATLAB routines in the Information Theory Toolbox v1.0.[2] The decision time was measured on each trial as the difference in the latency for Net 1 to reach its

2 http://www.mathworks.com/matlabcentral/fileexchange/17993-information-theory-toolbox-v1-0

attractor state and Net 2 to reach its attractor state. The criterion for being in an attractor state was that the firing rate in one of the decision pools (D1 versus D2) had to be more than 10 spikes/s on average for each neuron than in the other pool, in a 500 ms period.

Network parameters		
$w_+ = 2.1$	$w_- = 0.877$	$w_I = 0.877$
$w_b/w_f = 1/3$	$N_E = 800$	$N_I = 200$
$N_{ext} = 800$	$\lambda_{ext} = 3.0$ Hz/synapse	

Table 3: The default parameter set used in the two network simulations

5.3 RESULTS

5.3.1 Information transmission between two coupled networks

A single trial of a simulation for the AMPA case (prone to gamma oscillations) is shown in in Figure 28. This illustrates that after a 1 s period of spontaneous activity, the decision cues were applied to Net 1, which took the correct decision that Net 1 should win, with a latency of approximately 400 ms. The forward connection weights w_f from pool N1D1 to pool N2D1 in this case were 0.03, and these were sufficiently strong for information to be transmitted to Net 2 pool D1 (N2D1) and for it then to win the competition in Net 2 and enter a decision attractor state with a high firing rate. Figure 28b shows the average (over 50 ms) of the firing rates of the neurons in the D1 pools of both networks. (The rapid increase of rate from a mean of 3 spikes/s in the spontaneous period to approximately 75 spikes / s when a decision has been made illustrates that an increase by 10 spikes/s from the spontaneous rate is a good criterion for a decision.) The spiking nature of the activity is illustrated in the rastergrams in Figure 28a.

The spectral analyses for the same trial are illustrated in Figure 28c. The Power Spectral Density (PSD) for the local field potential in Net 1 D1 showed that there is no gamma activity in the spontaneous period, when the mean firing rates of the neurons in the excitatory neuron pools is 3 spikes/s. The power spectral density only increased in the gamma band when the D1 neurons started to fire with high firing rates in response to their inputs, reflecting what is found neurophysiologically (Fries, Womelsdorf, et al., 2008). Similarly, the Power Spectral Density (PSD) for the local field potential in Net 2 D1 showed that there is no gamma activity in the spontaneous period, when the mean firing rates of the neurons in the excitatory neuron pools is 3 spikes/s. The power spectral density only increased in the gamma band when the Net 2 D1 neurons started to fire with high firing rates in response to the inputs received from Net 1. This immediately raises a fundamental question: how could oscillations contribute to the information transmission if they do not become established until information transmission has increased the firing rates?

Next, Figure 28c shows that the coherence between the N1D1 and N2D1 populations remains low throughout the trial. This indicates that although both N1D1

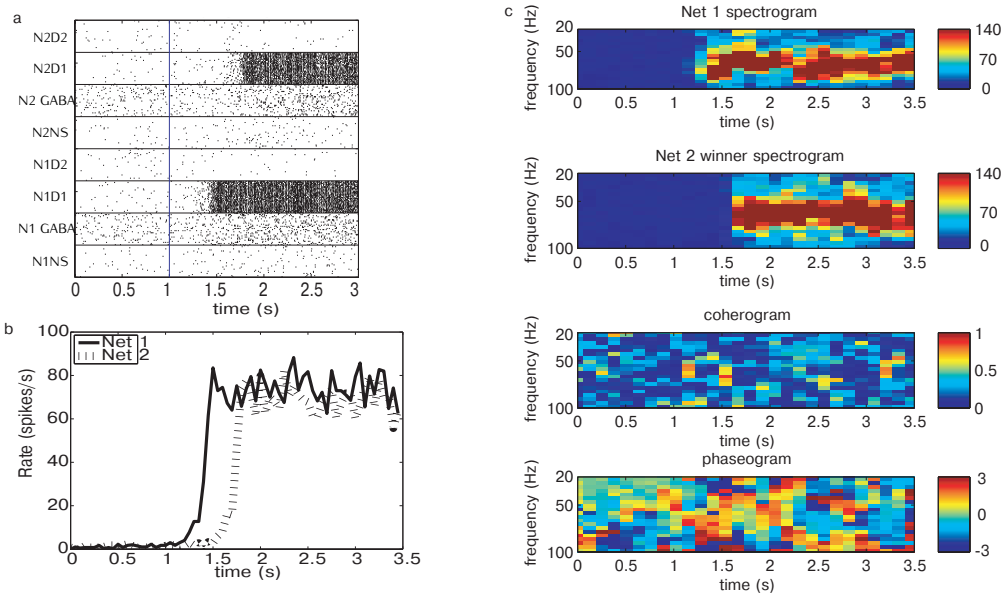

Figure 28: (a) Rastergram of the spiking activity of each pool from a single trial of the simulation to illustrate the responses of the network in the AMPA case as a function of time. The decision cues for Net 1 were switched on at $t = 1.0$ s and stayed on for the remainder of the trial. $w_f = 0.03$. Net 1 took its decision at 1.4 s, and Net 2 at 1.7 s. Each row of the rastergram providing the spike times for one of 30 neurons in each pool, with pool labels on the left side of the figure. There is a 1 s period of spontaneous activity from 0–1 s, and then the decision cues are applied to the neurons in pools D1 and D2 of Net 1 for the remainder of the trial. The lower four pools are for Net 1. NS: non-specific excitatory. GABA: inhibitory. D1, D2: the decision pools for Net 1. The upper four pools are for Net 2, with the pool names preceded by N2. (b) The firing rates of the D1 neurons in Net 1 and in Net 2. (c) The spectral analyses for this trial. Top: Power Spectral Density (PSD) for the LFP in Net 1 D1. Next: Power Spectral Density (PSD) for the LFP in Net 2 D1 Bottom: Phaseogram between Net 1 pool D1 and Net 2 pool D1.

and N2D1 have gamma oscillations when their firing rates are high (as shown by their PSDs), the oscillations were without any fixed phase relationship. (A case for comparison which does show coherence building up is in Figure 29a, the AMPA case with $w_f = 0.45$.) Similarly, the phaseogram at the bottom of Figure 28c also shows no fixed phase in the gamma band between the gamma oscillations in N1D1 and N2D1. (Again, a case for comparison which does show phase locking is in Figure 29a, the AMPA case with $w_f = 0.45$.) The generic results shown in Figure 28 are prototypical for the operation of the networks, confirmed over thousands of trials with the averaged data illustrated in the next few figures. First, gamma oscillations only become clearly evident when the neurons leave their spontaneous firing rate state and are driven by inputs to reach high firing rates. Second, at low values of w_f, in the AMPA case oscillations are present in both Net 1 and Net 2, but there is no coherence between the oscillations in the two nets, no fixed phase relationship. Thus information has been transmitted from Net 1 to Net 2, and the firing rates in Net 2 D1 increased

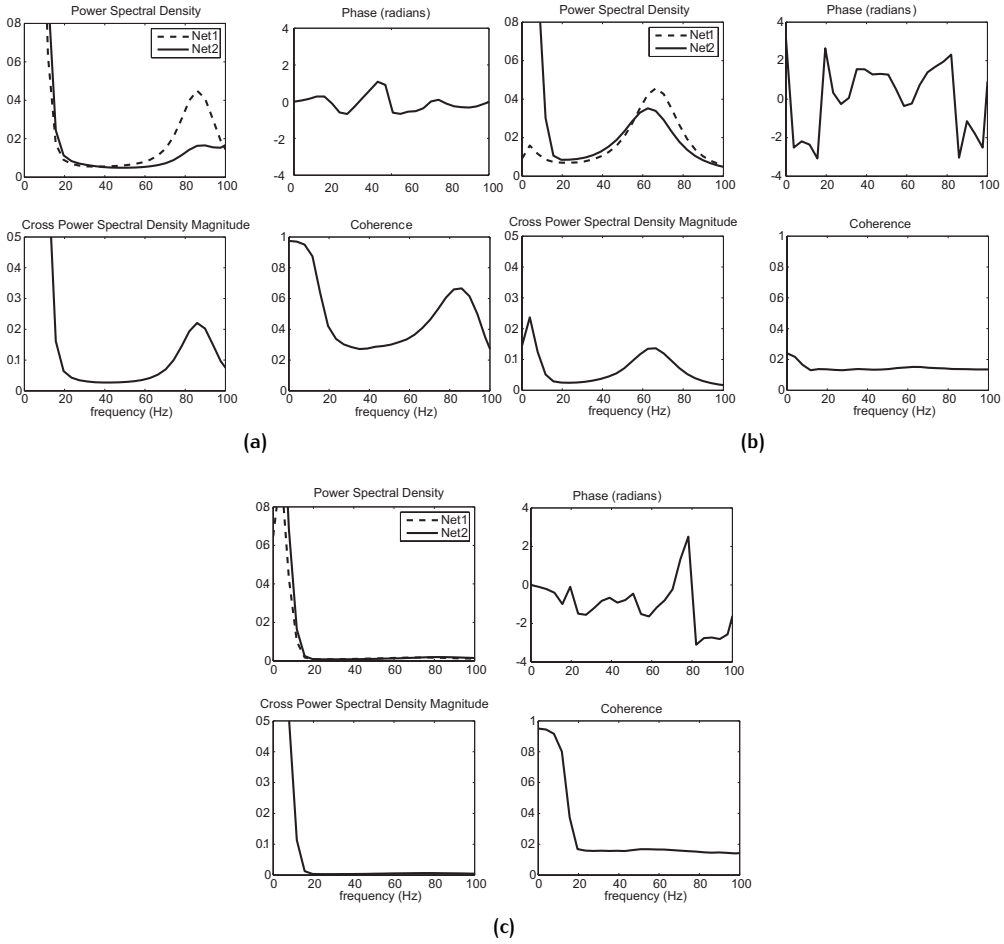

Figure 29: LFP frequency analyses for (a) the AMPA case with $w_f = 0.45$, (b) the AMPA case with $w_f = 0.021$, and (c) the NMDA case with $w_f = 0.45$. The abscissa is the frequency in Hz. The spectra are for the 500 ms time period in which the decision is made. Each set of plots shows:
Power Spectral Density: LFP power in Net 1 D1 and Net 2 D1, the winning pool;
Cross Power Spectral Density Magnitude: the square of this is the unnormalised coherence;
Phase: phase (radians) between the LFPs in Net 1 D1 and Net 2 D1 (In the 0.45 AMPA case shown in (a), the phase between the spikes in Net 1 D1 and Net 2 D1 was very close to 0 radians;)
Coherence: coherence between the LFPs in Net 1 D1 and Net 2 D1.
The results are each averaged over 1,000 trials, except for the phase which will be for a single trial.

relative to those in Net 2 D2, yet this occurred without coherent oscillations between the two networks, which, as we shall see, only become established at much higher values of w_f than are needed for information transmission from Net 1 to Net 2.

Next, further analyses of the performance found on single trials with the different types of simulation are shown in Figure 29 and Figure 30 to illustrate the operation of the network.

Figure 29 shows local field potential (LFP) frequency analyses for (a) the AMPA case with $w_f = 0.45$, (b) the AMPA case with $w_f = 0.03$, and (c) the NMDA case. The spectra are for the 500 ms time period in which the decision is made. The AMPA case refers to simulations where the g_{AMPA}/g_{NMDA} ratio β was set to 0.1 to emphasize AMPA at the expense of NMDA conductances, and to promote oscillations in the gamma range. Figure 29a shows that with $w_f = 0.45$, oscillations were present in both networks Net 1 and Net 2 in the gamma range of 50–100 Hz as shown by the Power Spectral Density analyses (for the LFP power in Net 1 D1 and in Net 2 D1, the winning pool). (Although most of the power was in the gamma range of 50–80 Hz in most simulations, it was found that with $w_f = 0.45$ the frequency was a little higher, and hence the larger frequency range was used for the quantitative analyses.) The Cross Spectral Density Magnitude (CSM) was large in the gamma range. At this value of $w_f = 0.45$, the phase (measured in radians) between the LFPs in Net 1 D1 and Net 2 D1, was locked close to zero. (In fact, not illustrated, the phase between the spikes in Net 1 D1 and the spikes in Net 2 D1 was very close to 0 radians, and the LFP phase illustrated corresponds to this case.) The coherence between the LFPs in Net 1 D1 and Net 2 D1 was high in the gamma range. In this case of AMPA domination and $w_f = 0.45$, oscillations occurred in both Net 1 and Net 2, and were locked in phase. This was a true case of synchrony and coherence. Figure 29b shows that in the AMPA case where β was set to 0.1, gamma oscillations were still present in Net 1 and Net 2 (as shown in the Power Spectral Density analyses illustrated in Figure 28c), but with the lower value of $w_f = 0.03$, the coherence between the LFPs in Net 1 D1 and Net 2 D1 was low in the gamma range, and so was the Cross Spectral Density Magnitude. Moreover, the phase in the gamma range was no longer close to zero, and was very variable within a trial and across trials. These measures indicate that with this weaker value of the forward coupling, synchrony was no longer present. [We note here that on single trials the Cross-Spectral Magnitude (which when squared forms the unnormalised coherence) was a better measure of coherence on a single trial than the coherence measure itself, as the coherence measure is normalised by the product of the PSDs of the two timeseries, and so can take high and misleading values when either or both PSDs are low, that is when either Net 1 and/or Net 2 is not oscillating. This is an important point when interpreting neurophysiological studies that report coherence. We further note that coherence indicates whether repeated estimates (in our case, measures repeated at different times in the 500 ms analysis window) of the cross-spectrum have consistent phases, but does not indicate whether the phase is zero. We further note, as shown in Figure 31d, that the cross-spectral magnitude measure does not take a zero value when the two networks are not coupled by synapses.]

Figure 29c shows that in the NMDA case where the β factor was set to its normal value for investigations of this network as shown in Table Table 3, no

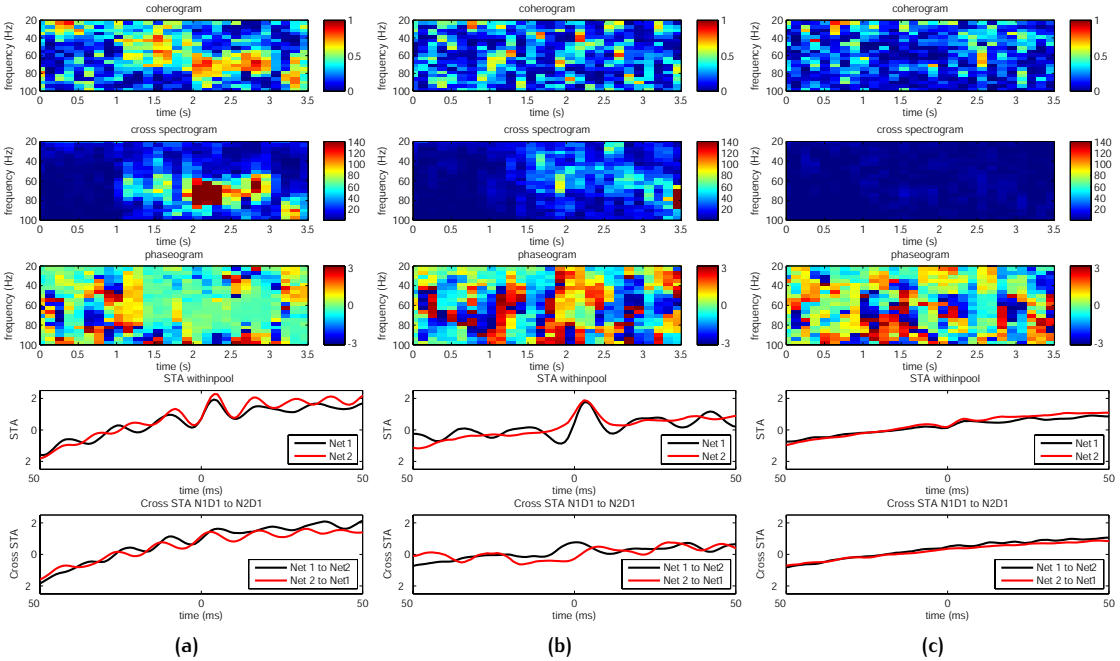

Figure 30: Spectral analyses as a function of time for a single trial. (a) the AMPA case with $w_f = 0.45$. (b) the AMPA case with $w_f = 0.03$. (c) the NMDA case. Top 3 plots, the abscissa is trial time is s, and the abscissa is the frequency in Hz. The frequency analyses are for the 500 ms time period in which the decision is made. Each plot shows:
Top: coherogram between the LFPs in Net 1 D1 and Net 2 D1;
Plot 2: cross spectrogram between the LFPs in Net 1 D1 and Net 2 D1;
Plot 3: phaseogram between the LFPs in Net 1 D1 and Net 2 D1. (In the 0.45 AMPA case shown in (a), the phase between the spikes in Net 1 D1 and Net 2 D1 was very close to 0 radians;)
Plot4: Black: the spike-triggered average (STA) between the spikes in Net 1 D1 and the LFPs in Net 1 D1; Red: The STA between the spikes in Net 2 D1 and the LFPs in Net 2 D1. Plot5 Black: the cross spike-triggered average (cross STA) between the spikes in Net 1 D1 and the LFPs in Net 2 D1; Red: The cross STA between the spikes in Net 2 D1 and the LFPs in Net 1 D1.

gamma oscillations were present in Net 1 and Net 2 (as shown by the PSDs). Accordingly, even with the high value of 0.45 for w_f the Cross-Spectral Density Magnitude (CSM) was very low in the gamma range and the gamma range phase was variable and not locked close to 0 (though, as in Figure 29b the coherence was not an especially good indicator of the lack of phase coupling in the gamma range due to its normalisation by the PSDs). Thus there is no synchrony in the NMDA case of the two networks, and no oscillations.

These analyses were extended to show how the oscillations and synchrony if present developed during the time course of a trial using Slepian filters. Results of typical trials are shown in Figure 30. Figure 30a shows the analyses for the AMPA case with $w_f = 0.45$. On the trial illustrated, with this strong forward coupling w_f of 0.45 (and backward coupling w_b set to 1/3 of this as for all

the results described), Net 1 took its decision at approximately 150 ms after the decision cues were applied, i.e. at 1,150 ms into the trial, and Net 2 took its decision at approximately the same time. The cross spectrogram for the LFP showed an increase at approximately the time of the decision, that is, when the neurons fired fast as they entered the attractor. The oscillations in each of the networks evident in the firing rates increased at approximately the same time (not illustrated), that is, the spontaneous firing rate did not support significant gamma oscillations. The coherogram also showed an increase at the decision time. [When interpreting the exact timing of events in Figure 30, it is important to appreciate that the time window in which the Slepian filters operated was 256 ms of data, with the results plotted at the start of that time window. The values plotted at a point in time thus reflect what happened in the following 256 ms.] The phase analysis shown in Figure 30a shows that the phase of the LFPs in Net 1 D1 and Net 2 D2 actually became locked close to 0 radians from about 1.4 s into the trial, that is, after the decision had been taken in both networks. The spike triggered average (STA) within Net 1 D1 (i.e. the relation between the spikes in N1D1 and the LFP in N1D1) calculated in the 500 ms period starting at the time at which the decision was taken showed a significant peak close to 0 ms, reflecting coupling between the spikes and the LFPs. (The strong oscillations are indicated by further peaks away from the central peak.) The same strong STA effect occurred in N2D1, the winning pool in Net 2. The cross STA from Net 1 to Net 2, and vice versa, also indicate the strong phase-linked coupling between the networks. (The cross STA from Net 1 to Net 2 shows the LFP in Net 2 D1 that is related to a spike in Net 1 D1, during the 500 ms decision period.) It is important to note that none of the measures described showed any relation to the decision-making if they were taken in the period before Net 2 took its decision as indicated by an increase of firing rate in one of its decision pools, even immediately before.

Figure 30b shows the analyses for the AMPA case with $w_f = 0.03$ for a typical single trial. On this trial, Net 1 took its decision at approximately 400 ms after the decision cues were applied, i.e. at 1.4 s into the trial, and Net 2 took its decision approximately 300 ms later. (The decision time for Net 2 was thus 300 ms). The cross spectrogram for the LFP (scaled to the same maximum as in Figure 30a) showed a small increase in the gamma range at approximately the time of the decision in Net 2, that is, when the neurons fired fast as they entered the attractor, but the coherogram showed little change, and there was no phase locking evident in the gamma range. The oscillations in each of the networks evident in the LFPs increased to high values in each of the networks at approximately the same time (not illustrated), and are evident in the STA analyses shown in Figure 30b The cross STA from Net 1 to Net 2, and vice versa, also indicate only weak phase-linked coupling between the networks. Thus in this case, strong oscillations were present in each of the networks separately, but with this lower value of $w_f = 0.03$ there was no phase-locking or synchrony between the two networks Net 1 and Net 2.

Figure 30c shows the analyses for the NMDA case with $w_f = 0.45$ for a typical single trial. On this trial, Net 1 took its decision at approximately 300 ms after the decision cues were applied, i.e. at 1.3 s into the trial, and Net 2 took its decision approximately 50 ms later. The cross spectrogram for the LFP (scaled to the same maximum as in Figure 30a) showed no effects, the coherogram

showed no change, and there was no phase locking evident in the gamma range. There were no gamma oscillations in either of the networks, and this is evident in the STA analyses shown in Figure 30c The cross STA from Net 1 to Net 2, and vice versa, also indicate no phase-linked coupling between the networks. Thus in this case, no gamma oscillations were present in each of the networks separately, and even with a high value of $w_f = 0.45$ there was no gamma phase-locking or synchrony between the two networks Net 1 and Net 2.

The time course analysis of the spectra based on the local field potentials (LFPs) in Figure 30 shows that the oscillations started in a network at approximately the time that a network took a decision for one of its attractor pools to fall into a high firing rate decision state. As the gamma oscillations were not apparent before this time, the analyses described next using 1000 trials for each data point started at the time that the second Net took a decision, and were for a 500 ms period. We did perform analyses for earlier periods, including 400 ms before the decision in Net 2 was reached until 112 ms after the Net 2 decision was taken, but no gamma oscillation-related effects were found, as there were no gamma oscillations evident even in the LFPs before the decision was reached in Net 2, as illustrated in Figure 28c. In particular, when the coherence between Net 1 and Net 2 was measured in the period before Net 2 took a decision (in fact, in the 512 ms period starting 400 ms before Net 2 responded), there was no measurable coherence different from that in uncoupled networks that could have influenced the decision in Net 2.

Then analyses based on 1,000 trials for each data point are shown in Figure 31. The operation of the system as a function of the forward connection strength w_f is shown in Figure 31. The spectral analyses were set to include the gamma frequency band in the range 50–100 Hz in which oscillations were induced in the networks when β was increased (the AMPA case). The information transmitted (Figure 31a) and the percent correct (Figure 31b) increased as w_f was increased from a low value of 0.015 up to a value of 0.09, by which value the information transmission saturated at 1 bit (perfect decision-making by Net 2) and the percent correct saturated at 100%. The information transmission and percentage correct curves as a function of the forward connection strength w_f were indistinguishable for the AMPA (gamma oscillating) and NMDA (non-gamma-oscillating) cases. Results are shown for values of w_f of 0, 0.015, 0.03, 0.045, 0.06, 0.09, 0.15 and 0.45.

Figure 31c shows that the oscillations in Net 1 and 2 in the AMPA case were almost independent as indicated by the gamma band coherence measure for the whole range of w_f values up to and including 0.09, the range in which the information transmission was shown to be taking place to reach saturation. Moreover, the measured coherence in this range was almost identical to that for the NMDA case (Figure 31c). [Because coherence is normalized by the power, the values can be similar for the NMDA case without much gamma power and the AMPA case with much gamma power. The coherence provides a measure in the range 0–1 of whether there are consistent phase relations in the different samples, in this case trials, between Net 1 and Net 2. The cross-spectral magnitude (CSM) shown in Figure 31d does reflect the un-normalized gamma power. As shown in the Methods, the square of this is the unnormalised coherence, and was a particularly useful measure on single trials in these analyses, as a high value indicated significant power in both Nets 1 and 2, as well as coherence.] In

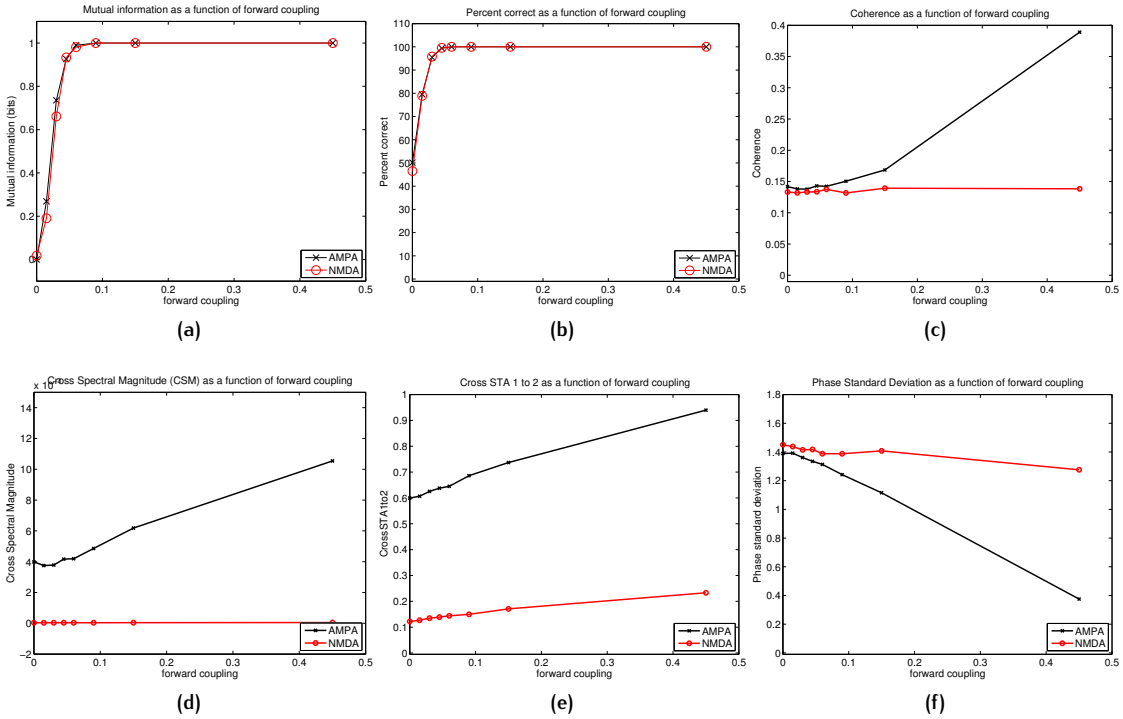

Figure 31: Performance of the network as a function of the value of the forward coupling weight w_f. The spectral analyses were set to include the gamma frequency band in the range $50 - 80$ Hz in which oscillations were induced in the networks when the β ratio was increased (the AMPA case). The NMDA case is with the normal value ratio of β as shown in Table 1.
(a) Information transmission between Net 1 and Net2. The measure is Shannon mutual information.
(b) Percent correct for Net 2.
(c) Coherence between Net 1 and Net 2.
(d) Cross-Spectral Density Magnitude (CSM) between Net 1 and Net 2.
(e) Cross Spike Triggered Average Net 1 (spikes) to Net 2 (LFP).
(f) The standard deviation of the phase in the gamma frequency band across trials. The low standard deviation at $w_f = 0.45$ for the AMPA case reflects phase-locking.

the AMPA case, the coherence only increased significantly for high values (relative to those needed for information transmission) of w_f of 0.15 and 0.45. Also in the AMPA case, the unnormalised coherence also only increased at values of w_f greater than 0.09, by which value information transmission was almost perfect. The implication is that information transmission can occur in the network at much lower values of connection strength than those necessary to support coherent oscillations between the networks. *It is in this sense that there is communication before coherence, that is before the connections are sufficiently strong to support coherent oscillations.* That analysis is supported by the cross spike triggered average (cross STA) between spikes in Net 1 D1 and the LFP in Net2 D1 shown in Figure 31e, which is a sensitive measure of synchrony between neu-

ronal populations (Gregoriou et al., 2009). The cross STA for the AMPA case at $w_f = 0$ indicates what would be measured by chance, and the measure shows only a small increase for values of w_f of 0.09 by which information transmission saturates. The major part of the increase of the cross STA, reflecting increasing synchrony, occurs for w_f values in the range 0.09–0.45. The cross STA is much smaller in the NMDA case, reflecting the fact that in this case there are no clear LFP oscillations in Net 2 to be in synchrony or not with spikes in Net 1. This measure thus indicates that coupling of gamma oscillations between the networks only becomes large after information transmission has saturated (the AMPA case), and is essentially absent in the NMDA case even though information transmission is perfect.

The analysis is also supported by the phase analysis shown in Figure 31f. The standard deviation of the phases across trials is large (close to 1.6 radians) when there is no coupling between the networks, and remains high in the NMDA case when w_f is increased. In the AMPA case, significant phase locking only becomes evident at the very large connection strength w_f value of 0.45, far beyond the value of 0.015 at which significant information transmission occurs, and the value of 0.09 at which the information transmission saturates.

The decision times as a function of the forward coupling w_f in Figure 32a show that the major decrease in the decision time took place for values of $w_f <= 0.06$. Within this range, for the AMPA condition the coherence hardly changed, as shown in Figure 31c. Similarly, the Cross Spectral Magnitude changed very little within this range of values of $w_f <= 0.06$ (Figure 32b). This is the range within which information was being transmitted between Net 1 and Net 2. At higher values of w_f the CSM increased in the AMPA case, and the decision time decreased, as shown in Figure 32b. However, this effect was just related to the somewhat higher firing rates that were present in the AMPA than in the NMDA case, as shown in Figure 32c. (It is well established that factors that increase the firing rates of an attractor decision-making network decrease the decision times (E. T. Rolls, Grabenhorst, and Deco, 2010a,b).) In fact, taking a particular value of the firing rate such as 60 spikes/s in Figure 32c, it is seen that the decision time is in fact faster in the NMDA (non-oscillating) than in the AMPA (oscillating) case. Thus the presence of oscillations did not speed decision times in this set of coupled networks. Further, taking the two highest values of w_f, 0.45, produced similarly fast decision times in the NMDA and AMPA networks (Figure 32a), though the AMPA network when in its synchronous firing state had much higher firing rates (Figure 32c). (The fact that the firing rates when in the attractor state were higher in the AMPA case indicates that the compensation for the g_{AMPA} vs g_{NMDA} change in the AMPA-case networks described in the Methods, which was designed to make the spontaneous firing rates similar when the β ratio was changed, did not achieve this for the much higher firing rates when in the attractor state.) Moreover, the decision times did not depend on the oscillations per se, as shown by the decision times in the NMDA case, which were independent of the gamma range cross-spectral magnitude which remained close to 0 for all decision times in the NMDA case (Figure 32b).

Further evidence that the decision times within the range of values of w_f that influenced information transmission did not depend on coherence is provided by the phase analysis shown in Figure 32d for $w_f = 0.03$. This shows for 1,000

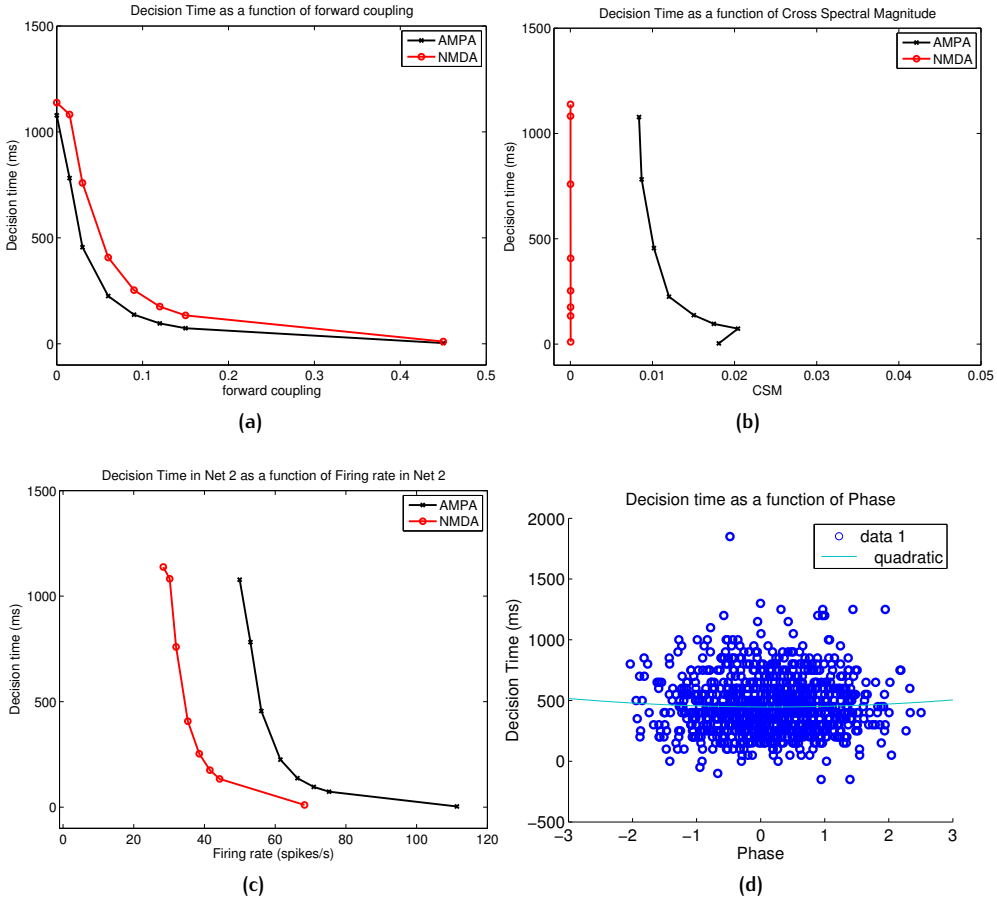

Figure 32: Decision time for Net 2 as a function of (a) the value of the forward coupling weight w_f, (b) the Cross-Spectral Density Magnitude (CSM), and (c) the firing rate in the winning pool in Net 2. (d) The relation between the decision time and the gamma phase relation (radians) between Net 1 and Net 2 for 1,000 trials with $w_f = 0.03$. A quadratic fit is shown.

trials that the decision time was not a function of the gamma phase that happened to be present between Net 1 and Net 2.

The implication is that the speed of information transmission, and information transmission itself, do not depend on coherence, or synchrony (phase locking) between two weakly coupled attractor networks in which the coupling is nevertheless sufficiently strong to support information transmission to 100 percent correct between the two networks. The small increase in coherence at higher values of w_f than 0.06, and even the phase locking at $w_f = 0.45$, appear just to reflect the stronger connections between Net 1 and Net 2, after information transmission has almost saturated.

It must be emphasized that we are considering here the transmission of information about an external stimulus (λ_1) through one Net (1) to a second (Net 2). This is not what was studied in previous work in which effectively the influence of oscillations in one network on oscillations in a second network has been

shown to be phase-dependent, at least at high values of w_f (Buehlmann and Deco, 2010). Indeed, a considerable part of the literature on oscillations involving LFPs and also spiking has measured this type of influence, for example by the correlation between two networks as a function of phase (Fries, 2005, 2009). We are concerned with a different type of information transmission, about external events through brain networks, in this chapter.

5.3.2 Information transmission when the phase between two coupled networks is externally controlled

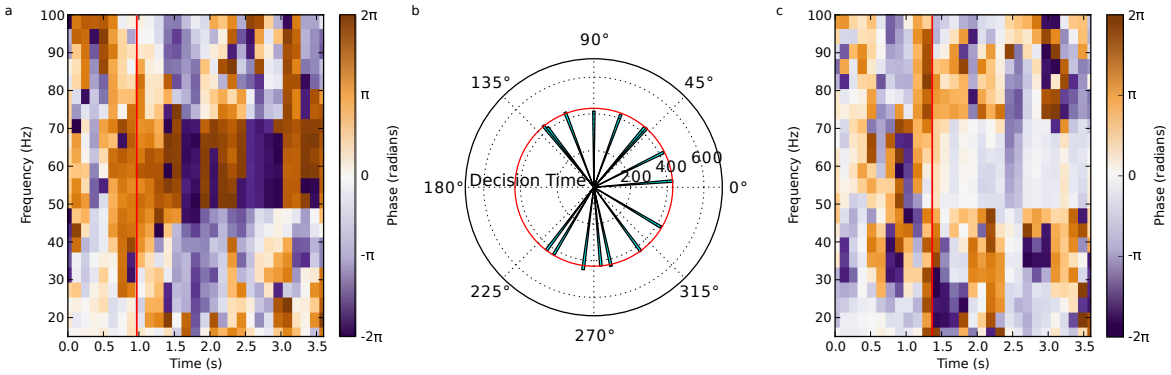

Figure 33: Decision time with phase control (N1D1–N2D1). (b) Polar plot showing the mean decision time (ms) (across 1,000 trials) as a function of the relative phases of Net 1 D1 to Net 2 D2 produced by 60 Hz sine waves applied to the neurons in Net 1 D1 and Net 2 D1. (a) Phase at different frequencies as a function of time in the trial, showing that after the decision cues and the external sine waves are applied with a phase of 180 degrees starting at 1,000 ms, the relative phases of the firing rates of N1D1 and N2D2 are well separated. (c) Phase at different frequencies as a function of time in the trial, showing that after the decision cues and the external sine waves are applied with a phase of 0 degrees starting at 1,000 ms (red line), the relative phases of the firing rates on N1D1 and N2D2 are close to 0 degrees apart. Phase control of the firing of N1D1 and N2D2 did not affect the decision times. w_f was 0.021.

The results described above show that the information transmission occurs at values of the coupling w_f that are much smaller than those needed to produce marked coherence or synchrony. We were nevertheless interested to investigate whether the relative phases of Net 1 and Net 2, if coherence was present, might influence the information transmission or the decision time. We therefore ran further simulations where the external input to particular pools of neurons had a 60 Hz sine wave modulating it. The modulation had a mean value of 0 (i.e. it was a modulation and not an addition) and amplitude (peak to peak) equivalent to 0.4 spikes/s per synapse (in the context that the external input apart from this was typically 3.05 spikes/s per synapse). This modulation value of 0.4 spikes/s per synapse was sufficient to influence the firing rates of the neurons in a pool, and to influence the phase plots of the firing rates and the LFPs, as

will be shown. This value was also chosen to be relatively small, so as not to impair the ability of the connections w_f between the two networks to produce information transmission.

Figure 33 shows a case in which we achieved phase control in this way of the firing times of neurons in Net 1 D1 and Net 2 D1. The phase control achieved is shown in Figure 33a (the phase applied was 180 degrees apart) and Figure 33b (0 degrees). Figure 33b is a polar plot showing that the mean decision time (ms) (across 1,000 trials) as a function of the relative phases achieved in the network of N1D1 vs N2D1 did not affect the decision times. w_f was 0.015, a value that does not saturate information transmission, so that the network is sensitive to its important parameters. There was no effect either of the relative phases on the information transmitted or percentage correct. Thus in this well controlled system of two networks, even when the phases of the two networks were locked by artificial external control firing rates applied to each network, the phase, and whether synchrony was present (as it was at 0 degrees), had no influence on the communication between the networks. Consistent results, of the phase having no effect on decision times, were obtained with $w_f = 0.15$, and in this case the decision times were approximately 70 ms.

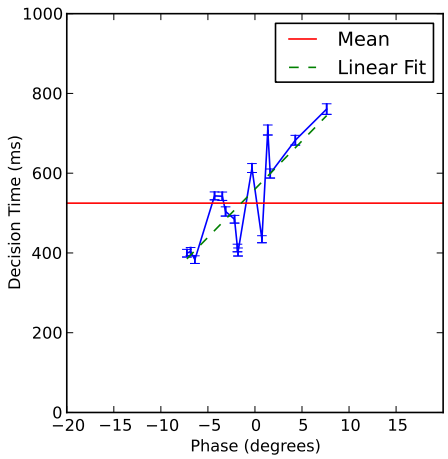

Figure 34: Decision time with phase control (N1D1–N2GABA). Polar plot showing the mean decision time (ms) (across 1,000 trials) as a function of the relative phases of the firing rates in pools N2D1 and N2GABA. The phase shift was achieved by applying 60 Hz sine waves to the neurons in Net 2 pool 1 (N2D1) vs the Net 2 GABA pool (N2GABA). w_f was 0.15.

5.4 DISCUSSION

One of the important conclusions is that information transmission between coupled cortical networks may occur at values of the interconnection strengths between the networks that are much lower than those necessary to induce synchronization. This is shown by the results in Figure 31b and Figure 31c. Fig-

ure 31b shows that the percentage correct of the second network rises to very close to 100% correct whereas the coherence remains at the 'chance' value that is measured when there is no coupling at all between the networks ($w_f = 0$, the first point on the x axis) for values of w_f up to 0.09 (the first three data points greater than 0 in Figure 31). In this sense communication occurs before coherence. The point is fully supported by the information transmission values shown in Figure 31a. Coherent oscillations only occur when much higher values of the synaptic coupling strength between the networks is present, e.g. $w_f = 0.45$ (Figure 31c). Thus information transmission between coupled networks that model pairs of interconnected networks in the same cortical area or in different cortical areas occurs at much lower values of the synaptic coupling strengths than are necessary to induce synchrony of gamma oscillations.

We emphasize that we are investigating a biologically realistic situation in which there are firing rate differences between the neuronal populations that are part of the encoding of the information to be transmitted, for differences in firing rates between different neurons are part of the normal representation of information in cortical areas including the inferior temporal visual cortex, hippocampus, orbitofrontal cortex, anterior cingulate cortex, and insular taste cortex (E. T. Rolls, 2008; E. T. Rolls and A. Treves, 2011). Hence, if one were to argue that coherence was only important in information transmission when there were no firing rate differences in the transmitting populations of neurons representing the different stimuli, the hypothesis would be so restrictive that it would apply to rare cases in the cerebral cortex.

Another important conclusion is that even when synchrony was artificially induced by external inputs, the information transmission between the two coupled networks and the speed of response were not influenced by the phase of their gamma oscillations (Figure 33). In a positive control condition, we were able to show that the relative phase of the gamma oscillations between the GABA inhibitory interneurons and the excitatory cells within the *same* network did influence the decision time (Figure 34).

Another conclusion is that the same findings and conclusions follow for neural systems that have quite different dynamics and fluctuations. In the AMPA case when there are gamma oscillations and the dynamics are fast, the result was that the information transmission between the coupled networks was not affected by the coherence in the gamma range of the two networks. In the NMDA case where the dynamics are slower and there are no gamma oscillations, information transmission occurred in quantitatively the same way as when there were oscillations in the AMPA case, as shown by the similar percentage correct and information transmission in the AMPA and NMDA scenarios as a function of the synaptic coupling w_f between the networks (Figure 31).

We note that three ways have been described of producing synchrony in a single network or 'cortical minicolumn' (Tiesinga and Sejnowski, 2009). First, by inheritance of synchrony from previous areas via the feedforward projection; second, by activation of inhibitory networks via the interneuron gamma (ING) mechanism; and third, by activation of reciprocally connected networks of excitatory and inhibitory neurons via the pyramidal-interneuron gamma (PING) mechanism within a single network (Tiesinga and Sejnowski, 2009). However, the results of such analyses (Tiesinga and Sejnowski, 2009) apply to what happens within a single network (or minicolumn), for example within Net 2 in

Figure 27. We instead in this chapter examine a different and new situation higly relevant to cortical function, the information transmission between two networks (Net 1 and Net 2 in Figure 27) or minicolumns.

The results found here show the way in which the information transmission between two coupled networks is influenced by the strength of the associative synaptic coupling w_f between the two networks (Figure 31a and Figure 31b). Relatively weak synaptic connections between the two networks relative to those within the network required to maintain an attractor state are sufficient for the information transmission. Whether the network is having gamma oscillations (the AMPA dominated case) or not (the NMDA case) does not influence the information transmission (Figure 31a and Figure 31b). Thus oscillations, coherence, and synchrony are not necessary for information transmission in these networks.

The system we have investigated thus operates with strong coupling within each network (e.g. within Net 1 and within Net 2), but relatively weak coupling between the two networks. This is exactly the system that applies in the cortex (Renart, Parga, and E. T. Rolls, 1999a,b; E. T. Rolls and A. Treves, 1998), where the connections between networks must be less than in the order of 0.01 of the internal recurrent collateral strength for the two networks to have the potential to operate separately (see further E. T. Rolls and A. Treves (1998) and E. T. Rolls (2008)). Consistently, in the investigations described here, information transmission between the coupled nets took place when the relative value of the inter-network connectivity to the intra-network (intra decision-pool) connectivity was $0.015/2.1 = 0.007$. Indeed, in the phase control experiments, it was difficult to move the phases of the oscillations between the D1, D2, and GABA neurons and LFPs within Net 1 or Net 2, due to the strong recurrent connection weights between the within-network pools of neurons. However, it was possible to move the phase of the oscillations between Net 1 and Net 2 (Figure 33), as the connections between the two networks w_f and w_b were relatively much weaker.

We emphasize that even when oscillations are present (the AMPA case), phase-locking and thus synchrony only become strong at the highest value of w_f, 0.45 (Figure 31f), whereas information transmission has saturated at 1 bit with w_f values of 0.09 (Figure 31a and Figure 31b). Even at $w_f = 0.15$ and 0.09, there is only a limited degree of phase coupling (Figure 31f), coherence (Figure 31c), cross-spectral magnitude (Figure 31d) or cross STA (Figure 31e). Thus information transmission saturates at much lower values of the coupling between these neural systems (Nets 1 and 2) than are needed to induce coherence and synchrony in networks that are oscillating. *In this sense, communication occurs before coherence.*

The implication of the findings in Figure 32 is that the speed of information transmission (as well as information transmission itself), do not depend on coherence, or synchrony (phase locking) between two weakly coupled attractor networks in which the coupling is nevertheless sufficiently strong to support information transmission to 100 percent correct between the two networks. The small increase in coherence at higher values of w_f than 0.06, and even the phase locking at $w_f = 0.45$, appear just to reflect the stronger connections between Net 1 and Net 2, after information transmission has almost saturated. Further evidence that the decision times within the range of values of w_f that influenced

information transmission did not depend on coherence is provided by the phase analysis shown in Figure 32d for $w_f = 0.03$. This shows for 1,000 trials that the decision time was not a function of the gamma phase that happened to be present between Net 1 and Net 2.

It must be emphasized that we are considering here the transmission of information about an external stimulus (λ_1) through one Net (1) to a second (Net 2). This is different to and extends what has been found in earlier work. In that earlier work, the influence of oscillations in one network on oscillations in a second network has been shown to be phase-dependent, at least at high values of w_f (Buehlmann and Deco, 2010). Indeed, a considerable part of the literature on oscillations involving LFPs and also spiking has measured this type of influence, for example by the power correlation between two networks as a function of phase, and by the STA (Fries, 2005, 2009). Those findings were replicated in the present findings. For example, considering the period in which a decision had just been taken, the power correlation between the LFPs in Nets 1 and 2 was maximal at zero phase, in the AMPA case. This indicates that ongoing fluctuations in the firing rates, including those produced by oscillations, are present in this network when high firing rate decision states are present in both Net 1 and Net 2. In this chapter we have taken matters forward by asking a different question, whether the information transmission, about external events through connected brain networks, which is prototypical of the function of cortical neuronal networks (E. T. Rolls, 2008), is influenced by the oscillations and their phase in the coupled networks. The results of this new type of analysis presented here indicate that this type of information transmission in this prototypical case of two coupled networks is not influenced by oscillations or by their phase if oscillations are present, nor is the speed of information transmission. We suggest that it will be important to measure the role of oscillations in this scenario in future in neurophysiological experiments. We note that the system we investigated is two connected integrate-and-fire networks, and that the effects found apply to that system, and leave open the possibility that communication through coherence, in the strong, information transmission, sense analysed here, may be found in other model networks, and in the brain. However, the model described here is rather prototypical of connected cortical networks (E. T. Rolls, 2008).

Furthermore, we showed that when the network was in a spontaneous firing rate state, before stimuli were applied, then no gamma oscillations were present. The gamma only started in the networks when inputs produced high firing rates (in practice typically 20 spikes/s or higher). We were able to show this by the use of the multitaper time spectrograms (Fries, Womelsdorf, et al., 2008; Mazzoni et al., 2008) which are important during neurophysiological investigations of cortical communication to examine exactly when gamma coherence may start in relation to the transmission of information. Indeed, that is one of the important points and predictions for neurophysiological investigations that arise from the present work: gamma oscillations and coherence with input networks are predicted not to be present in receiving networks when they are in the spontaneous firing rate state, and may only arise after the receiving network had increased its firing rate as a result of the information transmission. In this situation the research described here makes the important point that information transmission can occur with synaptic connection strengths between networks and signal

strengths in the first network that may not be sufficient to produce coherence between the networks. It will be important to test that prediction neurophysiologically, taking care with spectrograms and coherence analysis as a function of time to measure when coherence may start between the networks in relation to when the second network shows influences from the first network and thus information transmission. Indeed, at least part of what is predicted, and thereby the applicability of the model described here, is already known: neurophysiological investigations have shown that cortical networks in V4 have little gamma band oscillation (30–70 Hz) in the spontaneous firing rate state, and gamma oscillations only become pronounced when the neurons have been induced to increase their firing rates by an input stimulus 2008. It is exactly this issue that is at the heart of this chapter: if coherence becomes present between cortical networks, does it just reflect information transmission that has already occurred, and has produced high firing rates in two strongly coupled networks which then begin to oscillate? If coherence between neurons increases with for example attentional modulation (Fries, Womelsdorf, et al., 2008), is this effect distinct from effects of firing rates, with higher firing rates tending to be related to more coherence, as described here. However, we note that in the present work we have gone beyond previous neurophysiological investigations that described spike coherence within networks in V4 (Fries, Womelsdorf, et al., 2008) to a situation in which information communication between different networks is being investigated, in the present investigation from Net 1 to Net 2.

We note that correlative evidence suggesting communication through coherence (Fries, 2005, 2009), such as the finding that gamma band synchronization predicts speed of change detection (Womelsdorf, Fries, et al., 2006) and selective attention (Fries, Womelsdorf, et al., 2008), must be carefully evaluated in the light of the present findings. For example, gamma synchronization tends to become high when the coupling between networks is increased to high values (Figure 31). This could be produced by any change such as increased attention or arousal on some trials which influenced synaptic transmission, for example increasing synaptic transmission by the release of acetylcholine, which would effectively increase the synaptic coupling between networks by reducing synaptic adaptation (E. T. Rolls, 2008). However, in addition, a change that was associated with increasing the synaptic coupling w_f and w_b in our simulations was that the firing rate was also increased (Figure 32), and that alone is an important factor that can increase the speed of information processing and decrease decision times (E. T. Rolls, 2008; E. T. Rolls, Grabenhorst, and Deco, 2010a,b; E. T. Rolls and A. Treves, 2011). For these reasons, care must be taken before concluding that synchronization affects even the speed of information transmission, as well as the information transmission, as the underlying causal factors including any differences in firing rates must be analyzed. In the network described here, because the parameters were under full control, we were able to test whether in this system coherence facilitates communication as measured by information transmission and the speed of processing, and found that information transmission, and fast processing, occur before coherence sets in when oscillations are present (the AMPA case), and can occur without oscillations or synchrony just as well (the NMDA case (see Figure 31). Further, even on trials when phase synchronization was present, the synchronization was delayed to be often 100 ms or more later than the decision time.

Running correlations between the gamma-filtered LFPs in Net 1 and Net 2 confirmed this. This makes an important point: it is important to measure the oscillations and synchrony just at the time that the information transmission is occurring, not some time after that, as oscillations, and synchrony if present, occurred only when the firing rates of the neurons were becoming high in the attractor state, when the transition had already occurred from the spontaneous firing rate state. In the light of the present studies, further neurophysiological studies are needed to test whether synchrony plays a causal role in information transmission and the speed of information processing.

The results described here are consistent with previous studies which showed that fast ongoing fluctuation effects in model and real neural systems can be reflected in measures such as the power correlation, and the spike triggered average of the neuronal (including multiple unit) activity, and the LFPs (Buehlmann and Deco, 2010; Fries, 2005, 2009; Womelsdorf, Schoffelen, et al., 2007). What is new about the present investigation is that we measured how information transmission about an external stimulus from one network to a second network, i.e. information about which stimulus has been presented, is influenced by gamma oscillations and synchrony. We found in the system analysed that at values of the coupling strength between the two networks that were sufficient for information transmission in this strong sense relevant to brain function, coherence was not present, and phase did not affect the speed of information transmission, even though gamma oscillations were present. Thus communication in this strong sense of information transmission about an external event did not need coherence, and was not affected by the phase if coherence was present. The results were found for a simple and clearly defined model of coupled cortical attractor networks, and do not necessarily apply to all systems of coupled networks. Communication through coherence may be found in other scenarios.

The findings suggest that experimental investigations of whether information transmission in this strong sense is influenced by the coherence of oscillations, if oscillations are present, may be important for analysing the role of oscillations in information processing in the brain. The finding that gamma oscillations are not present during spontaneous firing, and only start in Net 2 when the neurons increase their firing rates, is illustrated by the single trial type of analysis shown in Figure 30. Yet when the Net 2 D1 neurons selectively increase their firing rates, the decision has effectively been taken, that is the bifurcation has been crossed. This is one of the implications of the investigations described here: great care has to be taken using single trial analyses with neurophysiological data to measure exactly when the gamma oscillations start, and also when any synchrony starts that may be present, in relation to the time of the decision or more generally of the information transmission.

6 DISCUSSION

This chapter is for additional discussion of the topics covered in this thesis. The main discussion is presented in each of the chapters presenting original results. The purpose here is to raise complementary issues to the discussion already presented. I will summarize the significance of the results and discuss possible directions for future work.

Simple as this model may be, it can capture a decision-making process and also the aspects of neural oscillations in the gamma frequency, we are also able to model relevant variables such as local field potential, which makes our results able to relate to experimental observations. The attractor networks natural analogy with working memory, mental states, and thoughts is also a very attractive hypothesis in search our goal.

6.1 SYNFIRE CHAINS

An open debate in neuroscience is whether information in the brain is either rate (M. Shadlen and W. Newsome, 1994) or temporally coded (Van Rullen, Guyonneau, and Thorpe, 2005). Because there is so much evidence on both sides, perhaps a better way to phrase the debate is "which information is rate coded and which is temporally coded"? On one hand, a rate coding scheme defends against the high variability of neuronal firing patterns that have been observed. On the other hand, rate coding seems to be far too slow for fast information transfer, yet this notion has been dispelled by Van Rossum, Turrigiano, and Nelson (2002).

The results presented in this thesis have primary focused on the recurrent dynamics inside decision pools; the final state of our network is determined by a rate code. In Chapter 5 I discussed a model that included forward communication between networks, and when high feedforward connections were established from neurons in one network to another, information communication happened over fast timescales, a hallmark of temporal coding.

Other modeling studies have looked more deeply into how forward communication may propagate through the brain through spike synchrony. One such modeling paradigm is *synfire chains*. Here, models consist of a feedforward network of neurons, with each neuron belonging to a layer (Abeles, 2009). A synfire chain is characterized by activity in one layers causing a subsequent wave of synchronous spiking activity in feedforward layers. This activity may loop back on itself causing persistent activity (Durstewitz and Seamans, 2002). Synfire chains have been shown to posses very interesting behavior. In a particular example, involving a rather complicated setup, one had an ability to compose primitives drawing strokes into more complex "paintings" (Schrader, Diesmann, and Morrison, 2010). In our current model, networks of neurons communicate with each other, not unlike the individual neurons in a synfire chain. This is similar

to the rate mode in a model for layered networks of IF neurons proposed by Van Rossum, Turrigiano, and Nelson (2002), in which rate coding was found to sufficiently fast enough coding scheme to work effectively. In this model, like ours, spike synchrony was not a requirement for communication.

Synfire chains account for is a temporal coding scheme governed by precise synchronous spiking (Diesmann, Gewaltig, and Aertsen, 1999). The numerous studies of synfire chains offer many examples of communication that is not governed by oscillations and coherence. Therefore, before this thesis it has already been demonstrated that meaningful communication can happen without coherence. Moreover, this has been a thoroughly researched topic since the inception of artificial network theory. The surprise to us was, in our model, coherence did not assist with communication.

Views diverge on the biological existence of synfire chains. A recent theoretical analysis sheds doubt on the biological plausibility of synfire chains embedded in balanced networks (Kunkel, Diesmann, and Morrison, 2010). Here, the authors used a mean-field analysis to show that the spike timing dependent plasticity (STDP) (Bi and Poo, 1998) is an ineffectual rule to produce synfire chains in balanced networks. Other results argue against the conjecture that temporal coding is incompatible with a more realistic STPD rule (Knoblauch et al., 2012). Aviel et al. (2003) have shown that under the right conditions (such as $N > 90{,}000$) it is possible to embed a synfire chain in the excitatory-excitatory synapses in a balanced excitatory-inhibitory network. However, these synfire chains were constructed, not learned through simulation. The implication is that neural networks can at least be artificially constructed that embody both a spontaneous state and a temporal code. Yet, no conclusive evidence for synfire chains have yet been discovered neurophysiologically. New methods in the analysis of parallel multi-cell spike train data (G. Gerstein et al., 2012) could lead to their detection in the near future, if they do exist.

The questions that arise here are larger than the scope of this thesis; and they reflect a need for a top-down approach to modeling the brain. By top-down, I mean a further reliance on experimental data from population recordings. This will lead us to better understand the brain's network structure. It is my own present view that possibly the next theoretical advances in resolving the structure of neural networks will involve a strong emphasis on biologically inspired learning rules inspired by empirical data. As I have historically noted, computation neuroscience moved from abstract models of neuronal networks to more detailed ones such as our integrate and fire network. Also, further advances in the field of detailed neural models are needed verify the results of less detailed neural models. STPD learning is an biologically plausible approach (however challenging), and current sentiment also points the exciting promises of simulating the effect of brain reward through reinforcement learning (Gerstner, Sprekeler, and Deco, 2012; Montague, Hyman, and J. Cohen, 2004).

6.2 OTHER SOURCES OF NOISE IN THE BRAIN

The importance of noise on brain performance is highly significant. Network noise, caused by the variability in spike arrival at synapses, is just one aspect in the noisy brain. (Faisal, Selen, and Wolpert, 2008) reviews experimental ev-

idence on the presence of noise in the nervous system and lists sensory noise, cellular noise, action potential noise, synaptic noise, and motor noise as all being characteristic of the nervous system. Some authors use the term *channel noise* to refer to the stochasticity arising from ion channels (White, Rubinstein, and Kay, 2000). In our model, there is an absence of noise at the synaptic and membrane level (instead, noise was produced by the Poisson process that the stimulus and background activity consisted of); so, I will discuss the implications of these other sources here.

Due to the probabilistic release of neurotransmitters, the postsynaptic response to an action potential is variable (Ribrault, Sekimoto, and Triller, 2011). For instance, the evoked PSP from AMPA and NMDA quantal release coefficient of variation has been measured between 0.30 and 0.39 in rat CA1 hippocampal neurons (Hanse and Gustafsson, 2001). The mechanism for stochastic synaptic transmission is now being better understood. As neurotransmitters diffuse across the synaptic gap, they obey laws of Brownian motion (Ribrault, Sekimoto, and Triller, 2011), an inherently stochastic process. Ca^{2+} ion diffusion, the process that triggers the release of synaptic vesicles, is also a source of stochasticity (Lisman, Raghavachari, and Tsien, 2007; Schneggenburger and Neher, 2005).

In considerations that look at larger than synaptic scales, ion channel noise many hold interesting implications for neural network simulations, but unfortunately the computational costs has limited simulation study in this area (Cannon, O'Donnell, and Nolan, 2010). Approaches using stochastic differential equations (Fox, 1997; Goldwyn, Imennov, et al., 2011) or Markov chains methods (Buesing et al., 2011) attempt to simulate the effects of channel noise on individual Hodgkin-Huxley neurons. More computationally efficient and accurate algorithms using a diffusion approximation have recently been proposed (Goldwyn and Shea-Brown, 2011; Linaro, Storace, and Giugliano, 2011; Orio and Soudry, 2012), which may soon lead to more computational network-level research.

6.3 CONTRIBUTIONS TO UNDERSTANDING THE STOCHASTIC FUNCTIONING OF THE BRAIN

This thesis used a spiking neural model consisting of two decision pools that have connections to a common population of inhibitory neurons. The spiking activity of this network has let us investigate how noise is effected by changes to network structure in Chapter3 and Chapter 4. Previous work had addressed the reaction time distribution of this network (Deco and E. T. Rolls, 2006; Loh, E. T. Rolls, and Deco, 2007b); however, no previous work had investigated the effect of graded firing rates or diluted connectivity on the performance of the model. As these are present biologically in the brain, the effects of these network structures on noise are important to understand.

Graded firing rates is one way we discovered how to change the level of noise by altering the synaptic strengths of the network. As noise in a neural network is not a well defined quantity, because it is generated at many different network levels, we first defined that the time to escape the spontaneous state and jump to

an attractor to be a quantity that could represent the overall noise in the network. In the mathematical analyses in Chapter 3 (see Equation 22) we found that that the variance of input into a neuron was also greater in a network with graded firing patterns. Another way to interpret our results is that in a network with graded firing rates, the pools behave as if they made up of less neurons then they actually are.

Technically, there was no available software to set the weight matrix needed to produce graded firing rates, I first needed to write new code to generate a matrix that would produce similar graded firing patterns to the graded patterns of the firing rate based network investigated by E. T. Rolls et al. (1997a). The graded firing rate implementation required a full synaptic weight matrix for the recurrent collaterals. This slowed down the simulation greatly to previous investigations, where the synaptic input to each neuron was uniform across a pool. In addition I wrote all the new code to implement the attractor with diluted connectivity. The weight matrix needed to be expanded in similar way to the graded simulations. In order to run the number of simulations required to investigate the stochastic behavior of the attractor network we employed the HPC cluster available at the University of Warwick.

Diluted connectivity is another way to change the noise in the network. In this case we observed a decrease in overall noise as measured by reaction times. More diluted representations along the mossy fiber input to the CA3 region from the dentate gyrus was found to help in the separation of the representations of memory patterns that would stored by the CA3 region, which may have a positive effect on performance and efficiency (O'Reilly and McClelland, 1994). Besides the role it may play in stabilizing attractor networks in the brain, another effect of diluted connectivity is that in recurrent networks it has been shown to be to decrease correlations between neurons with shared inputs (Renart, Rocha, et al., 2010). Balanced networks with clustered connectivity have been shown replicate our Fano factor results of neural variability when stimuli were applied to specific clusters (Litwin-Kumar and Doiron, 2012). This experiment assumed a weak uniform synaptic weight distribution, which was strengthened in the case of neurons belonging to the same cluster, so clustering in effect created pools analogous to our decision pools.

It of interest that there are two naturally occurring mechanisms that have opposing effects on the level of noise in the brain. As we have mentioned previously, the number of connections per neuron is likely fixed due to biological limitations or difficulty in utilization at approximately 20,000. One proposed hypothesis is that diluted connectivity allows the biological mechanisms that structure the synaptic connections of the brain to prefer one synaptic connection between each pair of neurons (E. T. Rolls, 2012).

The discussion in each of these two chapters describe advantages of both increased and decreased noise that appear to be in contrast with each other. However, we observed a speed-accuracy trade off affected by noise that is consistent across the results from each chapter. Both chapters show that increased noise in the system decreases stability and improves reaction time, and that decreased noise increases stability and decreases reaction time. These results add a new mechanism to the existing theory of drift diffusion models that indicates that a speed-accuracy trade off is controlled by changing the distance from baseline activity to a decision threshold (Bogacz, Wagenmakers, et al., 2010). In this thesis

I have given two structural mechanisms in areas of the brain that may encode decisions that could affect this trade-off. A question that naturally arises is what is biologically preferred, speed or stability? Clearly speed and accuracy are both important to a behaving animal, and an analysis of some of the different two alternative forced choice models mentioned in subsection 1.1.1 point to these models having optimal parameters in different paradigms (Bogacz, Brown, et al., 2006). Furthermore, recent advances in the understanding of neurobiology indicates that modulation of the speed-accuracy trade off occurs in association and pre-motor areas, which are similar to the areas modeled in this thesis (Bogacz, Wagenmakers, et al., 2010; Ivanoff, Branning, and Marois, 2008; Van Veen, Krug, and C. Carter, 2008).

6.4 CONTRIBUTIONS TO THE CTC HYPOTHESIS

Chapter 5 dealt with the unanswered question, how do neurons collectively communicate with each other? The CTC hypothesis states that phase locking between the oscillatory neuronal groups helps with transmission of messages in the brain, and even goes as far to say that communication is facilitated when regions are phase locked, and inhibited when they are not. The mechanisms which facilitate phase locking are well understood theoretically. The theory of phase reduction describes how neurons will shift phases as a response to synaptic input (X.-J. Wang, 2010). Often the CTC hypothesis is described in these terms; I quote Fries (2009) to explain the consequences of rhythmic synchronization in the case where there are two populations of neurons, all gamma oscillating, that are both providing competing synaptic input to a feedforward population:

> *If there is rhythmic synchronization among the neurons in group A and among the neurons in group B, but not between those in A and B, then group C will most likely synchronize to either A or B but not to both at the same time (Börgers and Kopell, 2008). This is due to the inhibitory interneurons in group C. When the interneurons in C have fired a synchronous barrage of spikes, then C's neurons are collectively inhibited and collectively return from inhibition. When C is synchronized with A, then input from A will arrive around the time that C is again ready to receive this input. But input from B (which is not synchronized with A) will arrive mostly when C is not receptive. Thus, in short, the locking of C to either A or B implements a winner-takes-all mechanism between the competing inputs of A and B into C (Fries, 2009).*

Our results show that the level of feedforward weight needed to achieve spike synchrony in our network was beyond the range in which the attractors would act with some independence, i.e. still be able to make their own decision with some uncertainty. Essentially, if synapses are so strong that coherence is produced between the connected networks, then the networks act as one attractor. It is a well established that information processing in the brain is highly distributed, and it goes against this to say that neuronal groups are so strongly

connected that the brain will operate as one attractor. Having the feed-forward weight w_f in our network set at a value where attractors only loosely influence each other is in line with a highly distributed brain.

We do not dispute the substantial body of experimental evidence that has observed spike synchrony across cortical regions. Womelsdorf and Fries (2007) outlines the supporting evidence for phase synchronization in selective attention, from numerous studies involving EEG and MEG recordings in animals and humans, and LFP electrode recording in animals. However, not all recent evidence supports the CTC hypothesis; Ray and Maunsell (2010) found that power in the gamma band between nearby neural populations were over too wide a frequency band to support reliable information transmission, and also that these rhythms were unstable. Instead the authors suggested that that gamma oscillations are arising from the inhibitory-excitation feedback loops that are local to the different populations. This feedback loop is well understood in phase reduction theory (X.-J. Wang, 2010), and there are several modeling studies that show gamma oscillations resulting from this architecture. In these networks the spike to spike coherence arises from the dynamical relationship of excitatory and inhibitory firing. It is very likely that this is the case in our network and that is why the two networks were unable to lock in phase coherence with each other.

It is our feeling that experimental CTC observations are probably due to some factor other than forward projecting EPSPs entraining spike firing across regions. The experimental observations could be explained by intrinsic gamma oscillations (X.-J. Wang, 2010) occurring after the onset of communication. In our framework, the high recurrent weight w_+, which is essential for an attractor network, locks a neuron's phase in with the gamma oscillations excitatory-inhibitory feedback loop of its pool. The weaker connections between networks is unable to phase lock the oscillations between the networks purely through excitatory phase advance.

If oscillations are generated intrinsically inside regions, how does phase locking occur at weak couplings? As we demonstrated a top down sine wave at the proper strength would be sufficient to phase lock the networks. Recent studies that have attempted to explain the mechanism for CTC have either oscillations are generated through an external top-down sine wave modulated force (Masuda, 2009; Wildie and Shanahan, 2011), or by through a excitatory-inhibitory feedback loop that is lacking recurrent connections.

In any case, the difference between oscillations being generated intrinsically, through well understood feedback loops, and extrinsically, through top-down controllers, will be crucial to understanding neural communication. Our study differs from this previous work in that we have strong recurrent connections, and in our measures of communication. This discussion raises a question, is a top-down controller influencing the input to each network necessary to generate phase locking between networks, and if it is required, does this fit in with our views of a distributed brain? Having such a top-down controller seems to imply a decision being made in advance about which pools will be allowed to communicate. In any case, the difference between oscillations being generated intrinsically, through well understood feedback loops, and extrinsically, through yet to be described top-down controllers, will be crucial to understanding neural communication.

In order to generate oscillations in the attractor model in the gamma frequency band, we needed to change the g_{AMPA}/g_{NMDA} ratio (see subsection 5.2.1) by increasing the amount of AMPA and reducing the amount of NMDA current in the network. The ratio of g_{AMPA}/g_{NMDA} is important to the gamma band behavior of our network. The original g_{AMPA}/g_{NMDA} ratio used as parameters to the attractor network of working memory had the amount of g_{NMDA} current dominate the amount of g_{AMPA} current by several fold in the attractor state (Brunel and X.-J. Wang, 2001). g_{NMDA} with its long acting time constant ($\approx$ 100ms) stabilizes the attractor state and make it more impervious to external noise. However, this long time constant is unable to produce oscillations in the fast 60Hz gamma frequency band through a excitatory-inhibitory feedback loop, and therefore g_{AMPA} needs to increased to make it fire in regime with strong gamma. NMDAR antagonists (such as ketamine) have been shown to disturb or strengthen gamma rhythms *in vivo* and *in vitro* (Carlén et al., 2011). Such drugs have substantial side effects such as hallucinations and strong feelings of dissociation at high doses, suggesting high levels of instability in neural functioning.

One theory is that the brain is operating in a regime where AMPA is needed for fast responses, but this may result in unstable attractor states. For this reason, NMDA may be recruited to stabilize the attractor state, but only in the minimal amount necessary to keep fast responses and gamma oscillations. Reported g_{AMPA}/g_{NMDA} ratios have varied widely by different authors as surveyed by Myme et al. (2003). The authors of this study reported a g_{NMDA}/g_{AMPA} (note inversion) of 109% in the prefrontal cortex, suggesting that NMDAR mediated current could plausibly play a role in stabilizing attractor states.

In this thesis, we considered a rather simplified case where only two networks were involved in communication. It is likely that brain microcircuits are receiving multiple inputs. Akam and D. M. Kullmann (2010) performed a computational experiment and found that gamma oscillations helped transmit information when multiple populations are all connected in a feedforward fashion to another network. This setup lacked the strong recurrent connections that we theorize prevented coherence developing at low levels of feedforward weight strength in our experiments. In their architecture, neurons were population coded to be selective to a particular orientation, for example like that found in MT cells in the macaque (Albright, Desimone, and Gross, 1984). Four different input neuron pools were constructed to be selective to a different specific stimuli orientation. Each input pool neuron had a feedforward connection to a corresponding cell in a receiving pool. This receiving pool retrieved information from a single network only when it was set to fire in an oscillating regime. The orientation of the input stimulus could be read off from the spacial firing pattern evoked in the receiving network. These results are plausible because their was no top-down controller generating shared oscillations between the sending and receiving networks. They are also very interesting because the receiving pool was basically able to filter out asynchronous input from distracting networks. In later work, the same authors of this study set up another similar experiment; and they found that performance becomes highly degraded because of distracting inputs that are incoherently oscillating in the same frequency band of the preferred pool (Akam and D. Kullmann, 2012), which sheds some further doubt on a realism of the CTC hypothesis.

In my opinion, the validity of the CTC hypothesis remains an open question. I believe that so-called biologically plausible frameworks — such as ours and others like it — make many assumptions about the feedforward connectivity patterns between different microcircuits and the strength of recurrent connections inside them. Until we know what are these strengths, we may not have a definite answer. This is because, while CTC can be shown in feedforward networks, our results point to the opinion that synchrony between networks is much more difficult to achieve in between recurrent networks. Also,gamma band oscillations may not be stable *in vivo*. Modeling and experimental work also state that the brain may be too noisy and possibly incoherent for the CTC hypothesis. It is also quite possible that in the brain recurrent connections are not as dominate as we modeled. A more complex and numerous set of inputs to microcircuits may negate the need to have strong recurrent connections to evoke persistent activity. We should explore these possibilities further with future modeling and experimental work.

6.5 POSSIBLE FUTURE WORK

A fit to the biological process of perceptual decision-making has been implemented in the attractor network model studied in this thesis. It is highly likely that the results pertaining to graded firing rates and diluted connectivity will generalize to other neuron models and methodologies, because these features are not architecture dependent. Future work could address a few key aspects that are missing from our model.

6.5.1 Formation of graded weight patterns

What are the rules of synaptic plasticity that will allow for graded weight patterns to form? The Hebbian rule in its most abstract rate based form, see Equation 10, does not provide a local learning rule algorithm for a spiking neuron simulation. Even more important than the exact formulation of a rule is the understanding of the rapidly changing synaptic connections in the brain. In an overview of the rapid (with changes present on the milliseconds to seconds scale) nature of synaptic plasticity, Haider and McCormick (2009) eloquently summarizes this

> *The highly interconnected local and large-scale networks of the neocortical sheet rapidly and dynamically modulate their functional connectivity according to behavioral demands. This basic operating principle of the neocortex is mediated by the continuously changing flow of excitatory and inhibitory synaptic barrages that not only control participation of neurons in networks but also define the networks themselves.*

We could consider a few possible extensions to our model that may allow the formation of graded weight patterns. STPD is a local leaning rule that can describe Hebbian learning at the level of spikes. Two factors certainly need to align for STDP to describe the formulation of graded weight patterns. One is

a homeostatic mechanism *in vivo*, suggested by (Urakubo et al., 2009). The other required mechanism is one that produces graded weight patterns. Using a standard STDP kernel in a recurrent network often ends up with the network drifting into unidirectional asymmetric synaptic weight distributions. A recent voltage-based biologically plausible STDP model has been proposed that is capable of producing the symmetric strong connections and unidirectional weak connections (Clopath et al., 2010).

6.5.2 Other methods to generate coherence between networks

The basic IF neuron model not does exhibit any sort of subthreshold resonance, a property of many biological neurons (Brunel, Hakim, and Richardson, 2003; Richardson, Brunel, and Hakim, 2003). All gamma band synchrony is generated through the previously mentioned inhibitory excitatory feedback loop. Therefore, it may be more difficult to generate synchrony in this model than one where neurons exhibit natural resonant frequencies. It could be possible to test our framework with more realistic neurons and observe if coherence is achievable at lower strengths of feedforward connections.

If we find that network communication alone cannot account for coherence, investigations could look further into stimulus that is carrying an oscillatory signal, such as a strobe light. Computational studies of the CTC hypothesis have had gamma oscillations generated through top-down control (Masuda, 2009). In our current simulations, we used a basic oscillating stimuli to look at top-down control, and we found that the amplitude of the oscillations had to dominate the signal in order for the network to oscillate at that frequency. By tuning the network to be more sensitive to the external oscillations, it could allow for further study in this area.

6.6 CONCLUSION

One grand goal certainly would be the understanding of how the brain's neural circuits work together to form our thoughts, feelings, and actions. This is the spirit of this thesis, and it has lead us to incorporate more biological plausibility into an attractor network model. This model consists of two decision pools that have connections to a common population of inhibitory neurons. Simple as this model may be, it can capture general processes such a decision-making and memory recall. Moreover, it is a suitable model to study the effects of neural oscillations in the gamma frequency. We are also able generate observational variables such as local field potentials, which makes our results relatable to experimental observations. The stochasticity of this network agrees with the trial to trial variability that is a common trait in neurophysiological data. Finally, An attractor network's natural analogy with working memory, mental states, and thought patterns lets us frame our results in the context of cognition.

It is my hope that the extensions to the attractor network model contained within this thesis will help guide us as we learn more about the synaptic connectivity of the actual brain. Denk, Briggman, and Helmstaedter (2012) concludes in a recent review that a detailed map of the mouse brain may be possible in next

decade. Detailed connectivity data such as this will provide many new modeling opportunities for investigators. With this data, our growing supercomputing ability, and our knowledge of ionic channels and synaptic vesicle release cycle, future neural network models will break new ground in realistically capturing the spiking behavior of the brain. As our skill in determining synaptic strength advances with new technology such as the imaging of intracellular calcium concentrations, we will rely on modeling studies such as this to help bridge the gap from knowing the brain's structure to determining its function. The next steps in the field of neuroscience will surely be a significant interdisciplinary combination of approaches that hopefully will lead to canonical models of different brain areas, much like the advances made in our understanding of genetics.

BIBLIOGRAPHY

Abbott, L. F. (1999). "Lapicque's introduction of the integrate-and-fire model neuron (1907)". *Brain Research Bulletin* 50, pp. 303–304.

Abeles, M. (1991). *Corticonics: Neural Circuits of the Cerebral Cortex*. Cambridge: Cambridge University Press.

Abeles, M. (2009). "Synfire chains". *Scholarpedia* 4, p. 1441.

Akam, T. and D. M. Kullmann (2010). "Oscillations and filtering networks support flexible routing of information". *Neuron* 67, pp. 308–320.

Akam, T. and D. Kullmann (2012). "Efficient "Communication through Coherence" Requires Oscillations Structured to Minimize Interference between Signals". *PLOS Computational Biology* 8, e1002760.

Albantakis, L. and G. Deco (2009). "The encoding of alternatives in multiple-choice decision making". *Proceedings of the National Academy of Science USA* 106, pp. 10308–10313.

Albright, T., R. Desimone, and C. Gross (1984). "Columnar organization of directionally selective cells in visual area MT of the macaque". *Journal of Neurophysiology* 51, pp. 16–31.

Alvarez, P. and L. R. Squire (1994). "Memory consolidation and the medial temporal lobe: a simple network model". *Proceedings of the National Academy of Sciences USA* 91, pp. 7041–7045.

Amaral, D. G. (1993). "Emerging principles of intrinsic hippocampal organization". *Current Opinion in Neurobiology* 3, pp. 225–229.

Amaral, D. and M. Witter (1989). "The three-dimensional organization of the hippocampal formation: a review of anatomical data". *Neuroscience* 31, pp. 571–591.

Amit, D. J. (1989). *Modeling Brain Function: The World of Attractor Neural Networks*. Cambridge: Cambridge University Press.

Amit, D. J. and N. Brunel (1997a). "Dynamics of a recurrent network of spiking neurons before and following learning". *Network* 8, pp. 373–404.

Amit, D. J. and N. Brunel (1997b). "Model of global spontaneous activity and local structured activity during delay periods in the cerebral cortex." *Cerebral Cortex* 7, p. 237.

Amit, D. J., H. Gutfreund, and H. Sompolinsky (1985). "Spin-glass models of neural networks". *Physical Review A* 32, p. 1007.

Aviel, Y. et al. (2003). "On embedding synfire chains in a balanced network". *Neural computation* 15, pp. 1321–1340.

Baddeley, R. J. et al. (1997). "Responses of neurons in primary and inferior temporal visual cortices to natural scenes". *Proceedings of the Royal Society* B264, pp. 1775–1783.

Beamish, D. et al. (2006). "Fifty years later: a neurodynamic explanation of Fitts' law". *Journal of The Royal Society Interface* 3, pp. 649–654.

Beck, J. M. et al. (2008). "Probabilistic population codes for Bayesian decision making". *Neuron* 60, pp. 1142–1152.

Bendat, J. S. and A. G. Piersol, eds. (2010). *Random Data: Analysis and Measurement Procedures*. 4th Edition. New York: Wiley.

Benzi, R., A. Sutera, and A. Vulpiani (1999). "The mechanism of stochastic resonance". *Journal of Physics A: mathematical and general* 14, p. L453.

Bi, G. and M. Poo (1998). "Synaptic modifications in cultured hippocampal neurons: dependence on spike timing, synaptic strength, and postsynaptic cell type". *The Journal of Neuroscience* 18, pp. 10464–10472.

Bliss, T. V. P. and A. Gardner-Medwin (1973). "Long-lasting potentiation of synaptic transmission in the dentate area of the unanaesthetized rabbit following stimulation of the perforant path". *The Journal of Physiology* 232, p. 357.

Bogacz, R., E. Brown, et al. (2006). "The physics of optimal decision making: A formal analysis of models of performance in two-alternative forced choice tasks". *Psychological Review* 113, pp. 700–765.

Bogacz, R., E. J. Wagenmakers, et al. (2010). "The neural basis of the speed-accuracy tradeoff". *Trends in Neurosciences* 33, pp. 10–16.

Börgers, C. and N. J. Kopell (2008). "Gamma oscillations and stimulus selection". *Neural Computation* 20, pp. 383–414.

Botvinick, M. M., J. D. Cohen, and C. S. Carter (Dec. 2004). "Conflict monitoring and anterior cingulate cortex: an update." *Trends in Cognitive Sciences* 8, pp. 539–46.

Bovier, A. and V. Gayrard (1992). "Rigorous bounds on the storage capacity of the dilute Hopfield model". *Journal of Statistical Physics* 69, pp. 597–627.

Braitenberg, V. and A. Schütz (1991). *Anatomy of the Cortex*. Berlin: Springer-Verlag.

Braun, J. and M. Mattia (2010). "Attractors and noise: Twin drivers of decisions and multistability". *Neuroimage* 52, pp. 740–751.

Bressloff, P. C. (2010). "Metastable states and quasicycles in a stochastic Wilson-Cowan model of neuronal population dynamics". *Physical Review E* 82, p. 051903.

Brette, R. and W. Gerstner (2005). "Adaptive exponential integrate-and-fire model as an effective description of neuronal activity". *Journal of Neurophysiology* 94, p. 3637.

Brette, R., M. Rudolph, et al. (2007). "Simulation of networks of spiking neurons: a review of tools and strategies". *Journal of Computational Neuroscience* 23, pp. 349–398.

Britten, K. et al. (1993). "Responses of neurons in macaque MT to stochastic motion signals". *Visual neuroscience* 10, pp. 1157–1157.

Brody, C., R. Romo, and A. Kepecs (2003). "Basic mechanisms for graded persistent activity: discrete attractors, continuous attractors, and dynamic representations". *Current Opinion in Neurobiology* 13, pp. 204–211.

Brunel, N. (2000). "Dynamics of sparsely connected networks of excitatory and inhibitory spiking neurons". *Journal of Computational Neuroscience* 8, pp. 183–208.

Brunel, N. and V. Hakim (1999). "Fast global oscillations in networks of integrate-and-fire neurons with low firing rates". *Neural Computation* 11, pp. 1621–1671.

Brunel, N., V. Hakim, and M. J. E. Richardson (2003). "Firing-rate resonance in a generalized integrate-and-fire neuron with subthreshold resonance". *Physical Review E* 67, p. 051916.

Brunel, N. and P. E. Latham (2003). "Firing rate of the noisy quadratic integrate-and-fire neuron". *Neural Computation* 15, pp. 2281–2306.

Brunel, N. and M. C. W. van Rossum (2007). "Lapicque's 1907 paper: from frogs to integrate-and-fire". *Biological Cybernetics* 97, pp. 337–339.
Brunel, N. and X.-J. Wang (2001). "Effects of neuromodulation in a cortical network model of object working memory dominated by recurrent inhibition". *Journal of Computational Neuroscience* 11, pp. 63–85.
Brunel, N. and X.-J. Wang (2003). "What determines the frequency of fast network oscillations with irregular neural discharges? I. Synaptic dynamics and excitation-inhibition balance". *Journal of Neurophysiology* 90, pp. 415–430.
Brunel, N., S. Sergi, et al. (1998). "Firing frequency of leaky integrate-and-fire neurons with synaptic current dynamics". *Journal of Theoretical Biology* 195, pp. 87–96.
Buehlmann, A. and G. Deco (2008). "The neuronal basis of attention: rate versus synchronization modulation". *Journal of Neuroscience* 28, pp. 7679–7686.
Buehlmann, A. and G. Deco (2010). "Optimal information transfer in the cortex through synchronization". *PLoS Computational Biology* 6, e1000934.
Buesing, L. et al. (2011). "Neural dynamics as sampling: A model for stochastic computation in recurrent networks of spiking neurons". *PLoS computational biology* 7, e1002211.
Bullmore, E. and O. Sporns (2009). "Complex brain networks: graph theoretical analysis of structural and functional systems". *Nature Reviews Neuroscience* 10, pp. 186–198.
Bullock, T. H. et al. (2005). "The neuron doctrine, redux". *Science* 310, p. 791.
Burkitt, A. N. (2006). "A review of the integrate-and-fire neuron model: I. Homogeneous synaptic input". *Biological Cybernetics* 95, pp. 1–19.
Burkitt, A. N. and G. M. Clark (2000). "Calculation of interspike intervals for integrate-and-fire neurons with Poisson distribution of synaptic inputs". *Neural Computation* 12, pp. 1789–1820.
Busemeyer, J. R. (1993). "Decision field theory: a dynamic-cognitive approach to decision making in an uncertain environment." *Psychological Review*, pp. 432–459.
Buzsáki, G. (1997). "Functions for interneuronal nets in the hippocampus". *Canadian Journal of Physiology and Pharmacology* 75, pp. 508–515.
Cannon, R., C. O'Donnell, and M. Nolan (2010). "Stochastic ion channel gating in dendritic neurons: morphology dependence and probabilistic synaptic activation of dendritic spikes". *PLoS computational biology* 6, e1000886.
Caporale, N. and Y. Dan (2008). "Spike timing-dependent plasticity: a Hebbian learning rule". *Annual Reviews of Neuroscience* 31, pp. 25–46.
Carlén, M. et al. (2011). "A critical role for NMDA receptors in parvalbumin interneurons for gamma rhythm induction and behavior". *Molecular Psychiatry*.
Carpenter, G. A. (1997). "Distributed learning, recognition and prediction by ART and ARTMAP neural networks". *Neural Networks* 10, pp. 1473–1494.
Carpenter, R. H., B. A. Reddi, and A. J. Anderson (2009). "A simple two-stage model predicts response time distributions". *Journal of Physiology* 587, pp. 4051–4062.
Cessac, B. and T. Viéville (2008). "On dynamics of integrate-and-fire neural networks with conductance based synapses". *Frontiers in Computational Neuroscience* 2.

Churchland, A. K., R. Kiani, R. Chaudhuri, et al. (2011). "Variance as a signature of neural computations during decision making". *Neuron* 69, pp. 818–831.
Churchland, A. K., R. Kiani, and M. N. Shadlen (2008). "Decision-making with multiple alternatives". *Nature Neuroscience* 11, pp. 693–702.
Churchland, M. M. et al. (2010). "Stimulus onset quenches neural variability: a widespread cortical phenomenon". *Nature Neuroscience* 13, pp. 369–378.
Clopath, C. et al. (2010). "Connectivity reflects coding: a model of voltage-based STDP with homeostasis". *Nature Neuroscience* 13, pp. 344–352.
Compte, A. et al. (2003). "Temporally irregular mnemonic persistent activity in prefrontal neurons of monkeys during a delayed response task". *Journal of Neurophysiology* 90, pp. 3441–3454.
Cover, T. M. and J. A. Thomas (1991). *Elements of Information Theory*. New York: Wiley.
Crisanti, A., D. J. Amit, and H. Gutfreund (1986). "Saturation level of the Hopfield model for neural network". *EPL (Europhysics Letters)* 2, p. 337.
Criss, A., M. Wheeler, and J. McClelland (2012). "A differentiation account of recognition memory: evidence from fMRI". *Journal of Cognitive Neuroscience*, pp. 1–15.
Dayan, P. and L. F. Abbott (2001). *Theoretical Neuroscience: Computational and Mathematical Modeling of Neural Systems*. Cambridge: MIT Press.
Deco, G., V. Jirsa, et al. (2008). "The Dynamic Brain: From Spiking Neurons to Neural Masses and Cortical Fields". *PLoS Computational Biology*.
Deco, G. and E. T. Rolls (2004). "A neurodynamical cortical model of visual attention and invariant object recognition". *Vision Research* 44, pp. 621–642.
Deco, G. and E. T. Rolls (2005). "Synaptic and spiking dynamics underlying reward reversal in the orbitofrontal cortex". *Cerebral Cortex* 15, pp. 15–30.
Deco, G. and E. T. Rolls (2006). "Decision-making and Weber's law: a neurophysiological model". *European Journal of Neuroscience* 24, pp. 901–916.
Deco, G., E. T. Rolls, et al. (2012). "Brain mechanisms for perceptual and reward-related decision-making". *Progress in Neurobiology*, in.
Deco, G., E. Rolls, and R. Romo (2009). "Stochastic dynamics as a principle of brain function". *Progress in Neurobiology* 88, pp. 1–16.
Deco, G., V. K. Jirsa, and A. R. McIntosh (Jan. 2011). "Emerging concepts for the dynamical organization of resting-state activity in the brain." *Nature Reviews Neuroscience* 12, pp. 43–56.
Denk, W., K. L. Briggman, and M. Helmstaedter (2012). "Structural neurobiology: missing link to a mechanistic understanding of neural computation". *Nature Reviews Neuroscience*, pp. 351–358.
Derrida, B., E. Gardner, and A. Zippelius (1987). "An exactly solvable asymmetric neural network model". *Europhysics Letters* 4, pp. 167–173.
Devroye, L. (1986). *Non-uniform random variate generation*. Vol. 4. Springer-Verlag New York.
Diesmann, M., M. Gewaltig, and A. Aertsen (1999). "Stable propagation of synchronous spiking in cortical neural networks". *Nature* 402, pp. 529–533.
Ditterich, J. (2006). "Evidence for time-variant decision making". *European Journal of Neuroscience* 24, pp. 3628–3641.
Ditterich, J., M. Mazurek, and M. Shadlen (2003). "Microstimulation of visual cortex affects the speed of perceptual decisions". *Nature neuroscience* 6, pp. 891–898.

Durstewitz, D. and J. K. Seamans (2002). "The computational role of dopamine D1 receptors in working memory". *Neural Networks* 15, pp. 561–572.
Eliasmith, C. (2007). "Attractor network". *Scholarpedia* 2, p. 1380.
Elston, G. N. et al. (2006). "Specializations of the granular prefrontal cortex of primates: implications for cognitive processing". *Anatomical Record A* 288, pp. 26–35.
Faisal, A. A., L. P. Selen, and D. M. Wolpert (2008). "Noise in the nervous system". *Nature Reviews Neuroscience* 9, pp. 292–303.
Feller, W. (1968). *An introduction to probability theory and its applications*. Third. New York: Wiley.
Feng, J. and B. Tirozzi (1997). "Capacity of the Hopfield model". *Journal of Physics A* 30, pp. 3383–3392.
Fourcaud-Trocmé, N. et al. (2003). "How spike generation mechanisms determine the neuronal response to fluctuating inputs". *The Journal of Neuroscience* 23, p. 11628.
Fox, R. (1997). "Stochastic versions of the Hodgkin-Huxley equations". *Biophysical journal* 72, pp. 2068–2074.
Franco, L. et al. (2007). "Neuronal selectivity, population sparseness, and ergodicity in the inferior temporal visual cortex". *Biological Cybernetics* 96, pp. 547–560.
Fries, P. (2005). "A mechanism for cognitive dynamics: neuronal communication through neuronal coherence". *Trends in Cognitive Sciences* 9, pp. 474–480.
Fries, P. (2009). "Neuronal gamma-band synchronization as a fundamental process in cortical computation". *Annual Reviews of Neuroscience* 32, pp. 209–224.
Fries, P., J. Reynolds, et al. (2001). "Modulation of oscillatory neuronal synchronization by selective visual attention". *Science* 291, pp. 1560–1563.
Fries, P., T. Womelsdorf, et al. (2008). "The effects of visual stimulation and selective visual attention on rhythmic neuronal synchronization in macaque area V4". *Journal of Neuroscience* 28, pp. 4823–4835.
Furman, M. and X.-J. Wang (2008). "Similarity effect and optimal control of multiple-choice decision making". *Neuron* 60, pp. 1153–1168.
Galán, R. F. et al. (2004). "Odor-driven attractor dynamics in the antennal lobe allow for simple and rapid olfactory pattern classification". *Neural Computation* 16, pp. 999–1012.
Gammaitoni, L. et al. (1998). "Stochastic resonance". *Reviews of Modern Physics* 70, p. 223.
Gerstein, G. L. and B. Mandelbrot (1964). "Random walk models for the spike activity of a single neuron". *Biophysical Journal* 4, pp. 41–68.
Gerstein, G. et al. (2012). "Detecting synfire chains in parallel spike data". *Journal of neuroscience methods* 206, pp. 54–64.
Gerstner, W. and W. M. Kistler (2002). *Spiking Neuron Models: Single Neurons, Populations, Plasticity*. Cambridge: Cambridge University Press.
Gerstner, W., H. Sprekeler, and G. Deco (2012). "Theory and Simulation in Neuroscience". *science* 338, pp. 60–65.
Gigante, G. et al. (2009). "Bistable perception modeled as competing stochastic integrations at two levels". *PLoS Comput Biol* 5, e1000430.

Gold, J. I. and M. N. Shadlen (2001). "Neural computations that underlie decisions about sensory stimuli". *Trends in cognitive sciences* 5, pp. 10–16.
Gold, J. I. and M. N. Shadlen (2007). "The neural basis of decision making". *Annual Review of Neuroscience* 30, pp. 535–574.
Goldberg, J., U. Rokni, and H. Sompolinsky (2004). "Patterns of ongoing activity and the functional architecture of the primary visual cortex". *Neuron* 42, pp. 489–500.
Goldman, D. E. (1943). "Potential, impedance, and rectification in membranes". *The Journal of General Physiology* 27, p. 37.
Goldwyn, J., N. Imennov, et al. (2011). "Stochastic differential equation models for ion channel noise in Hodgkin-Huxley neurons". *Physical Review E* 83, p. 041908.
Goldwyn, J. and E. Shea-Brown (2011). "The what and where of adding channel noise to the Hodgkin-Huxley equations". *PLoS Computational Biology* 7, e1002247.
Gray, C. M. et al. (1989). "Oscillatory responses in cat visual cortex exhibit intercolumnar synchronization which reflects global stimulus properties". *Nature* 338, pp. 334–337.
Gregoriou, G. et al. (2009). "High-frequency, long-range coupling between prefrontal and visual cortex during attention". *Science* 324, pp. 1207–1210.
Gutfreund, H. (1990). "From statistical mechanics to neural networks and back". *Physica A* 163, pp. 373–385.
Gütig, R. and H. Sompolinsky (2006). "The tempotron: a neuron that learns spike timing–based decisions". *Nature neuroscience* 9, pp. 420–428.
Haider, B. and D. A. McCormick (2009). "Rapid neocortical dynamics: cellular and network mechanisms". *Neuron* 62, pp. 171–189.
Hanse, E. and B. Gustafsson (2001). "Quantal variability at glutamatergic synapses in area CA1 of the rat neonatal hippocampus". *The Journal of physiology* 531, pp. 467–480.
Hansel, D., G. Mato, et al. (2001). "Existence and stability of persistent states in large neuronal networks". *Physical Review Letters* 86, pp. 4175–4178.
Hebb, D. O. (1949). *The Organization of Behavior*. New York: Wiley.
Hernandez, A., A. Zainos, and R. Romo (2002). "Temporal evolution of a decision-making process in medial premotor cortex". *Neuron* 33, pp. 959–972.
Hertz, J. A., A. Krogh, and R. G. Palmer (1991). *Introduction to the Theory of Neural Computation*. Wokingham, UK: Addison-Wesley.
Herz, A. V. M. et al. (2006). "Modeling single-neuron dynamics and computations: a balance of detail and abstraction". *Science* 314, p. 80.
Holroyd, C. B. et al. (2004). "Dorsal anterior cingulate cortex shows fMRI response to internal and external error signals". *Nature Neuroscience* 7, pp. 497–498.
Hopfield, J. J. (1982). "Neural networks and physical systems with emergent collective computational abilities". *Proceedings of the National Academy of Sciences USA* 79, pp. 2554–2558.
Hopfield, J. J. (1984). "Neurons with graded response have collective computational properties like those of two-state neurons". *Proceedings of the National Academy of Sciences* 81, pp. 3088–3092.
Hopfield, J. J. (2007). "Hopfield network". *Scholarpedia* 2, p. 1977.

Ishizuka, N., W. M. Cowan, and D. G. Amaral (1995). "A quantitative analysis of the dendritic organization of pyramidal cells in the rat hippocampus". *The Journal of Comparative Neurology* 362, pp. 17–45.

Ivanoff, J., P. Branning, and R. Marois (2008). "fMRI evidence for a dual process account of the speed-accuracy tradeoff in decision-making". *PLoS One* 3, e2635.

Izhikevich, E. M. (2001). "Resonate-and-fire neurons". *Neural Networks* 14, pp. 883–894.

Izhikevich, E. M. (2004). "Which model to use for cortical spiking neurons?" *IEEE Transactions on Neural Networks* 15, pp. 1063–1070.

Izhikevich, E. M. and G. M. Edelman (2008). "Large-scale model of mammalian thalamocortical systems". *Proceedings of the National Academy of Sciences USA* 105, p. 3593.

Kadohisa, M., E. T. Rolls, and J. V. Verhagen (2005a). "Neuronal representations of stimuli in the mouth: the primate insular taste cortex, orbitofrontal cortex, and amygdala". *Chemical Senses* 30, pp. 401–419.

Kadohisa, M., E. T. Rolls, and J. V. Verhagen (2005b). "The primate amygdala: neuronal representations of the viscosity, fat texture, grittiness and taste of foods". *Neuroscience* 132, pp. 33–48.

Kandel, E., J. Schwartz, and T. Jessell (2012). *Principles of Neural Science*. Fifth. New York: McGraw-Hill Medical, p. 1414.

Kanter, I. and H. Sompolinsky (1987). "Associative recall of memory without errors". *Physical Review A* 35, p. 380.

Knight, B. (2000). "Dynamics of encoding in neuron populations: some general mathematical features". *Neural Computation* 12, pp. 473–518.

Knoblauch, A. et al. (2012). "Does spike-timing-dependent synaptic plasticity couple or decouple neurons firing in synchrony?" *Frontiers in Computational Neuroscience* 6.

Kunkel, S., M. Diesmann, and A. Morrison (2010). "Limits to the development of feed-forward structures in large recurrent neuronal networks". *Frontiers in Computational Neuroscience* 4.

Lapicque, L. (1907). "Recherches quantitatives sur l'excitation électrique des nerfs traitée comme une polarisation". *Journal de Physiologie et de Pathologie Générale* 9, 620–635.

Lebowitz, J. L. (1993). "Macroscopic laws, microscopic dynamics, time's arrow and Boltzmann's entropy". *Physica A* 194, pp. 1–27.

Levy, W. B. and R. A. Baxter (1996). "Energy efficient neural codes". *Neural Computation* 8, pp. 531–543.

Li Hegner, Y. et al. (2009). "Comparing tactile pattern and vibrotactile frequency discrimination: a human fMRI study". *Neuroimage* 47, S108.

Li, X. et al. (1994). "The hippocampal CA3 network: an in vivo intracellular labeling study". *The Journal of comparative neurology* 339, pp. 181–208.

Linaro, D., M. Storace, and M. Giugliano (2011). "Accurate and fast simulation of channel noise in conductance-based model neurons by diffusion approximation". *PLoS computational biology* 7, e1001102.

Lisman, J. (2005). "The theta/gamma discrete phase code occuring during the hippocampal phase precession may be a more general brain coding scheme". *Hippocampus* 15, pp. 913–922.

Lisman, J., S. Raghavachari, and R. Tsien (2007). "The sequence of events that underlie quantal transmission at central glutamatergic synapses". *Nature Reviews Neuroscience* 8, pp. 597–609.
Little, W. (1974). "The existence of persistent states in the brain". *Mathematical Biosciences* 19, pp. 101–120.
Litwin-Kumar, A. and B. Doiron (Nov. 2012). "Slow dynamics and high variability in balanced cortical networks with clustered connections". *Nat Neurosci* 15, pp. 1498–1505.
Liu, Y. H. and X.-J. Wang (2008). "A common cortical circuit mechanism for perceptual categorical discrimination and veridical judgment". *PLoS Computational Biology*, e1000253.
Loh, M., E. T. Rolls, and G. Deco (2007a). "A dynamical systems hypothesis of schizophrenia". *PLoS Computational Biology* 3 (11), e30228.
Loh, M., E. T. Rolls, and G. Deco (2007b). "Statistical fluctuations in attractor networks related to schizophrenia". *Pharmacopsychiatry* 40, S78–84.
London, M. and M. Häusser (Jan. 2005). "Dendritic computation." *Annual Review of Neuroscience* 28, pp. 503–32.
Luce, R. D. (1986). *Response Time: Their Role in Inferring Elementary Mental Organization*. New York: Oxford University Press.
Luczak, A. and J. MacLean (2012). "Default activity patterns at the neocortical microcircuit level". *Frontiers in Integrative Neuroscience* 6.
Luna, R. et al. (2005). "Neural codes for perceptual discrimination in primary somatosensory cortex". *Nature neuroscience* 8, pp. 1210–1219.
Lundervold, A. (2010). "On consciousness, resting state fMRI, and neurodynamics". *Nonlinear Biomedical Physics* 4, pp. 1–18.
Lynch, G., T. Dunwiddie, and V. Gribkoff (1977). "Heterosynaptic depression: a postsynaptic correlate of long-term potentiation". *Nature*, pp. 737–739.
Ma, W., J. Beck, A. Pouget, et al. (2008). "Spiking networks for Bayesian inference and choice". *Current opinion in neurobiology* 18, p. 217.
Marti, D. et al. (2008). "A fluctuation-driven mechanism for slow decision processes in reverberant networks". *PLoS ONE* 3, e2534.
Masuda, N. (2009). "Selective population rate coding: A possible computational role of gamma oscillations in selective attention". *Neural Computation* 21, pp. 3335–3362.
Mattia, M. and P. Del Giudice (2002). "Population dynamcs of inhibitory and excitatory interacting spiking neurons". *Physical Review E* 66, pp. 51917–51919.
Mattia, M. and P. Del Giudice (2004). "Finite-size dynamics of inhibitory and excitatory interacting spiking neurons". *Physical Review E* 70, p. 052903.
Mazzoni, A. et al. (2008). "Encoding of naturalistic stimuli by local field potential spectra in networks of excitatory and inhibitory neurons". *PLoS Computational Biology* 4.
McCulloch, W. S. and W. Pitts (1943). "A logical calculus of the ideas immanent in nervous activity". *Bulletin of Mathematical Biology* 5, pp. 115–133.
McDonnell, M. and D. Abbott (2009). "What is stochastic resonance? Definitions, misconceptions, debates, and its relevance to biology". *PLoS computational biology* 5, e1000348.
McDonnell, M. and L. Ward (2011). "The benefits of noise in neural systems: bridging theory and experiment". *Nature Reviews Neuroscience* 12, pp. 415–426.

McEliece, R. et al. (July 1987). "The capacity of the Hopfield associative memory". *IEEE Transactions on Information Theory* 33, pp. 461–482.
McNaughton, B. L. et al. (1996). "Deciphering the hippocampal polyglot: the hippocampus as a path integration system". *Journal of Experimental Biology* 199, pp. 173–185.
McNaughton, B. and R. G. M. Morris (1987). "Hippocampal synaptic enhancement and information storage within a distributed memory system". *Trends Neurosci* 10, pp. 408–415.
Miller, P. (2006). "Analysis of spike statistics in neuronal systems with continuous attractors or multiple, discrete attractor States". *Neural Compututation* 18, pp. 1268–1317.
Miller, P. and D. B. Katz (2010). "Stochastic transitions between neural states in taste processing and decision-making". *Journal Neuroscience* 30, pp. 2559–2570.
Miller, P. and X.-J. Wang (2006). "Power-law neuronal fluctuations in a recurrent network model of parametric working memory". *Journal of Neurophysiology* 95, pp. 1099–1114.
Montague, P., S. Hyman, and J. Cohen (2004). "Computational roles for dopamine in behavioural control". *Nature* 431, pp. 760–767.
Moreno-Bote, R. (2010). "Decision confidence and uncertainty in diffusion models with partially correlated neuronal integrators". *Neural Computation* 22, pp. 1786–1811.
Moreno-Bote, R. and N. Parga (2006). "Auto- and crosscorrelograms for the spike response of leaky integrate-and-fire neurons with slow synapses". *Physical Review Letters* 96, p. 028101.
Moreno-Bote, R., J. Rinzel, and N. Rubin (2007). "Noise-induced alternations in an attractor network model of perceptual bistability". *Journal of Neurophysiology* 98, pp. 1125–1139.
Mountcastle, V., M. Steinmetz, and R. Romo (1990). "Frequency discrimination in the sense of flutter: psychophysical measurements correlated with postcentral events in behaving monkeys". *The Journal of Neuroscience* 10, pp. 3032–3044.
Myme, C. I. O. et al. (2003). "The NMDA-to-AMPA ratio at synapses onto layer 2/3 pyramidal neurons is conserved across prefrontal and visual cortices". *Journal of Neurophysiology* 90, pp. 771–779.
Newsome, W. T., K. H. Britten, and J. A. Movshon (1989). "Neuronal correlates of a perceptual decision". *Nature* 341, pp. 52–54.
Noble, D., A. Garny, and P. J. Noble (2012). "How the Hodgkin–Huxley equations inspired the cardiac Physiome Project". *The Journal of Physiology* 590, pp. 2613–2628.
Nowotny, T. (2011). "Flexible neuronal network simulation framework using code generation for NVidia® CUDA™". *BMC Neuroscience* 12, p. 239.
O'Keefe, J. and L. Nadel (1978). *The Hippocampus as a Cognitive Map*. Oxford: Clarendon Press.
O'Reilly, R. C. (1998). "Six principles for biologically based computational models of cortical cognition". *Trends in Cognitive Sciences* 2, pp. 455–462.
O'Reilly, R. and J. McClelland (1994). "Hippocampal conjunctive encoding, storage, and recall: avoiding a trade-off". *Hippocampus* 4, pp. 661–682.

Orio, P. and D. Soudry (2012). "Simple, fast and accurate implementation of the diffusion approximation algorithm for stochastic ion channels with multiple states". *PloS one* 7, e36670.

Palmer, J., A. C. Huk, and M. N. Shadlen (2005). "The effect of stimulus strength on the speed and accuracy of a perceptual decision". *Journal Vision* 5, pp. 376–404.

Panzeri, S., G. Biella, et al. (1996). "Speed, noise, information and the graded nature of neuronal responses". *Network* 7, pp. 365–370.

Panzeri, S., E. T. Rolls, et al. (2001). "Speed of feedforward and recurrent processing in multilayer networks of integrate-and-fire neurons". *Network: Computation in Neural Systems* 12, pp. 423–440.

Perez Castillo, I. and N. S. Skantzos (2004). "The Little-Hopfield model on a sparse random graph". *Journal of Physics A* 37, pp. 9087–9099.

Polavieja, G. G. de (2002). "Errors drive the evolution of biological signalling to costly codes". *Journal of Theoretical Biology* 214, pp. 657–664.

Purves, D. (2007). *Neuroscience*. 4th Edition. Sunderland: Sinauer Associates, Inc.

Ratcliff, R. and G. McKoon (1978). "Priming in item recognition: Evidence for the propositional structure of sentences". *Journal of Verbal Learning and Verbal Behavior* 17, pp. 403–417.

Ratcliff, R. and G. McKoon (2008). "The diffusion decision model: theory and data for two-choice decision tasks". *Neural Compututation* 20, pp. 873–922.

Ratcliff, R. and J. F. Rouder (1998). "Modeling response times for two-choice decisions". *Psychological Science* 9, pp. 347–356.

Ratcliff, R., T. V. Zandt, and G. McKoon (1999). "Connectionist and diffusion models of reaction time". *Psychological Reviews* 106, pp. 261–300.

Ray, S. and J. H. R. Maunsell (2010). "Differences in gamma frequencies across visual cortex restrict their possible use in computation". *Neuron* 67, pp. 885–896.

Renart, A., N. Brunel, and X.-J. Wang (2004). "Mean-field theory of irregularly spiking neuronal populations and working memory in recurrent cortical networks". *Computational Neuroscience: A Comprehensive Approach*, pp. 431–490.

Renart, A., R. Moreno-Bote, et al. (2007). "Mean-driven and fluctuation-driven persistent activity in recurrent networks". *Neural Computation* 19, pp. 1–46.

Renart, A., N. Parga, and E. T. Rolls (1999a). "Associative memory properties of multiple cortical modules". *Network* 10, pp. 237–255.

Renart, A., N. Parga, and E. T. Rolls (1999b). "Backprojections in the cerebral cortex: implications for memory storage". *Neural Computation* 11, pp. 1349–1388.

Renart, A., J. de la Rocha, et al. (Jan. 2010). "The asynchronous state in cortical circuits." *Science* 327, pp. 587–90.

Resulaj, A. et al. (2009). "Changes of mind in decision-making". *Nature* 461, pp. 263–266.

Ribrault, C., K. Sekimoto, and A. Triller (2011). "From the stochasticity of molecular processes to the variability of synaptic transmission". *Nature Reviews Neuroscience* 12, pp. 375–387.

Richardson, M. J. E. (2004). "Effects of synaptic conductance on the voltage distribution and firing rate of spiking neurons". *Physical Review E* 69, p. 051918.

Richardson, M. J. E., N. Brunel, and V. Hakim (2003). "From subthreshold to firing-rate resonance". *Journal of Neurophysiology* 89, pp. 2538–2554.
Ringach, D. (2009). "Spontaneous and driven cortical activity: implications for computation". *Current opinion in neurobiology* 19, p. 439.
Rinzel, J. (1986). "A formal classification of bursting mechanisms in excitable systems". In: *Proceedings of the International Congress of Mathematicians*. Vol. 1, pp. 1578–1593.
Rinzel, J. et al. (1998). "Propagating activity patterns in large-scale inhibitory neuronal networks". *Science* 279, p. 1351.
Roitman, J. D. and M. N. Shadlen (2002). "Response of neurons in the lateral intraparietal area during a combined visual discrimination reaction time task". *Journal of Neuroscience* 22, pp. 9475–9489.
Rojas, R. (1996). *Neural Networks: A Systematic Introduction*. Berlin: Springer-Verlag.
Rolls, E. T. (1996). "A theory of hippocampal function in memory". *Hippocampus* 6, pp. 601–620.
Rolls, E. T. (2003). "Consciousness absent and present: a neurophysiological exploration". *Progress in Brain Research* 144, pp. 95–106.
Rolls, E. T. (2005). *Emotion Explained*. Oxford: Oxford University Press.
Rolls, E. T. (2008). *Memory, Attention, and Decision-Making. A Unifying Computational Neuroscience Approach*. Oxford: Oxford University Press.
Rolls, E. T. (2010). "A computational theory of episodic memory formation in the hippocampus". *Behavioural Brain Research* 215, pp. 180–196.
Rolls, E. T. (2011). "Glutamate, obsessive-compulsive disorder, schizophrenia, and the stability of cortical attractor neuronal networks". *Pharmacology, Biochemistry and Behavior*, pp. 736–751.
Rolls, E. T. (2012). "Advantages of dilution in the connectivity of attractor networks in the brain". *Biologically Inspired Cognitive Architecture* 1, in.
Rolls, E. T., H. D. Critchley, and A. Treves (1996). "The representation of olfactory information in the primate orbitofrontal cortex". *Journal of Neurophysiology* 75, pp. 1982–1996.
Rolls, E. T., H. Critchley, et al. (2010). "The representation of information about taste and odor in the primate orbitofrontal cortex". *Chemosensory Perception* 3, pp. 16–33.
Rolls, E. T. and G. Deco (2010). *The Noisy Brain: Stochastic Dynamics as a Principle of Brain Function*. Oxford: Oxford University Press.
Rolls, E. T. and G. Deco (2011). "A computational neuroscience approach to schizophrenia and its onset". *Neuroscience and Biobehavioral Reviews* 35, pp. 1644–1653.
Rolls, E. T., F. Grabenhorst, and G. Deco (2010a). "Choice, difficulty, and confidence in the brain". *Neuroimage* 53, pp. 694–706.
Rolls, E. T., F. Grabenhorst, and G. Deco (2010b). "Decision-making, errors, and confidence in the brain". *Journal of Neurophysiology* 104, pp. 2359–2374.
Rolls, E. T., M. Loh, and G. Deco (2008). "An attractor hypothesis of obsessive-compulsive disorder". *European Journal of Neuroscience* 28, pp. 782–793.
Rolls, E. T., M. Loh, G. Deco, and G. Winterer (2008). "Computational models of schizophrenia and dopamine modulation in the prefrontal cortex". *Nature Reviews Neuroscience* 9, pp. 696–709.

Rolls, E. T., S. M. Stringer, and T. Elliot (2006). "Entorhinal cortex grid cells can map to hippocampal place cells by competitive learning". *Network: Computation in Neural Systems* 17, pp. 447–465.

Rolls, E. T. and M. J. Tovee (1995). "Sparseness of the neuronal representation of stimuli in the primate temporal visual cortex". *Journal of Neurophysiology* 73, pp. 713–726.

Rolls, E. T., M. J. Tovee, and S. Panzeri (1999). "The neurophysiology of backward visual masking: information analysis". *Journal of Cognitive Neuroscience* 11, pp. 335–346.

Rolls, E. T. and A. Treves (1990). "The relative advantages of sparse versus distributed encoding for associative neuronal networks in the brain". *Network* 1, pp. 407–421.

Rolls, E. T. and A. Treves (1998). *Neural Networks and Brain Function*. Oxford: Oxford University Press.

Rolls, E. T. and A. Treves (2011). "The neuronal encoding of information in the brain". *Progress in Neurobiology*, pp. 448–490.

Rolls, E. T., A. Treves, R. G. Robertson, et al. (1998). "Information about spatial view in an ensemble of primate hippocampal cells". *Journal of Neurophysiology* 79, pp. 1797–1813.

Rolls, E. T., A. Treves, M. Tovee, et al. (1997). "Information in the neuronal representation of individual stimuli in the primate temporal visual cortex". *Journal of Computational Neuroscience* 4, pp. 309–333.

Rolls, E. T., J. V. Verhagen, and M. Kadohisa (2003). "Representations of the texture of food in the primate orbitofrontal cortex: neurons responding to viscosity, grittiness, and capsaicin". *Journal of Neurophysiology* 90, pp. 3711–3724.

Rolls, E. T. et al. (1997a). "Simulation studies of the CA3 hippocampal subfield modelled as an attractor neural network". *Neural Networks* 10, pp. 1559–1569.

Rolls, E. T. et al. (1997b). "Simulation studies of the CA3 hippocampal subfield modelled as an attractor neural network". *Neural Networks* 10, pp. 1559–1569.

Romo, R., C. Brody, et al. (1999). "Neuronal correlates of parametric working memory in the prefrontal cortex". *Nature* 339, pp. 470–473.

Romo, R., A. Hernandez, and A. Zainos (2004). "Neuronal correlates of a perceptual decision in ventral premotor cortex". *Neuron* 41, pp. 165–173.

Romo, R., A. Hernandez, A. Zainos, et al. (2002). "Neural correlates of decision-making in secondary somatosensory cortex". *Nature Neuroscience* 5, pp. 1217–1225.

Romo, R. and E. Salinas (2003). "Flutter discrimination: Neural codes, perception, memory and decision making". *Nature Reviews Neuroscience* 4, pp. 203–218.

Rudolph, M. and A. Destexhe (2006). "Analytical integrate-and-fire neuron models with conductance-based dynamics for event-driven simulation strategies". *Neural Computation* 18, pp. 2146–2210.

Sakai, Y., H. Okamoto, and T. Fukai (2006). "Computational algorithms and neuronal network models underlying decision processes". *Neural Networks* 19, pp. 1091–1105.

Salinas, E. and T. J. Sejnowski (2001). "Correlated neuronal activity and the flow of neural information". *Nature Reviews Neuroscience* 2, pp. 539–550.

Scanziani, M. and M. Häusser (2009). "Electrophysiology in the age of light". *Nature* 461, pp. 930–939.
Schall, J. (2001). "Neural basis of deciding, choosing and acting". *Nature Review Neuroscience* 2, pp. 33–42.
Schall, J. (2003). "Neural correlates of decision processes: neural and mental chronometry". *Current opinion in neurobiology* 13, pp. 182–186.
Schneggenburger, R. and E. Neher (2005). "Presynaptic calcium and control of vesicle fusion". *Current opinion in neurobiology* 15, pp. 266–274.
Schrader, S., M. Diesmann, and A. Morrison (2010). "A compositionality machine realized by a hierarchic architecture of synfire chains". *Frontiers in computational neuroscience* 4.
Schwartz, E. L. (1990). *Computational Neuroscience*. Cambridge: MIT Press.
Shadlen, M. and W. Newsome (1996). "Motion perception: seeing and deciding". *Proceedings of the National Academy of Science USA* 93, pp. 628–633.
Shadlen, M., K. Britten, et al. (1996). "A computational analysis of the relationship between neuronal and behavioral responses to visual motion". *The Journal of neuroscience* 16, pp. 1486–1510.
Shadlen, M. and W. Newsome (1994). "Noise, neural codes and cortical organization". *Current opinion in neurobiology* 4, pp. 569–579.
Shadlen, M. and W. Newsome (2001). "Neural basis of a perceptual decision in the parietal cortex (area LIP) of the rhesus monkey". *Journal of Neurophysiology* 86, pp. 1916–1936.
Shannon, C. E. (1948). "A mathematical theory of communication". *AT&T Bell Laboratories Technical Journal* 27, pp. 379–423.
Shepherd, G. M. (1988). *Neurobiology* . Oxford: Oxford University Press.
Smerieri, A., E. T. Rolls, and J. Feng (2010). "Decision time, slow inhibition, and theta rhythm". *Journal of Neuroscience* 30, pp. 14173–14181.
Smith, P. and R. Ratcliff (2004). "Psychology and neurobiology of simple decisions". *Trends in Neurosciences* 23, pp. 161–168.
Softky, W. R. and C. Koch (1993). "The highly irregular firing of cortical cells is inconsistent with temporal integration of random EPSPs". *Journal of Neuroscience* 13, pp. 334–350.
Stein, R. B. (1965). "A theoretical analysis of neuronal variability". *Biophysical Journal* 5, pp. 173–194.
Stewart, R. D. and W. Bair (2009). "Spiking neural network simulation: numerical integration with the Parker-Sochacki method". *Journal of Computational Neuroscience* 27, pp. 115–133.
Stock, J. T. and M. V. Orna (1989). *Electrochemistry, Past and Present*. Washington, DC: American Chemical Society.
Sudhof, T. C. (Jan. 2004). "The synaptic vesicle cycle." *Annual review of neuroscience* 27, pp. 509–47.
Sun, Y. et al. (2009). "Library-based numerical reduction of the Hodgkin–Huxley neuron for network simulation". *Journal of computational neuroscience* 27, pp. 369–390.
Tesauro, G. (1986). "Simple neural models of classical conditioning". *Biological Cybernetics* 55, pp. 187–200.
Thurstone, L. L. (1987). "Psychophysical analysis. By L. L. Thurstone, 1927." eng. *Am J Psychol* 100, pp. 587–609.

Tiesinga, P. and T. J. Sejnowski (2009). "Cortical enlightenment: are attentional gamma oscillations driven by ING or PING?" *Neuron* 63, pp. 727–732.
Traub, R. D., J. G. Jefferys, and M. A. Whittington (1997). "Simulation of gamma rhythms in networks of interneurons and pyramidal cells". *Journal of Computational Neuroscience* 4, pp. 141–150.
Treves, A. (1991). "Dilution and sparse encoding in threshold-linear nets". *Journal of Physics A* 24, pp. 327–335.
Treves, A. and E. T. Rolls (1991). "What determines the capacity of autoassociative memories in the brain?" *Network* 2, pp. 371–397.
Treves, A. and E. T. Rolls (1994a). "A computational analysis of the role of the hippocampus in memory". *Hippocampus* 4, pp. 374–391.
Treves, A. and E. T. Rolls (1994b). "Computational analysis of the role of the hippocampus in memory". *Hippocampus* 4, pp. 374–391.
Treves A.and Panzeri, S. et al. (1999). "Firing rate distributions and efficiency of information transmission of inferior temporal cortex neurons to natural visual stimuli". *Neural Computation* 11, pp. 611–641.
Tsodyks, M. (1999). "Attractor neural network models of spatial maps in Hippocampus". *Hippocampus* 9, pp. 481–489.
Tversky, A. (1972). "Elimination by aspects: A theory of choice." *Psychological review* 79, p. 281.
Urakubo, H. et al. (2009). "Experimental and computational aspects of signaling mechanisms of spike-timing-dependent plasticity". *HFSP Journal* 3, pp. 240–254.
Usher, M. and J. McClelland (2001). "On the time course of perceptual choice: the leaky competing accumulator model". *Psychological Reviews* 108, pp. 550–592.
Van Rossum, M., G. Turrigiano, and S. Nelson (2002). "Fast propagation of firing rates through layered networks of noisy neurons". *The Journal of Neuroscience* 22, pp. 1956–1966.
Van Rullen, R., R. Guyonneau, and S. J. Thorpe (2005). "Spike times make sense". *Trends in Neuroscience* 28, pp. 1–4.
Van Veen, V., M. Krug, and C. Carter (2008). "The neural and computational basis of controlled speed-accuracy tradeoff during task performance". *Journal of Cognitive Neuroscience* 20, pp. 1952–1965.
Vandekerckhove, J. and F. Tuerlinckx (2007). "Fitting the Ratcliff diffusion model to experimental data". *Psychonomic Bulletin & Review* 14, pp. 1011–1026.
Varela, F. et al. (2001). "The Brainweb: phase synchronization and large-scale integration". *Nature Reviews Neuroscience* 2, pp. 229–239.
Verhagen, J. V., M. Kadohisa, and E. T. Rolls (2004). "The primate insular taste cortex: neuronal representations of the viscosity, fat texture, grittiness, and the taste of foods in the mouth". *Journal of Neurophysiology* 92, pp. 1685–1699.
Vickers, D. (1970). "Evidence for an accumulator model of psychophysical discrimination". *Ergonomics* 13, pp. 37–58.
Vickers, D. (1979). *Decision Processes in Visual Perception*. New York: Academic Press.
Vickers, D. and J. Packer (1982). "Effects of alternating set for speed or accuracy on response time, accuracy and confidence in a unidimensional discrimination task". *Acta Psychologica* 50, pp. 179–197.

Wang, X.-J. (1999). "Synaptic basis of cortical persistent activity: the importance of NMDA receptors to working memory". *Journal of Neuroscience* 19, pp. 9587–9603.
Wang, X.-J. (2002). "Probabilistic decision making by slow reverberation in cortical circuits". *Neuron* 36, pp. 955–968.
Wang, X.-J. (2008). "Decision making in recurrent neuronal circuits". *Neuron* 60, pp. 215–234.
Wang, X.-J. (2010). "Neurophysiological and computational principles of cortical rhythms in cognition". *Physiological Reviews* 90, pp. 1195–1268.
Watanabe, M. and K. Maemura (2002). "GABA and GABA receptors in the central nervous system and other organs". *International Review of Cytology*, pp. 1–47.
Webb, T. J. et al. (2011). "Noise in attractor networks in the brain produced by graded firing rate representations". *PLoS One* 6, e23620.
Welford, A. T., ed. (1980). *Reaction Times*. London: Academic Press.
White, J., J. Rubinstein, and A. Kay (2000). "Channel noise in neurons". *Trends in neurosciences* 23, pp. 131–137.
Wilbur, W. J. and J. Rinzel (1982). "An analysis of Stein's model for stochastic neuronal excitation". *Biological Cybernetics* 45, pp. 107–114.
Wildie, M. and M. Shanahan (2011). "Establishing communication between neuronal populations through competitive entrainment". *Frontiers in Computational Neuroscience* 5, p. 62.
Wills, T. J. et al. (2005). "Attractor dynamics in the hippocampal representation of the local environment". *Science* 308, pp. 873–876.
Willshaw, D., O. Buneman, and H. Longuet-Higgins (1969). "Non-holographic associative memory." *Nature*.
Wilson, R. C. (Mar. 2009). "Parallel Hopfield networks." *Neural computation* 21, pp. 831–50.
Womelsdorf, T. and P. Fries (2007). "The role of neuronal synchronization in selective attention". *Current Opinion in Neurobiology* 17, pp. 154–160.
Womelsdorf, T., P. Fries, et al. (2006). "Gamma-band synchronization in visual cortex predicts speed of change detection". *Nature* 439, pp. 733–736.
Womelsdorf, T., J. M. Schoffelen, et al. (2007). "Modulation of neuronal interactions through neuronal synchronization". *Science* 316, pp. 1609–1612.
Wong, K. F. and A. C. Huk (2008). "Temporal dynamics underlying perceptual decision making: insights from the interplay between an attractor model and parietal neurophysiology". *Frontiers in Neuroscience* 2, pp. 245–254.
Wong, K. F., A. C. Huk, et al. (2007). "Neural circuit dynamics underlying accumulation of time-varying evidence during perceptual decision-making". *Frontiers in Computational Neuroscience* 1, p. 6.
Wong, K. F. and X. Wang (2006). "A recurrent network mechanism of time integration in perceptual decisions". *Journal of Neuroscience* 26, pp. 1314–1328.
Wong, K. F. and X.-J. Wang (2006). "A recurrent network mechanism of time integration in perceptual decisions". *Journal of Neuroscience* 26, pp. 1314–1328.
Wu, S., K. Hamaguchi, and S. Amari (2008). "Dynamics and computation of continuous attractors". *Neural computation* 20, pp. 994–1025.
Zippelius, A. (1993). "Statistical mechanics of neural networks". *Physica A* 194, pp. 471–481.